An Investigation on the Corrosion Inhibition of Brazing Cu-Ag Alloy

By

Hooman Rahmani

A Dissertation Submitted in Fulfillment of the Requirements for the Degree of Doctor of Philosophy in Materials Science and Engineering

The University of Texas at Arlington

August 2020

Dedication

To my beloved parents for their limitless love, unconditional support, faith in me, and encouragement for the pursuit of my dreams.

Acknowledgments

First, I would like to extend my sincere thanks to my parents whom their support and love have always helped me in taking important steps in my life. I would also like to extend my deepest gratitude to Dr. Efstathios I. Meletis, whom I have always learned from, for giving me this opportunity in the first place. I would also like to acknowledge Dr. Choong-Un Kim, Dr. Krishnan Rajeshwar and Dr. Jiechao Jiang for their support and advice. I would also like to thank my group members and recognize their assistance.

Abstract

Adsorption and inhibition behavior of 1,2,3-benzotriazole (BTA) and 2,5-dimercapto-1,3,4-thiadiazole (DMTD) on brazing Cu-Ag alloy was studied in deionized water using corrosion potential measurement, potentiodynamic polarization, adsorption isotherm investigation, X-ray photoelectron spectroscopy (XPS), and electrochemical impedance spectroscopy (EIS). Pure Ag and pure Cu specimens were included to investigate the mere effect each component has on the alloy's behavior along with a high copper alloy for comparison purposes. The electrochemical responses show that BTA shifts the corrosion potential of Cu to the noble direction but has the opposite effect for Ag and a mixed behavior for the Cu-Ag alloys. However, DMTD in all cases shifts the corrosion potentials to the active region for the metals studied. The inhibition efficiency (η) of BTA for Cu and high Cu alloy reached around 95% through chemisorption. Nonetheless, η was significantly lower for Ag and the brazing Cu-Ag alloy having a partially chemisorbed-partially physiosorbed behavior while interacting with BTA. Results show the better inhibition of DMTD for Ag and the brazing Cu-Ag alloy by merely chemisorption. BTA was found to follow Langmuir isotherm while DMTD obeyed Temkin adsorption isotherm, despite both acting as a mixed type inhibitor. Combining the two inhibitors increased the inhibition efficiency over 80% for the Cu-Ag alloy.

XPS results showed the formation of Cu- and Ag-BTA organometallic complexes through the N tail of the inhibitor. In addition, formation of DMTD organometallic film was confirmed through DMTD's functional groups of pyrrolic N from the azole ring and thiol S from the mercapto anchoring group on Ag and thiol S on Cu. The lower inhibition efficiency of Ag and brazing alloy was attributed to the weak adsorption of BTA on the Ag phase leading to lower corrosion protection of Ag. The higher affinity of DMTD to Ag was attributed to the involvement of two heteroatoms with the Ag surface.

Furthermore, electrochemical impedance spectroscopy (EIS) was utilized to delve into the corrosion inhibition of eutectic Cu-Ag alloy and its components (Cu and Ag) in aqueous, aerated 0.1 M KNO_3 solutions. The corrosion inhibition slowly evolved over time as diagnosed by an increase in the charge transfer impedance and the gradual tendency of the Nyquist profiles to arc toward the real axis. This trend was attributed to the gradual formation of organometallic passivation layers replacing the interfacial water molecules on the metal surfaces. The EIS data underlined the specific affinity of BTA and DMTD toward the Cu and Ag surfaces, respectively. A transition of the double layer equivalent circuit element from ideal capacitance to a constant phase element was observed for the alloy compared to the pure metals. This was attributed to the heterogeneity induced by Cu-rich and Ag-rich phases in the alloy and by the formed oxides/protective film on the alloy surface.

Table of Contents

List of Tables

List of Figures

Chapter 1 Introduction

1. 1. Introduction

The search for efficient and economical methods to protect metals from corrosion is a key factor in industrial manufacturing. Addition of corrosion inhibitors, in very small amounts, is one of the most effective preventing methods especially for protection of closed water systems through the interaction of the inhibitor's molecules with the metal surface leading to corrosion rate reduction [1].

Water-cooled mainframes are being utilized as a vital component for maintaining the security and reliability of data storage centers. These water circulating cooling systems use high purity copper plates and straight/pin-shaped fins brazed with Cu-60 atom% Ag eutectic alloy (hereafter designated as Cu-60Ag) to operate as effective sinks to dissipate heat generated by the myriad of central processing units. However, the brazed joints experience corrosion that jeopardizes the safety and longevity of the data repository. Employing corrosion inhibitors on both the constituent α (Cu-rich) and β (Ag-rich) phases in the Cu-60Ag alloy, can address much of the reliability concern and improve the safety and lifetime of the overall system.

Even with exercising various corrosion protection strategies including the use of 1,2,3-benzotriazole (BTA) for inhibition, corrosion is not completely prevented, and the inhibitor is not highly effective in protecting the device. This poses serious concern to the information technology industry as future computing facilities that have planned to be built with water cooling systems

can face reliability issues. This study is going to investigate the involved mechanisms for the failure of such systems by studying the interaction of Cu-Ag alloy with BTA. In addition, based on the prevailing mechanism, it also explores an alternative inhibitor and the combination of inhibitors for a better corrosion protection utilizing 2,5-dimercapto-1,3,4-thiadiazole (DMTD).

Corrosion inhibition of copper with BTA has been the subject of numerous studies [2–4], but very limited research has been conducted on the interaction of silver with BTA which are contradictory [5–9]. Also, there is virtually no research on the inhibition of Cu-Ag alloys with BTA. Therefore, to secure the safety and longevity of the data repository and for a higher corrosion protection in structures with Cu-Ag alloys, it would only seem natural to conduct a corrosion study and to investigate the involved inhibition mechanisms.

This dissertation provides a unique opportunity to study the adsorption and inhibition behavior of BTA and DMTD on the Cu-Ag alloy surfaces by conducting electrochemical and surface characterization studies. Understanding the bonding nature of the inhibitor to the metal surface by XPS studies is important since it relates to its effectiveness in protecting the metal surface.

The following objectives are intended in this study to get a fundamental understanding of the involved mechanisms:

i. **Electrochemical studies of the Cu-Ag alloys as well as the particular phases present in them with the objective to recognize their corrosion behavior, inhibitor adsorption mechanisms, and to identify their susceptible component(s) in the specific environment.** Electrochemical studies provide the opportunity for these investigations through exploring the potential behavior, corrosion rate obtained by potentiodynamic testing, and electrochemical impedance spectroscopy [10].

ii. **Surface characterization studies to explore the chemical state, the plausible formed bonds from the inhibitor interaction with the Cu and Ag surface, as the Cu-Ag alloys' components, in order to trace the adsorption of inhibitor on these phases.** XPS is a highly-surface-sensitive technique in this matter. The inhibitor interaction with Cu and Ag is expected to form a very thin layer at the surface and XPS is an ideal technique to obtain

bonding information from such a small volume of surface layer. It is a well-established method in the literature for such surface characterizations [11,12].

iii. **Proposing the features of an effective inhibitor compound in the specific environment based on the fundamental understanding of the involved mechanisms led to corrosion failure.**

The study tasks mentioned above can bridge between the primary observations, the current understandings, and the objectives. They also provide ground to progress towards proposing solutions for a higher corrosion protection in structures involving Cu-Ag alloys that face corrosion risks, especially in data center facilities.

This dissertation is divided into five chapters, and the content is described briefly as follows:

Chapter 1 already presented, and it described the motivation, objectives, and the aim of this study.

Chapter 2 investigates a thorough review on the available knowledge on the subject.

Chapter 3 outlines the experimental details and methodology including the information about the materials, solutions, equipment, and characterization techniques.

Chapter 4 presents and discusses the obtained results on the interaction of the metal surfaces with the inhibitors used in the specific environment. The corrosion rates and potentials as well as the inhibition efficiencies are compared in different conditions, adsorption strength and behaviors are studied, and the electrochemical behaviors are modeled based on equivalent circuits. In addition, the chemical state of the metal surfaces and the plausible formed chemical bonds are determined to further shed light on the fundamental understanding behind the corrosion inhibition mechanisms.

Chapter 5 presents the major conclusions from the acquired results.

Chapter 2 Literature Review

2. 1. Corrosion

2. 1. 1. Definition of Corrosion

Corrosion is the chemical or electrochemical reaction of a material with the environment leading to its gradual deterioration. Generally, there are different types of corrosion including uniform corrosion, galvanic corrosion, pitting, crevice corrosion, hydrogen damage, erosion corrosion, intergranular corrosion, stress corrosion cracking, high temperature oxidation and dealloying [13,14]. Electrochemical corrosion is the result of specific cathodic and anodic reactions. For the electrochemical corrosion to occur, a third element is required which is the electrolyte to carry electrons and ions and to provide ground for the anodic and cathodic reactions to happen [13,15–17].

2. 1. 2. Anodic and Cathodic Reactions

As aforementioned, for the electrons to path in an electrochemical corrosion process, anodic and cathodic reactions occur. The process in which the metal loses electron(s) and metal dissolution takes place is called anodic reaction. This reaction is also known as oxidation as it follows [18]:

$$M \rightarrow M^{n+} + ne^{-} \qquad (2\text{-}1)$$

where *M* stands for the metal and *n* stands for the number of electrons. The cathodic reaction can be one of the followings depending on the specific environment to consume the electrons produced by the anodic reaction. In deaerated acidic electrolytes, hydrogen evolution is the main cathodic reaction [19]:

$$2H^+ + 2e^- \rightarrow H_2 \qquad (2\text{-}2)$$

in case of deaerated aqueous alkaline environments, the cathodic reaction is [16]:

$$2H_2O + 2e^- \rightarrow H_2 + 2OH^- \qquad (2\text{-}3)$$

for the aerated acidic and alkaline environments the cathodic reaction are as follows, respectively [15]:

$$O_2 + 4e^- + 4H^+ \rightarrow 2H_2O \qquad (2\text{-}4)$$

$$O_2 + 4e^- + 2H_2O \rightarrow 4OH^- \qquad (2\text{-}5)$$

and finally, metal reduction as the other type of cathodic reaction:

$$M^{n+} + e^- \rightarrow M^{(n-1)+} \qquad (2\text{-}6)$$

2. 1. 3. Corrosion of Brazed Joints

Common joining methods vary from mechanical attachment (e.g. bolt or rivet) to solid state joining (e.g. bonding to diffusion). Brazing is an alternative method where a filler material (the braze alloy) is heated to form metallurgical and mechanical bonds with the base (parent) materials intended to be joined. Compared to welding, brazing is a low temperature method (usually above 450˚C) in which the filler (braze material) is heated above its melting point but below that of the parent materials [20]. However, compared to soldering technique which is generally carried out at temperatures below 450˚C, brazing can be considered as a high temperature joining process.

Brazed joints experience corrosion attacks led by low quality in the brazing process, environmental conditions, and geometrical factors stemming from the joint design. They are also subjected to selective attacks owing to the microstructure or composition of the brazed joint. Therefore, these factors can cause various types of corrosion in the brazed joints such as uniform corrosion, pitting, selective dealloying, galvanic, intergranular, etc. [15,21,22].

As the base materials and the braze alloy have different chemical compositions, corrosion can happen when appropriate care is not taken during the material selection. The design of the brazed joint can also influence its corrosion susceptibility often through mechanical effects such as stress factors. For instance, with increasing brazed joint length and depth, the plausible destructive tension stress in the brazed joint turns into shear and compression stress leading to less corrosion vulnerability [23,24]. With respect to the joint design it is also important that the geometry of the joint allows the flow of pickling and cleaning solutions easily. The probability of the stagnant solution at the edge of the joint should be considered. Any form of discontinuity including entrapped flux, voids, incomplete joining, or porosities made by gases released from the fluxes or elsewhere should be avoided. Stress distribution must be as even as possible to avoid stress concentration that provide ground for local failure. The brazing is also a critical process. A uniform temperature distribution at a proper temperature range, duration, heating and cooling rate and atmosphere should be determined to avoid premature failures and susceptible spots with concentrated residual stress at the joint. After brazing, oxide scales formed during the brazing process and specially, flux residues which are chemically active and basically corrosive, must be cleaned [23,25].

2. 2. Corrosion Protection

Given the significant importance of corrosion in terms of waste of energy and materials as well as the economic loss it carries [26], there are various preventing methods for different types of corrosion. Usually, several preventing techniques can be applied based on the importance of the system and the availability of the resources. Changing the materials used, changing the corrosive environment, applying barrier films, inhibitors, and coatings, using electrochemical techniques such as sacrificial coatings, or cathodic protection are the main corrosion preventing methods used

in industry [27]. Application of corrosion inhibitors is common when neither the material and environments can be changed caused by the requirements of maintaining some desirable properties, nor the application of coatings and electrochemical methods is feasible owing to the technical and financial limitations.

2. 3. Corrosion Inhibitors

Corrosion inhibitors are chemical substances that lower or prevent corrosion when added in small amounts to a system to extend service lifetime [4,16]. They can interfere in the mechanisms and kinetics of the electrochemical anodic and/or cathodic reactions. For instance, by decelerating the movement or diffusion of ions to the metallic surface. They can form a protective barrier layer on the metal surface that lowers its interaction with the corrosive environment increasing the surface electrical resistant, or can operate by a combination of these methods [24,28]. Corrosion inhibitors are used in various applications including cooling water systems, acid pickling solutions, automobile engine coolants, potable water, oil and gas extraction and storage, etc. [17].

2. 4. Classification of Corrosion Inhibitors

The corroding material and the corrosive environment are the most significant items to consider in choosing an inhibitor for a system [29]. Corrosion inhibitors have been classified in different ways. Some have categorized them as organic and inorganic inhibitors [30]. Figure 2-1 illustrates a qualitative classification of inhibitors.

Corrosion inhibitors can be divided into interface inhibitors and environmental conditioners. Environmental conditioners slow down the corrosion process by decreasing and removing the corrosive species. That is why they are also called scavengers. For instance, hydrazine can lower the oxygen content as a common cathodic reaction (Equation 2-5) in alkaline and neutral environments as follows [16,17,28]:

$$5O_2 + 2(NH_2 - NH_2) \rightarrow 2H_2O + 4H^+ + 4NO_2^- \qquad (2\text{-}7)$$

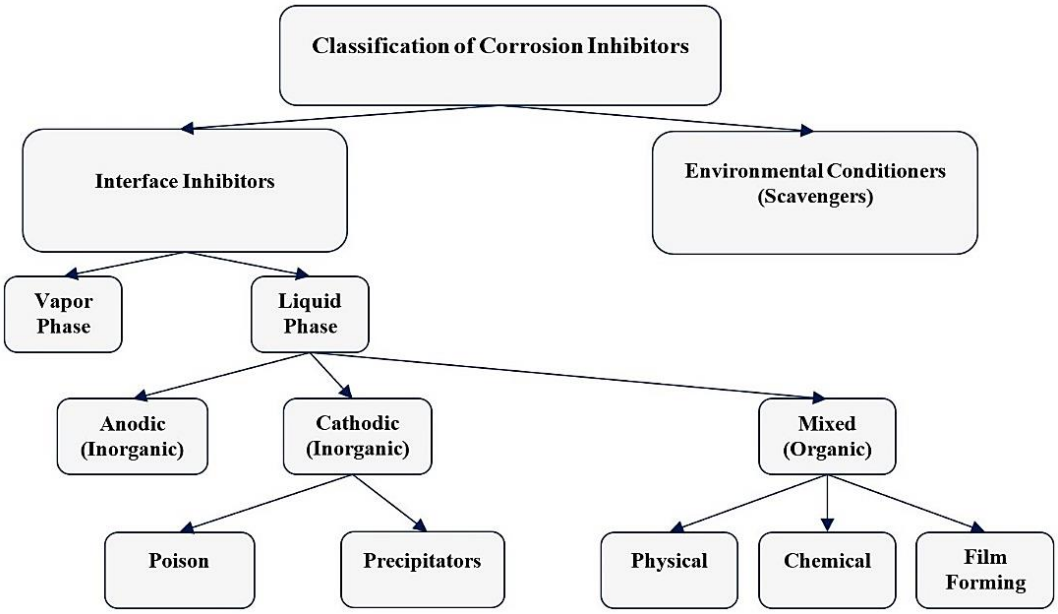

Figure 2-1. Schematic of inhibitor classification [16,17].

Interface inhibitors form a protective layer at the metal/surrounding interface [31]. These inhibitors have been also classified into liquid- and vapor-phase inhibitors. Vapor phase inhibitors, also known as volatile corrosion inhibitors (VCI), have the capability to vaporize and condense on the metal surfaces. The main advantage of these inhibitors is their gas-transportability nature that enables them to reach all metallic surfaces [32]. VCIs are usually transferred to the metal surface by diffusion through a closed environment followed by condensation on the desired surfaces. They either adsorb directly on the part surface or dissolve in a surface moisture layer [33]. Liquid phase inhibitors, depending on their inhibiting impact on each specific electrochemical reaction, are classified as anodic, cathodic, or mixed type inhibitors [16].

2. 4. 1. Anodic Corrosion Inhibitors

Anodic inhibitors decrease the anodic reaction by forming or facilitating the natural passivation of the metal surface along with forming an adsorbed protective layer on the metallic part [28]. In general, these inhibitors react with the initially formed corrosion products and develop an insoluble film on the metal surface [34]. As anodic inhibitors shift the corrosion potential to more positive (noble) values, there is a critical inhibitor concentration below which the corrosion

rate increases when inhibitor is applied for protection of an active-passive metal. As shown in Figure 2-2, in the absence of the inhibitor, the metal is corroding at the active state at a rate corresponding to point A. Increasing the concentration insufficiently, increases the corrosion rate corresponding to point B. After a critical concentration, the metal experiences a rapid transition to the passive state and the corrosion rate decreases significantly (point C) [15,16]. Insufficient concentrations of passivating (anodic) inhibitors also leads to local corrosion attacks caused by galvanic and/or pitting corrosion owing to the poor coverage of the inhibitor on the metal surface and the heterogeneity of the developed passivating layer [24].

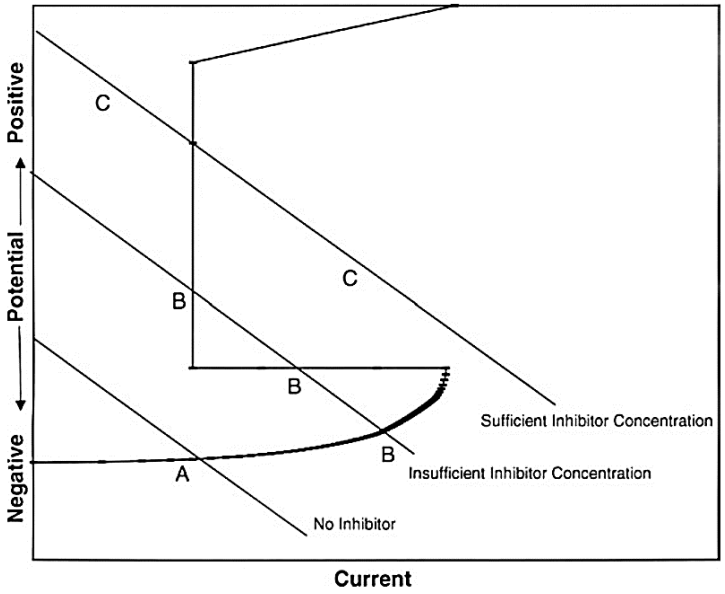

Figure 2-2. Polarization diagram of an active-passive metal illustrating the dependence of corrosion rate on the concentration of anodic type inhibitor [16].

As mentioned above, anodic inhibitors react with the corrosion products (metallic ions), generally forming insoluble hydroxides which are deposited on the metal surface. Hydrolysis of the inhibitors results in OH^- ions. Figure 2-3 shows the protective mechanism of anodic inhibitors. Nitrates, molybdates, sodium chromates, phosphates, hydroxides, silicates are examples of inorganic anodic type inhibitors [34].

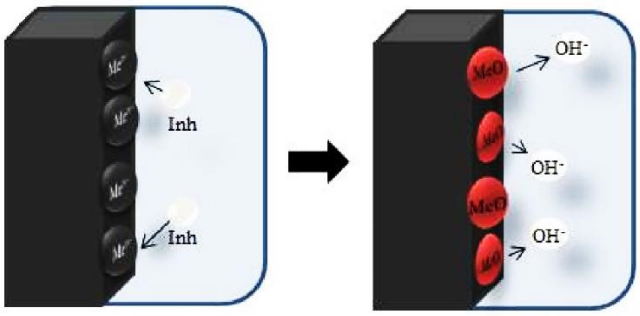

Figure 2-3. Schematic illustration of anodic inorganic inhibitors effect and their mechanism of action [34].

2. 4. 2. Cathodic Corrosion Inhibitors

Cathodic inhibitors restrain the corrosion process by either decreasing the reduction rate (cathodic poisons) or by selectively precipitating on the cathodic areas (cathodic precipitators) to increase the surface impedance and limit the diffusion of reducible species to these areas [16,28]. Cathodic poisons such as sulfides and selenides, are adsorbed on the metal surface, whereas compounds of arsenic, bismuth, and antimony are reduced and deposited at the cathode minimizing the release of hydrogen ions by making the recombination and discharge of hydrogen ions difficult in acidic environments. Cathodic precipitators are used in alkaline environments. They precipitate insoluble compounds on the metal surface. The most widely used cathodic precipitators are the carbonates of calcium, zinc, and magnesium that precipitate as oxides to form a protective layer on the metal surface [19,28,34]. In contrast with the anodic inhibitors, cathodic inhibitors do not cause intense local attacks and are generally known as safe inhibitors [15,24]. As illustrated in Figure 2-4, cathodic inhibitors shift the corrosion potential to the active regions (negative values) induced by their impact on the cathodic polarization curve altering its slope. Nevertheless, the anodic polarization curve would remain intact.

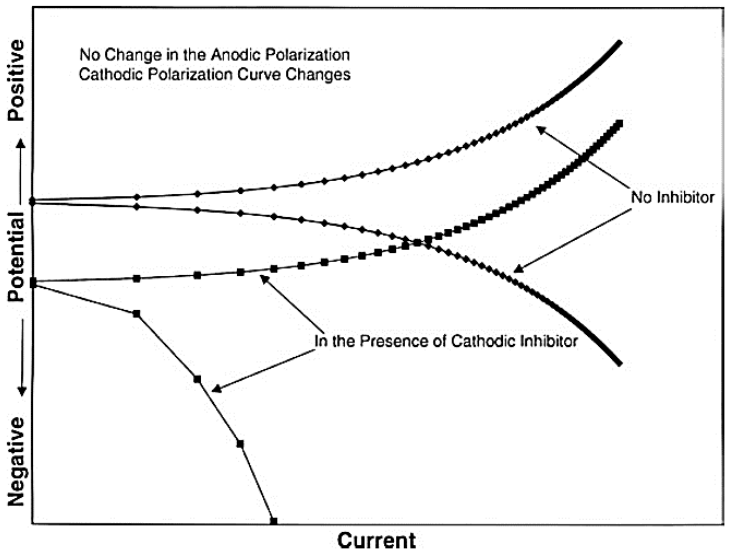

Figure 2-4. Polarization behavior of a metal in the presence of cathodic inhibitor [16].

Figure 2-5 demonstrates the inhibition behavior of the cathodic inhibitors acting as a mechanical barrier suppressing the corrosion process.

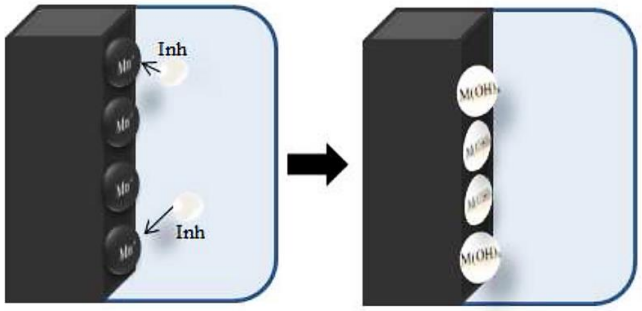

Figure 2-5. Schematic illustration of cathodic inorganic inhibitors and their mechanism of action [34].

2. 4. 3. Mixed Corrosion Inhibitors

Most of the inhibitors are organic compounds that cannot be categorized specifically as anodic or cathodic and are known as mixed type inhibitors [16,17,34]. The effectiveness of these inhibitors depends on the extent to which they adsorb and cover the metal surface known as surface coverage [35]. These inhibitors develop a hydrophobic protective layer that creates a physical barrier impeding the metal surface exposure to the environment, oxygen, or other corrosive agents. They also prevent from further dissolution of the metal [31,36]. Organic mixed inhibitors protect

the metal in three possible ways: physical adsorption, chemisorption, and film formation. Physical (or electrostatic) adsorption is a result of electrostatic attraction force between the ionic charges or dipoles on the inhibitor molecules and the electric charge on the metal surface. Physically adsorbed inhibitors interact rapidly, but they are also easily removed from the surface. The most effective inhibitors are those that chemically adsorb (chemisorb), a process that involves charge sharing or charge transfer between the inhibitor molecules and the metal surface. Adsorbed inhibitor molecules may undergo surface reactions, producing polymeric films. Corrosion protection increases considerably as the protective films grow from nearly two- dimensional adsorbed layers to three- dimensional films up to several hundred nanometers thick. Inhibition is effective only when the films are adherent, are homogeneous, are not soluble, and prevent access of the solution to the metal surface [16,37]. Figure 2-6 represents the formation of the protective film with mixed inhibitors schematically.

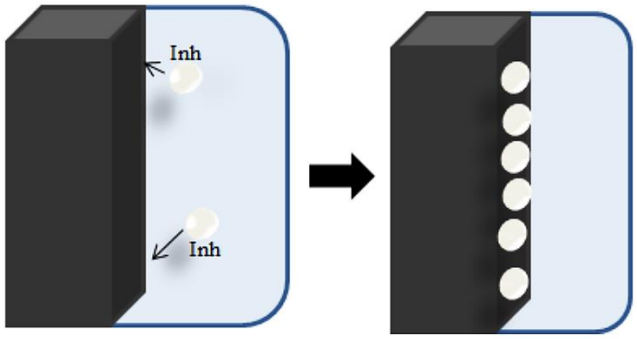

Figure 2-6. Schematic illustration of actuation of the organic (mixed) inhibitor: acting through inhibitor adsorption and film formation on the metal surface [34].

2. 5. Adsorption of Corrosion Inhibitors

Adsorption of organic inhibitors has been attributed to the tendency of their functional group to adsorb on the metal surface. However, there are several other important parameters involved. The efficiency of the mixed inhibitors and their adsorption process generally depends on the following features:

- Inhibitor chemical structure, like the size of the organic molecule;
- Inhibitor functional group (aromaticity and/or conjugated bonding, as the carbon chain length);
- Type and number of bonding atoms or groups in the molecule (either π or σ);

- Electron donating ability of the inhibitor molecule (nature and charges of the metal surface and the adsorption mode like bonding strength to the metal surface);
- Interaction of adsorbed inhibitor species (ability of the formed layer to become compact or cross-linked);
- Interaction of adsorbed inhibitor with the metal surface (capability to form a complex with the metal);
- Type of the electrolyte and the adequate inhibitor solubility in the specific environment [28,34].

Hence, inhibition is effective only when the films are adherent, are not soluble, and prevent access of the solution to the metal. The charge on the inhibitors depends on the presence of loosely bound electrons, lone pairs of electrons, π-electron clouds, aromatic (e.g., benzene) ring systems, and functional groups including elements of group V or VI of the periodic table. Most organic inhibitors have at least one functional group, considered as the reaction center or anchoring group. The strength of adsorption depends on the charge on the anchoring group, rather on the hetero atom (i.e., atoms other than carbon, including N, S, P, O, or Se (present in the anchoring group). The structure of the rest of the molecule influences the charge density on the anchoring group [14,15].

As mentioned above, the active ingredients of organic inhibitors invariably contain one or more functional groups containing one or more heteroatoms through which the inhibitors anchor onto the metal surface. Some common anchoring groups are listed in Table 2-1. These groups are attached to a parent chain (backbone), which enhances the ability of the inhibitor molecule to cover a large surface area.

Table 2-1. Some anchoring (functional) groups in mixed inhibitors [16].

Structure	Name	Structure	Name
$-OH$	Hydroxy	$-CONH_2$	Amide
$-C=C-$	-Yne	$-SH$	Thiol
$-C-O-C-$	Epoxy	$-S-$	Sulfide
$-COOH$	Carboxy	$-S=O$	Sulfoxide
$-C-N-C-$	Amine	$-C=S-$	Thio
$-NH_2$	Amino	$-P=O$	Phosphonium
$-NH$	Imino	$-P-$	Phospho
$-NO_2$	Nitro	$-As-$	Arsano
$-N=N-N-$	Triazole	$-Se-$	Seleno

Water molecules adsorb on the metal surface when the part is immersed in an aqueous phase. Organic molecules adsorb by replacing the water molecules:

$$[inhibitor]_{sol} + [nH_2O]_{ads} \rightleftarrows [inhibitor]_{ads} + [nH_2O]_{sol} \qquad (2\text{-}8)$$

where n is the number of water molecules displaced by one inhibitor molecule. The ability of the inhibitor to replace water molecules depends on the electrostatic interaction between the metal and the inhibitor. On the other hand, the number of water molecules displaced depends on the size and orientation of the inhibitor molecule. The first interaction between inhibitor and the metal surface is nonspecific with a low activation energy. This process, called, physical adsorption, is rapid and, in many cases, reversible [16]. It involves, electrostatic/ van der Waals forces [38].

Under favorable conditions, the adsorbed molecules involved in chemical interaction (chemisorption) form bonds with the metal surface. Chemisorption entails a higher heat of energy and is persistence, specific and irreversible [17,39]. The bonding occurs with electron transfer or sharing between metal and inhibitor. Electron transfer is typical for transition metals having vacant, low-energy electron orbitals. Table 2-2 compares some features of chemical and physical adsorption.

Table 2-2. Comparison between chemisorption and physisorption [17].

	Physisorption	Chemisorption
Type of electronic interaction	Van der Waals or electrostatic forces	Charge transfer or charge sharing
Reversibility	Adsorbed species readily removed by solvent washing	Adsorption is irreversible, more persistent
Energetics	Low heat of adsorption, <10 kcal/mol (40 kJ/mol)	Higher heat of adsorption, >10 kcal/mol (40 kJ/mol)
Kinetics	Rapid adsorption	Slow adsorption
Specificity	Adsorbed species relatively indifferent to identity of surface	Specific interaction, strong dependence on identity of surface

Inhibitors having relatively loosely bound electrons transfer charge easily. The inhibition efficiency of the homologous series of organic substances differing only in the heteroatom is usually in the following sequence: P > S > N > O. On the other hand, the electronegativity, that is, the ability to attract electrons, increases in the reverse order [17]. This might be hard to interpret, because oxygen with higher electronegativity is expected to have a higher inhibition efficiency than the other heteroatoms. The reason is that in oxygen, the outer electrons are firmly held around the atom. Consequently, the electron donating ability of nitrogen and sulfur are enhanced as shown in Figure 2-7 [40]. This leads to a higher affinity to make bond with the vacant d orbitals of the metal surface. Nevertheless, the inhibition efficiency depends on several parameters noted above, such as inhibitor molecular size, electronic structure, the number of adsorption sites, chemical characteristics of the inhibitor being adsorbed, etc. [41].

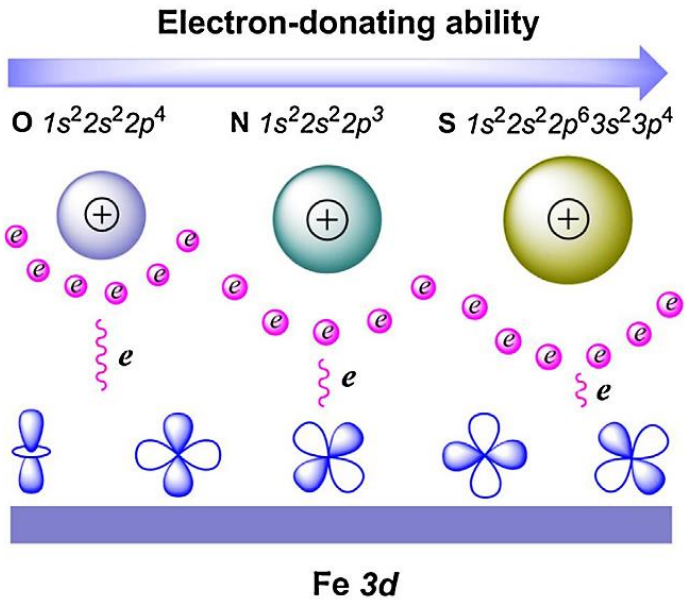

Figure 2-7. Electron donating ability comparison among heteroatoms of O, N and S [40].

2. 5. 1. Adsorption Isotherms

Adsorption mechanism and strength can be deduced from the adsorption isotherm, which shows the relation between the concentration of inhibitors in the corrosive environment (electrolyte) and the inhibitor coverage on the metal surface [37,42,43]. Table 2-3 represents the most commonly used isotherms valid for the formation of up to a monolayer of inhibitor on the metal surface. To evaluate the nature and strength of adsorption, the experimental data (e.g., surface coverage calculated from corrosion rate or impedance data) are fitted to the isotherms, and from the best fit, the thermodynamic data for adsorption are extracted [16,44–46]. Among all the adsorption isotherms, Langmuir isotherm is the simplest. It assumes that all metal surface adsorption sites are equal and molecular binding takes place independently from the neighboring sites regardless of whether or not the nearby sites are occupied [47]. The Temkin adsorption isotherm is also an empirical adsorption model that considers the chemisorption of molecules on heterogeneous surfaces [48]. The main assumption in this model is that heat of adsorption of all molecules in the adsorbed layer decreases linearly with an increase in the surface coverage. It also disregards the very low and high concentrations [39].

Table 2-3. Common inhibitor adsorption isotherms [16].

Name	***Isotherm***	***Verification Plot***
Langmuir	$\theta/(1-\theta)=K_{ads}c$	$Log[\theta/(1-\theta)]$ *vs.* $Log(c)$
Frumkin	$[\theta/(1-\theta)]e^{f\theta}=K_{ads}c$	θ *vs.* $Log(c)$
Bockris-Swinkels	$[\theta/(1-\theta)^n][\theta+n(1-\theta)]^{n-1}/n^n=ce^{-K_{ads}}/55.5$	$Log[\theta/(1-\theta)]$ *vs.* $Log(c)$
Temkin	$e^{f\theta}=K_{ads}c$	θ *vs.* $Log(c)$
Virial Parson	$\theta e^{2f\theta}=K_{ads}c$	θ *vs.* $Log(\theta/c)$

where θ is the inhibitor fractional surface coverage and is equal to $\eta/100$ in which η is inhibition efficiency percent and can be calculated through: $\eta=1-(inhibited\ corrosion\ rate/uninhibited)$; K_{ads} ($dm^3\ mol^{-1}$) equals to $e^{-\Delta G/RT}$ as the adsorption coefficient constant reflecting the affinity of the adsorbate molecules towards adsorption sites; ΔG (J mol^{-1}) is free energy of adsorption; R (J $mol^{-1}\ K^{-1}$) is the gas constant; T (K) is temperature; c (mol dm^{-3}) is inhibitor concentration; n, number of water molecules replaced per inhibitor molecule; and f, inhibitor molecular lateral interaction parameter (0, for no interaction; $+$, for attraction; and $-$, for repulsion) between the adsorbed molecules. Regardless of the adsorption mechanism, the electron density of the functional groups, polarizability, and electron donating ability are important parameters in controlling the effectiveness of an inhibitor for a specific environment [16,39,49].

2. 6. Cu-Ag Alloy in Nearly Neutral Environment

While exploring an alloy's corrosion behavior, studying its phase diagram provides useful information about its components. It is also reasonable to primarily look after the behavior of the involved constituents in the specific environment. Reciprocal solubility of Cu and Ag is negligible below 300˚C; so, all Cu-Ag alloys possess two phases containing a mixture of α and β phases (mainly Cu and Ag, respectively) [50]. With respect to the Pourbaix diagram of Cu- and Ag-H_2O

systems, they both show activity in the pH range of the circulating water used in the cooling system, pH=5.5-6 [51].

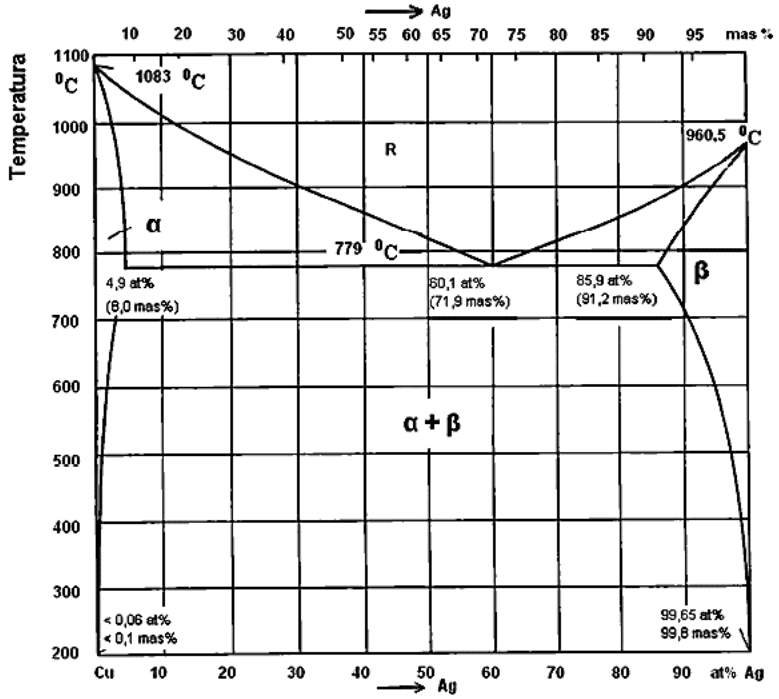

Figure 2-8. Phase diagram of Ag-Cu alloy [51].

Copper is sometimes used in aerated neutral environments as a strategic metal in industry. Oxygen reduction (Equation 2-5) is the most common reaction in that setting, and oxidation of copper is the initial anodic reaction. However, in case the solution pH drops resulting in an aerated acidic condition, the cathodic reaction would be oxygen reduction in acidic environment (Equation 2-4).

$$Cu \rightarrow Cu^{+} + e^{-} \qquad (2\text{-}9)$$

$$Cu^{+} \rightarrow Cu^{2+} + e^{-} \qquad (2\text{-}10)$$

Nearly neutral environments may also contain some aggressive ions such as chloride ions. Therefore, reaction between Cl^{-} and Cu^{+} can take place leading to the formation of a soluble and unstable film $(CuCl)$ on the surface. Poor cohesion and heterogeneity of this film on the metal surface can cause pitting corrosion [30].

$$Cu^{+} + Cl^{-} \rightarrow CuCl \qquad (2\text{-}11)$$

The formed layer again reacts with chloride ion and transforms to cuprous chloride $(CuCl_2^-)$ which also has a poor cohesion with the metal surface, and can later be oxidized to cupric ion (Cu^{2+}) [52].

$$CuCl + Cl^{-} \rightarrow CuCl_2^- \qquad (2\text{-}12)$$

$$CuCl_2^- \rightarrow Cu^{2+} + 2Cl^- + e^- \qquad (2\text{-}13)$$

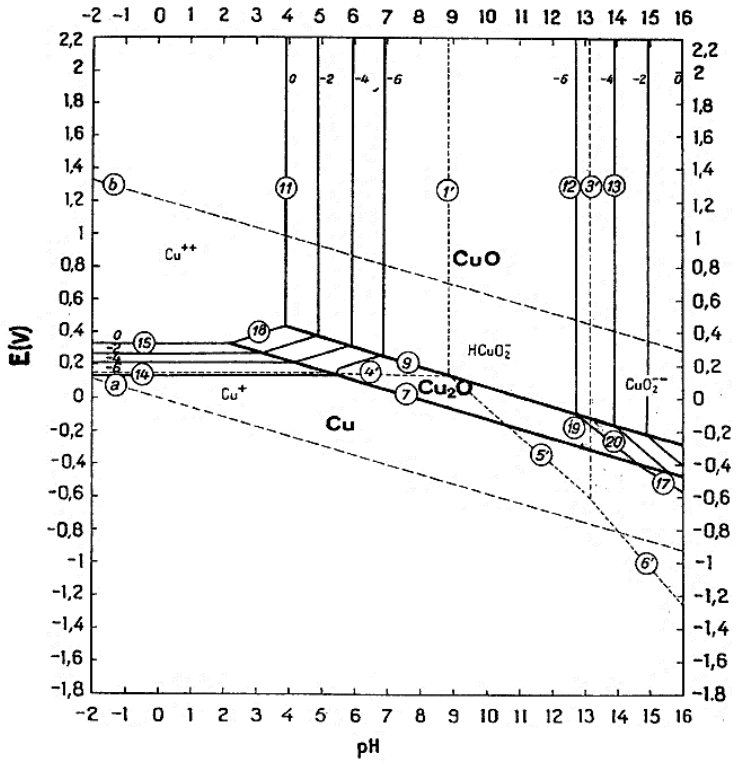

Figure 2-9. E-pH diagrams for the Cu-H_2O system [51].

With respect to silver, it is more stable and noble than copper in nearly neutral environments, but it tarnishes through exposure to ozone (O_3) and other environments such as hydrogen sulfide, air containing sulfur oxide, strong halogenated mineral acids (e.g., *HCl*), nitric acid, and sulfuric acid [53]. In an aerated condition, the neutral medium (electrolyte) can adsorb the atmospheric gases that ultimately leads to the dissolution of the metal. The cathodic reaction

could be reduction of oxygen (Equation 2-5), and the anodic reaction would be the oxidation of silver [54]:

$$Ag \rightarrow Ag^{+} + e^{-} \tag{2-14}$$

Depending on the pH level, various forms of silver oxide can form [16,55] as represented in the Pourbaix diagram of Ag-H_2O system (Figure 2-10).

$$Ag^{+} + O_3 \rightarrow AgO + O_2 \tag{2-15}$$

$$Ag^{+} + AgO + O_2 \rightarrow Ag_2O_3 \tag{2-16}$$

$$Ag_2O_3 + 2H_2O + 4e^{-} \rightarrow Ag_2O + 4OH^{-} \tag{2-17}$$

$$2Ag + H_2O \rightarrow Ag_2O + 2H^{+} + 2e^{-} \tag{2-18}$$

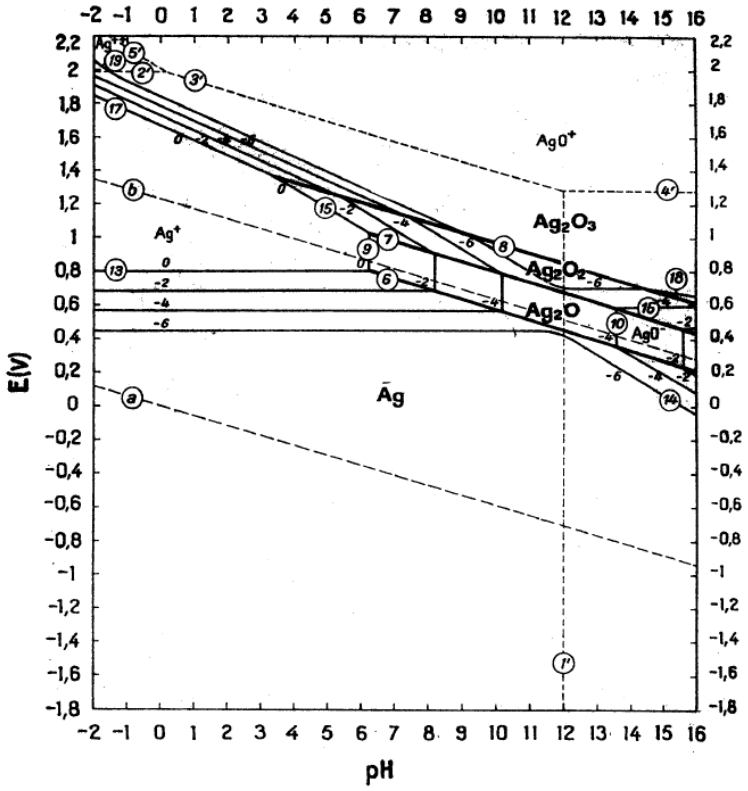

Figure 2-10. E-pH diagrams for the Ag-H_2O system [51].

Much the same as the case with copper ions, silver ions can react with the plausible chloride ions present in the medium. Cl^- ions can enter the environment from airborne particles in the case of neutral environment, if not from an acid (e.g., *HCl*), and form a solid product, $AgCl$, that can later transform to $AgCl_2^-$ leading to pitting corrosion [54].

$$Ag^+ + Cl^- \rightarrow AgCl_{(s)} \quad (2\text{-}19)$$

$$AgCl_{(s)} + Cl^- \rightarrow AgCl_2^- \quad (2\text{-}20)$$

Therefore, for Cu-Ag alloys containing a mixture of α-Cu and β-Ag phases, corrosion inhibition practices should consider the activity of both phases involved.

2. 7. Inhibition of Cu-Ag Alloy in Nearly Neutral Medium

As noted above, Cu-Ag alloys possess two rich phases of α-Cu and β-Ag. Thus, for the corrosion inhibition of these alloys, inhibition of each phase must be considered individually and in conjunction. Several inhibitors have been used so far for corrosion protection of Cu. As illustrated in Table 2-4, azole compounds, especially BTA and its derivatives, are the main type of inhibitors used for the inhibition of Cu in nearly neutral environments. Sometimes, additives such as surfactants have been also used for a higher protection. Besides, BTA is being used in cooling systems in supercomputing and data center facilities with Cu-Ag alloy structures which are still suffering from corrosion.

However, less study has been carried out on the inhibition of Ag, probably due to its relatively noble properties. Even in the case of Ag inhibition with BTA, sometimes the findings are in contrast with each other. As per Table 2-5 that summarizes the research results on the silver corrosion inhibition in different environments, thiadiazole (TD) compounds can be good candidates for the inhibition of Ag. Some of TD derivatives have shown more than 90% inhibition efficiency in corrosive medium.

Therefore, the following sections focus on the previous studies on the interaction of Cu and Ag with BTA and some of its derivatives, effect of surfactants, and effect of flow rate on the inhibition of BTA. The latter of which was included to study the background on the effect of

agitation on inhibition with BTA. This is because the coolant is in circulation in the actual cooling system. But, first let's concisely explore TD's properties and briefly review the findings obtained on corrosion inhibition with TD.

Meanwhile, Figure 2-11 shows the molecular structure of amines used as corrosion inhibitors for silver by Wanees et al. [48]. They found that inhibition efficiency also increases up to ~67% with n-Butylamine as it possesses the longest alkyl chain providing a higher surface coverage on the metal surface. This is an evidence for the effect of alkyl chain length on the inhibition efficiency of the inhibitor.

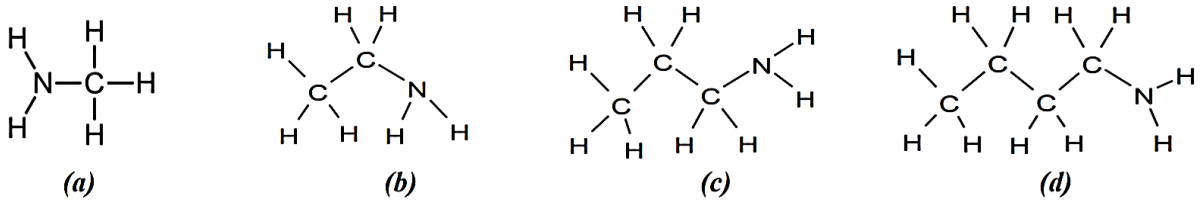

Figure 2-11. Molecular structure of (a) Methylamine, (b) Ethylamine, (c) n-Propylamine, (d) n-Butylamine [56].

The high inhibition efficiency of TD ($C_2H_2N_2S$) on Ag can stem from the presence of two heteroatoms of N and S in its structure willing to participate in bonding with the metal surface. Hence, increasing the odds of adsorption. In general, thiadiazole and benzotriazole compounds are examples of the category of *"five-membered rings with two heteroatoms and fused carbocyclic derivative(s)"* heterocyclic compounds in organic chemistry [57]. They both possess features of a good inhibitor such as the presence of several heteroatoms to bond with the vacant orbitals of the metal, and complexity of the structure capable to make the molecule size big enough to properly block the electrochemical reactions, especially when fused with carbocyclic derivatives. As discussed earlier, electron donating ability and affinity of N and S are higher than O. Thus, they can be better candidates for a higher inhibition efficiency. In addition, among different thiadiazole isomers, 1,3,4-thiadiazole probably provides a better inhibition efficiency as its heteroatoms are located on the both side of the azole ring enhancing the odds of adsorption regardless of the direction of the molecule in the environment. Figure 2-12 demonstrates the structure of four possible thiadiazole isomers.

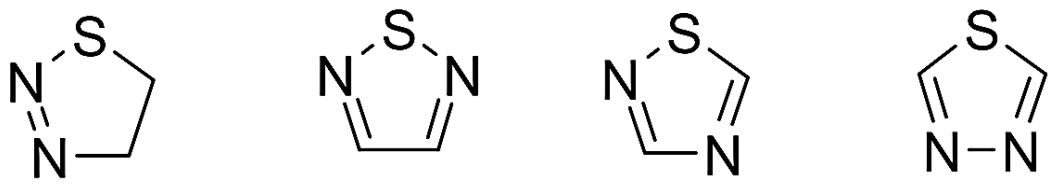

Figure 2-12. Thiadiazole isomers; from left to right: (1,2,3- ; 1,2,5- ; 1,2,4- ; and 1,3,4-thiadiazole) [58].

As shown in Table 2-5, much the same as for the amines, increasing the TD's chain length has increased the inhibition efficiency on Ag. This can be attributed to the higher metal surface coverage with the inhibitors possessing longer chains as well as the possibility of a better/stronger inhibitor molecular lateral interaction between the adsorbed molecules. In this case, a much dense and a more homogenous protective film can form.

2. 8. Benzotriazole

BTA is a well-known organic inhibitor compound used for more than 50 years for copper [3,12] in different corrosive media: neutral [59], acidic [37,60,61], alkaline [45,50], reducing and oxidizing containing various ions [62], chlorides [12], and sulfates [63]. BTA has a chemical formula ($C_6H_5N_3$) [4] possessing benzene and triazole rings [2,6] as illustrated in Figure 2-13.

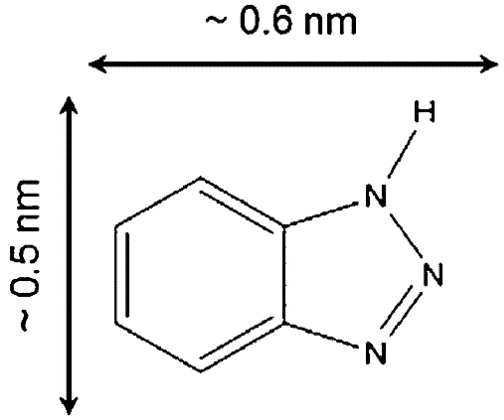

Figure 2-13. Chemical structure of BTA with approximate molecular dimensions [3].

Table 2-4. Summarized research results on the copper corrosion inhibition in non-acidic aqueous solutions.

Inhibitor group	Inhibitor	Symbol(s)	Concentration	Solution	Condition	Adsorption isotherm	Efficiency (%)	Ref.
Azole	Tolytriazole	TTA	1 ppm TTA	Cooling water	pH=8.5	Langmuir	61.9	[64]
			1 ppm TTA + 0.5 ppm (cholorine)				39.4	
	Benzotriazole	BTA	1 mM	Ethanol	Temporarily immersed.		NA (Effective)	[35]
	Benzotriazole	BTA	100 ppm	Distilled water	Immersed for a month		NA (Effective)	[62]
	Benzotriazole	BTA	3 mg/l	Simulated cooling water	Circulated at 0.85 m/s for 200 h		NA (Effective)	[65]
	Tolytriazole	TTA	3 mg/l	Simulated cooling water	Circulated at 0.85 m/s for 200 h		NA (Effective)	
	Benzotriazole. 1-(2-pyrrole carbonyl) benzotriazole + SDS + TBTA	TBTA+SDS+Mo PBTA+SDS+Mo		Groundwater	303 K		94.5 96.8	[66]
	Triazo phosphonates	3-Cinnamyledene amino 1,2,4-triazole phosphonate (CATP)	15 ppm	Lake water	Added inhibitor after 24 h		82.5	[67]
	Tolytriazole	TTA	10 ppm	DI water			95.48	[68]
	Benzotriazole	BTA	10 ppm	DI water	After 24 h, 60˚C	Langmuir	84.48	[69]
	Tolytriazole	TTA					95.48	
	1-(2-pyrrole carbonyl)-benzotrizole (PCBT)+ Triton X-100 (TX-100)	0.095 + 0.16 mM		Groundwater	28˚C		91.34	[70]
Organic	Carboxylates	Monocarboxylates $\left(C_nH_{2n+1}COO^-\right)n=10$	5 mM	near neutral aqueous	Aerated, mildly saline		99.00	[71]
		α,ω-Dicarboxylate analog $(-OOC[CH_2]_nCOO^-)n=11$					98.00	
Natural inhibitor (green inhibitor)	Nigella sativa	(NS)	30 ppm	Aerated make-up water	pH=7.5	Langmuir	90.30	[72]
	Natural honey	(NH)	900 ppm				98.00	
	Sodium carboxymethyl cellulose	(Na-CMC)	5 g/l	Cooling water	20˚C	Langmuir	77.35	[73]
	Emblica officinalis	(AMLA)	1000 ppm	Natural seawater	30˚C		79.99	[74]
	Vitis vinifera		1000 ppm	Natural seawater	After 24 h, 25˚C	Langmuir	76.08	[75]

Table 2-5. Summarized research results on the silver corrosion inhibition.

Inhibitor group	Inhibitor	Symbol(s)	Concentration	Solution	Condition	Adsorption isotherm	Efficiency (%)	Ref.
Amine	Methylamine	CH_3NH_2	0.01 M	0.01 M HNO_3	13˚C	Temkin	43	[48]
	Ethylamine	$C_2H_5NH_2$					51	
	n-Propylamine	C_3H_9N					58	
	n-Butylamine	$C_4H_{11}N$					67	
Azole	Benzotriazole	BTA	0.01 mol/dm^3	0.1 mol/dm^3 NaCl	25˚C		NA	[9]
	Benzotriazole	BTA	1 M	Ethanol			NA	[76]
	2,5-dimercapto-1,3,4-thiadiazole	DMTD	40 mg/L	50 mg/L H_2S	After 96 h at 50˚C	Temkin	76.37	[41]
	5-methyl-2-mercapto-1,3,4-thiadiazole	MMTD	40 mg/L	50 mg/L H_2S	After 96 h at 50˚C	Temkin	74.63	
	2,5-dithiododecyl-1,3,4-thiadiazole	DDTD	40 mg/L	50 mg/L H_2S	After 96 h at 50˚C	Langmuir	91.76	
	2,5-diphenly-1,3,4-thiadiazole	DPTD	90 mg/L	50 mg/L S-ethanol	After 30 min at room T	Langmuir	81.3	[77]
	2,5-di(2-hydroxyphenly)-1,3,4-thiadiazole	2-DHPTD	90 mg/L	50 mg/L S-ethanol	After 30 min at room T	Langmuir	97.8	
	2,5-di(3-hydroxyphenly)-1,3,4-thiadiazole	3-DHPTD	90 mg/L	50 mg/L S-ethanol	After 30 min at room T	Langmuir	97.9	
	2,5-di(4-hydroxyphenly)-1,3,4-thiadiazole	4-DHPTD	90 mg/L	50 mg/L S-ethanol	After 30 min at room T	Langmuir	98.1	

2. 8. 1. Inhibition of Cu with BTA and Its Derivatives

BTA acts as a mixed type inhibitor with more impact on the anodic reaction [44,59,78]. Its inhibitory effect increases with increased concentration on Cu-based alloys [44,69]. It is well-accepted that the inhibition is due to the formation of predominantly Cu(I)-BTA along with Cu(II)-BTA organometallic complexes involving Cu-N bonds [1,3,5]. However, the exact structure of the complex, its molecular adsorption, orientation [3] and whether the complex film forms on the metal surface or it precipitates on the surface after formation in the electrolyte solution is up for debate [63,79]. Previous research has shown that the inhibitive film either forms perpendicular or

tilted and/or parallel relative to the Cu surface [2,63,80]. Different adsorption types of BTA on Cu and their corresponding properties are presented in Figure 2-14.

The BTA adsorption mechanism in neutral environment involves the adsorption of the inhibitor's molecules on the copper surface (Cu:$BTAH_{(ads)}$) along with the formation of a protective mono- or multilayer film known as polymeric [Cu(I)BTA] complex by anodic polarization or by having oxidants as follows [4,30,80]:

$$Cu_{(s)} + BTAH_{(aq)} = Cu:BTAH_{(ads)} + H^{+}_{(aq)} \quad (2\text{-}21)$$

$$Cu:BTAH_{(ads)} = Cu(I)BTA_{(S)} + H^{+}_{(aq)} + e^{-} \quad (2\text{-}22)$$

Dipoles of the adsorbed BTA molecules provide the lateral interaction to form the protective film. Increasing the inhibitor concentration shifts the above reactions to the right and increases the surface coverage; consequently, it provides more protection [80].

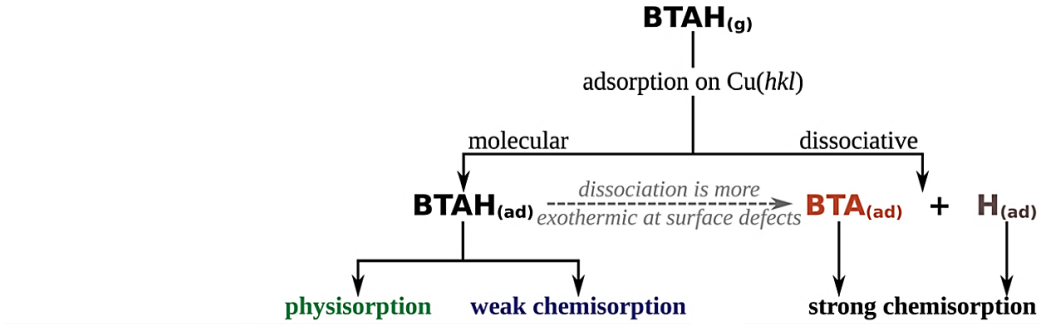

molecule-surface bond strength	weak	weak	strong	strong
sensitiveness to surface geometry	weak	strong	strong	weak
sensitiveness to surface coverage	weak	strong	weak	weak
intermolecular dipole-dipole interactions	weakly attractive	strongly repulsive	weakly repulsive	weak
adsorption induced work function change	weak reduction	strong reduction	weak reduction	insignificant

Figure 2-14. Features of molecular and dissociative adsorption of benzotriazole on the copper surface [78].

Gerengi et al. have reported that BTA shifts corrosion potentials towards cathodic values in artificial seawater for copper-manganese-aluminum (CMA) alloy [44]. Figure 2-15 shows the

polarization curves of this alloy in various BTA concentrations. In addition, both Tafel slopes (β_a and β_c) have changed indicating that BTA is a mixed type inhibitor.

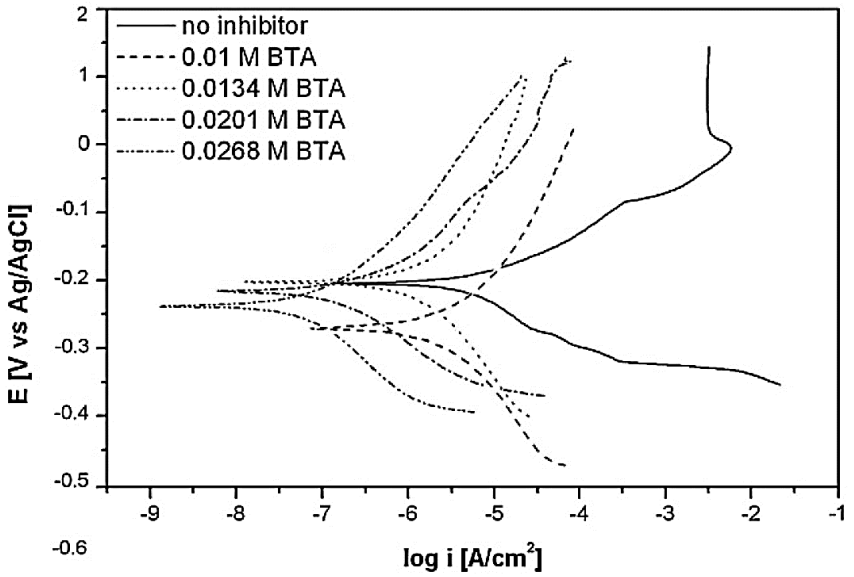

Figure 2-15. Potentiodynamic polarization of CMA alloy in artificial seawater in the absence and presence of different BTA concentrations [44].

The variation of conductivity for 100 ppm BTA-treated and non-treated distilled water in closed-circuit copper pipes was recorded by Wall and Davies [62] as displayed in Figure 2-16. The effectiveness of BTA was demonstrated by a low rate of conductivity increase over time. It was suggested there should be coolant flushing periods to avoid further increase in the conductivity stemming from the increasing rate of Cu^{2+} concentration over time and to maintain the BTA concentration by periodic inhibitor additions.

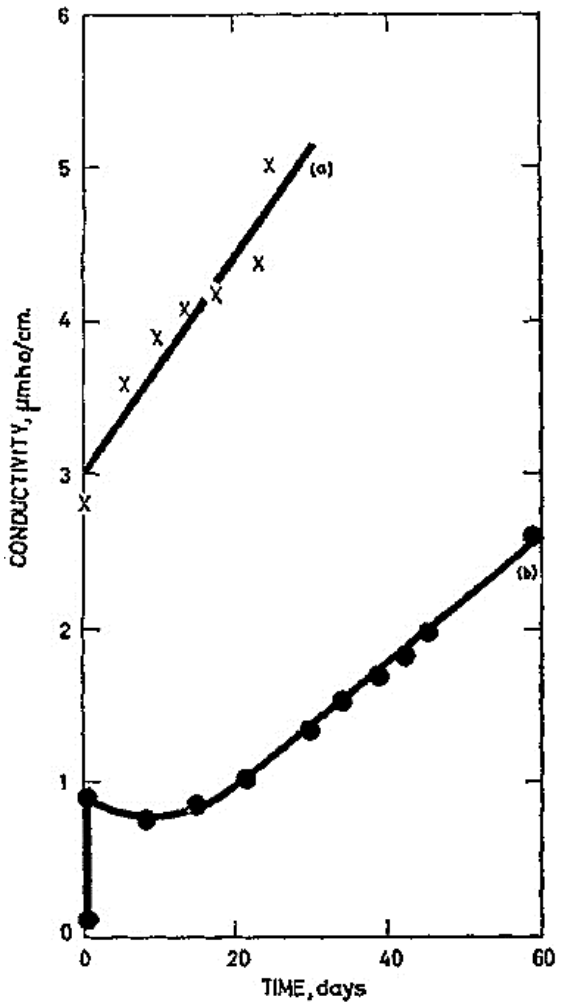

Figure 2-16. Variations in conductivity of distilled water in copper pipes; (a) without BTA, (b) with 100 ppm BTA [62].

Quantum chemical calculations have been also used to correlate inhibitor efficiencies with molecular properties such as orbital energy (the highest occupied molecular orbital energy, E_{HOMO}, and the lowest unoccupied molecular orbital energy, E_{LUMO}), dipole moment, heat of formation, charge density and ionization potential [81]. Employing these properties, density functional theory (DFT) calculations have illustrated that BTA can physiosorb or weakly chemisorb on the copper surface [3]. BTA also lowers the work function of copper; therefore, diminishing any reaction that donates electron; this is also consistent with the fact that BTA predominantly affects the anodic reactions although it is a mixed type inhibitor [78]. Johnson [82] used weight-loss and calorimetric methods to study the corrosion of copper and reported 0.5 mg/cm^2 weight change and 2.4 mg/cm^2 copper in the solution, respectively in DI water after 34 days. Also, using calorimetric analysis for

the corrosion of silver in the same environment and duration, no traces of soluble corrosion products for silver was found. Figure 2-17 shows the result of weight-loss method test for copper.

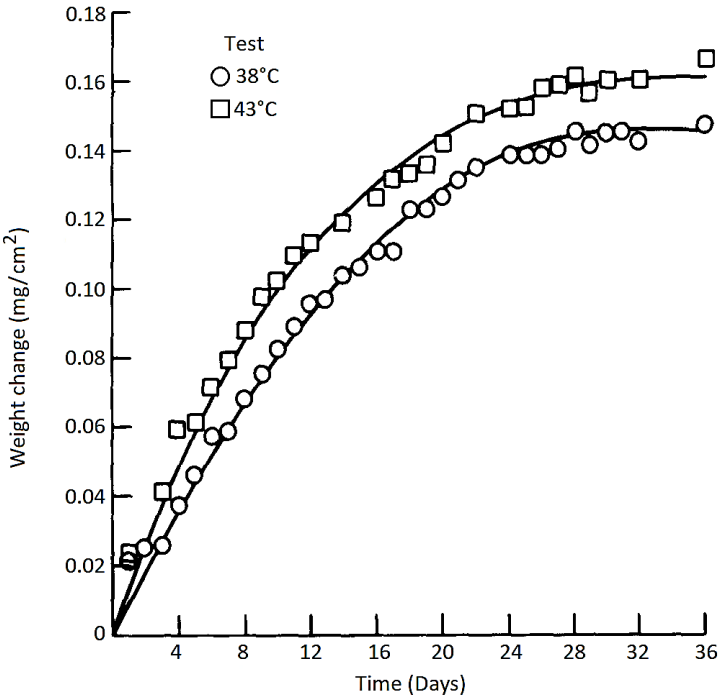

Figure 2-17. Copper weight per area released to DI water [82].

Szociński et al. [35] introduced a new AFM-based approach in a contact mode to investigate the copper surface coverage with BTA in electrolyte-less condition. This technique provided local DC maps along with the topographical images, and local electrical impedance spectra. The impedances utilized the DC bias voltage or AC perturbation signal between the conductive AFM tip and the metal. Polished copper samples were immersed in 1 mM solution of BTA and ethanol for 15 min. Subsequently, the samples were placed for 20 days in a container with saturated solution of potassium sulfate to provide the elevated humidity of 97%. Figure 2-18 displays the polished copper surface topography covered with BTA prior to and after exposure to elevated humidity. Prior to exposure, Figure 2-18(a), the surface is relatively smooth. Nevertheless, after 10 days of exposure, Figure 2-18(b), the surface is more corrugated, and roughness is higher reaching 2 µm. After 20 days of exposure, humidity has resulted in serious destruction of the inhibitor film, Figure 2-18(c). Figure 2-19 shows the AFM DC results for these samples. Before exposure, the inhibitor has a complete coverage over the copper surface acting as

an insulator for the DC current flow between the AFM tip and copper substrate. After 10 days of exposure to the elevated humidity, the investigated surface is no longer electrically uniform. As demonstrated in Figure 2-19(b), there are some spots depleted from the BTA resulting in DC current flowing reaching 40 pA in some cases as marked with C corresponding to the conductive region. Those areas marked by N, corresponds to a non-conductive region due to the presence of the protective BTA layer. Figure 2-20 demonstrates the local impedance spectra of N and C regions. In the non-conductive part, the impedance is of the GΩ order while it is of a few MΩ order for the conductive part.

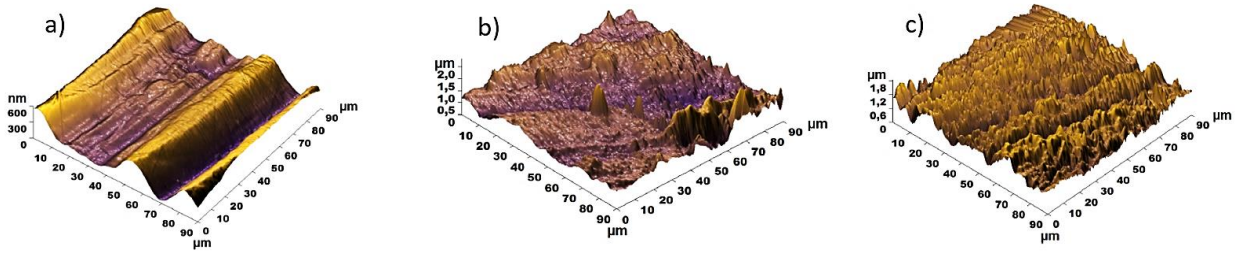

Figure 2-18. AFM topography of copper surface covered with BTA collected (a) prior to elevated humidity exposure;(b) after 10 days of elevated humidity exposure; (c) after 20 days of elevated humidity exposure [35].

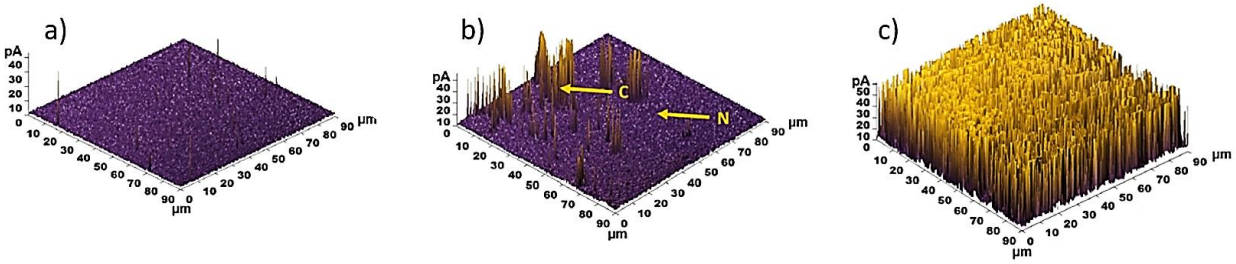

Figure 2-19. AFM DC map of copper surface covered with BTA collected (a) prior to elevated humidity exposure; (b) after 10 days of elevated humidity exposure; (c) after 20 days of elevated humidity exposure [35].

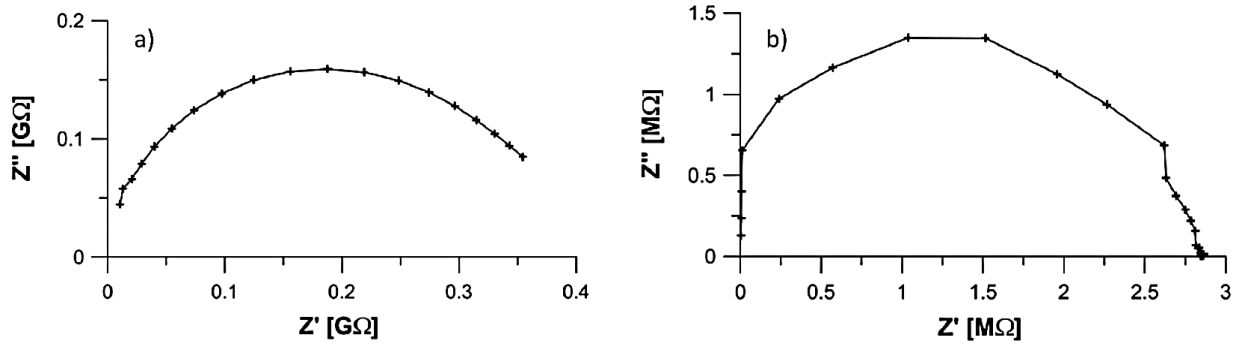

Figure 2-20. Local impedance spectrum of copper surface covered with BTA recorded via AFM set-up after 10 days of elevated humidity exposure. The spectrum corresponds to the (a) non-conductive region indicated as N and (b) conductive region indicated as C, in the DC current map in Figure 2-19(b) [35].

In view of employing the simple parallel RC circuit to interpret the impedance spectrum, resistance dropped, and capacitance increased upon transition from N to C region. This confirms the deteriorated protective effect of the inhibitor and reduction of the BTA film thickness. Therefore, inhibitor layer refurbishment was proposed to provide an effective protection, especially when the object is not in a medium with continuous supply of the inhibitor.

Table 2-6. Electrical parameters achieved via modeling of the local impedance spectra collected on non-conductive region and conductive region in Figure 2-19(b) of the investigated surface [35].

Location on sample surface	Resistance (MΩ)	Capacitance (fF)
Non-conductive region	341.2	3.9
Conductive region	2.8	8432

Yu et al. [69] investigated the effect of BTA and its derivative, tolytriazole (TTA), on the corrosion inhibition of copper in de-aerated DI water using purified nitrogen. As demonstrated in Figure 2-21, TTA has an extra methyl group in its chemical structure compared to BTA. They found that the inhibition efficiency is concentration-, temperature- and time-dependent. The pH was 6.4 in their experiments and 1 mM sodium sulfate (Na_2SO_4) was added to increase the ionic strength and to maintain the conductivity of the solution (1.25 µs/cm).

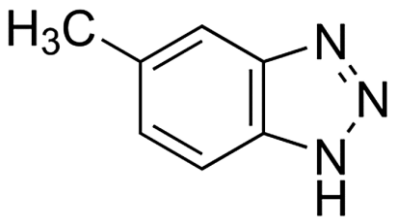

Figure 2-21. Chemical structure of TTA.

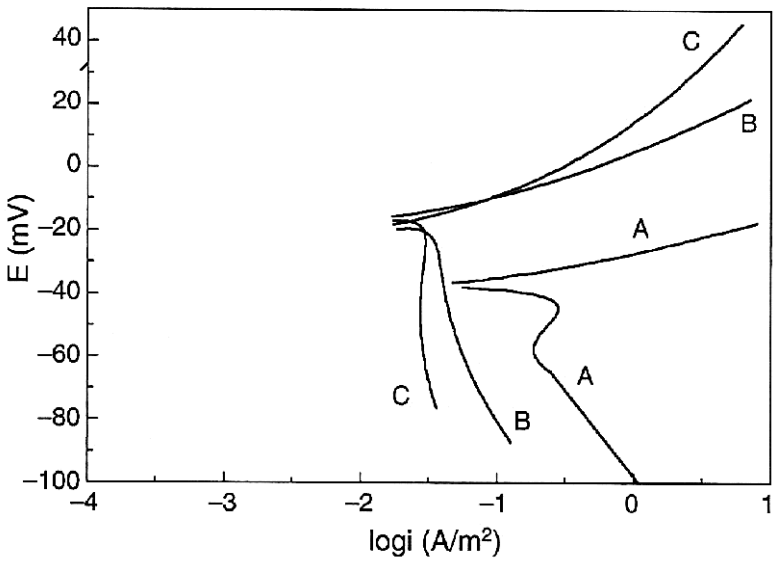

Figure 2-22. Potentiodynamic polarization curves for copper after 1 hour of exposure to (A) DI water + 1 mM Na_2SO_4, (B) 6 ppm BTA, and (C) 6 ppm TTA [69].

According to Figure 2-22, there is a small increase in the Cu corrosion potential due to the adsorption of the inhibitor molecules on the metal surface. This is a phenomenon known as blocking effect in which the surface-active centers get obstructed preventing the oxidation of the metal. Both TTA and BTA have reduced the Cu corrosion current density by virtually an order of magnitude. This proves the constructive role of these inhibitors on the corrosion protection of Cu. Table 2-7 shows the variation of inhibition efficiency of these two inhibitors versus their concentration. TTA has demonstrated a better efficiency over the same concentrations. Corrosion inhibition efficiency (IE), η, can be calculated by the following formula:

$$\eta = \frac{i_c - i_{c(inh)}}{i_c} \times 100 \qquad (2\text{-}23)$$

where i_c and $i_{c(inh)}$ are the corrosion current densities achieved from the potentiodynamic polarization curves in the absence and presence of inhibitor, respectively [44].

The copper-azole film has hydrophobic characteristic limiting the transport of hydrated ions to the metal surface. Also, the higher efficiency of TTA over BTA stems from its extra methyl group making it more hydrophobic [65].

Table 2-7. Corrosion efficiency of TTA and BTA on copper after 1 day of immersion in 250 mL DI water at 60°C [69].

Inhibitor Concentration (ppm)		Cu^{2+} in Solution (ppb)		η (%)	
TTA	BTA	TTA	BTA	TTA	BTA
0	0	248.18	248.18	0	0
0.5	0.5	150.97	176.31	39.17	28.96
1.0	1.0	98.49	142.74	60.31	42.48
1.5	1.5	84.79	117.02	65.84	52.85
2.0	2.0	76.63	95.85	69.14	61.38
3.0	3.0	50.78	72.10	77.93	70.95
4.0	4.0	52.86	65.64	78.70	73.55
6.0	6.0	29.29	52.86	88.19	78.70
8.0	8.0	22.95	42.81	90.75	82.75
10.0	10.0	11.23	37.63	95.48	84.48

Figure 2-23 shows the effect of temperature on the corrosion efficiency of BTA and TTA on Cu. As the adsorption process were exothermic, rising the temperature has led to lowering the inhibition efficiencies. In addition, temperature has lower impact on the adsorption of TTA in comparison with BTA. This can be attributed to the difference in the charge density of these inhibitors or the plausible stronger bonding between TTA and the Cu surface.

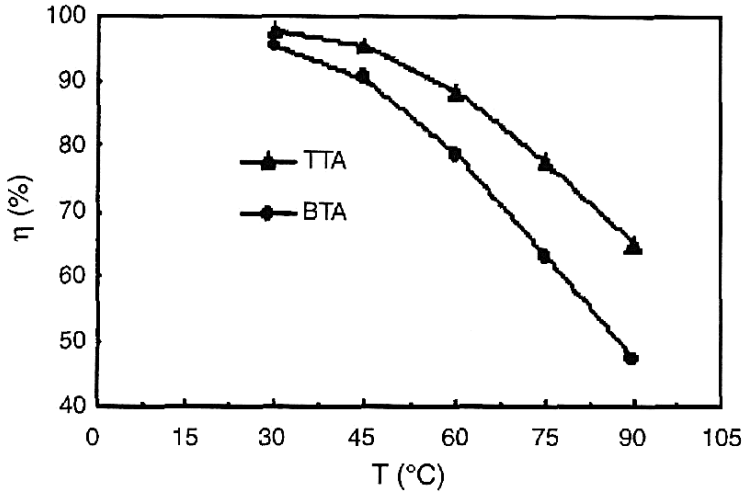

Figure 2-23. Corrosion efficiency of BTA and TTA versus temperature for copper in DI water [69].

The effect of exposure time, to the corrosive medium (DI water in this case), on the corrosion efficiency has been also studied for this system. As demonstrated in Figure 2-24, inhibition efficiency decreases after 3 days with BTA. However, copper concentration in the electrolyte has not been changed that much over the passage of time for TTA resulting in more persistence in corrosion efficiency. As noted above, presence of the extra methyl group in TTA has increased the hydrophobicity of the protective film leading to a higher corrosion efficiency [69].

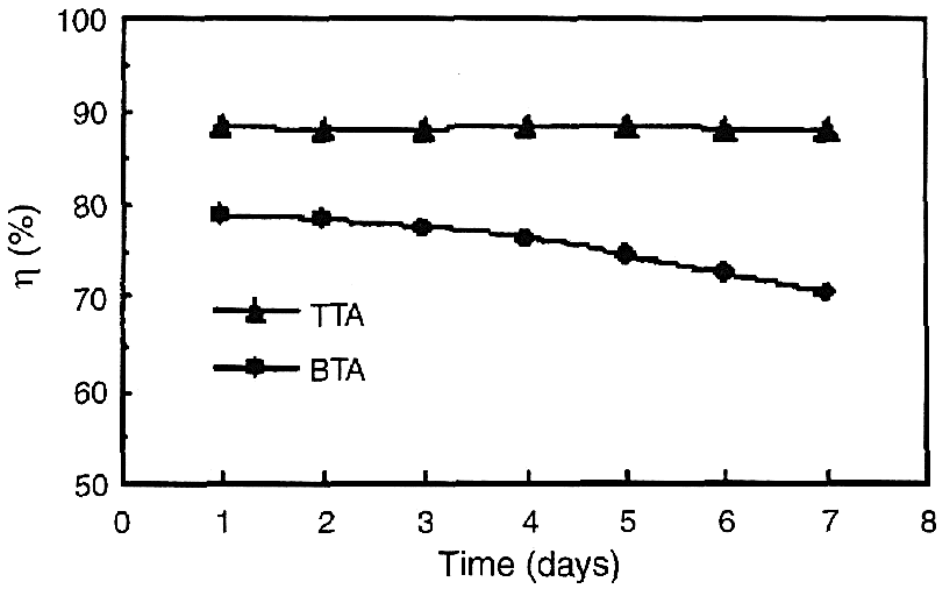

Figure 2-24. Corrosion efficiency of BTA and TTA versus exposure time for copper in DI water [69].

By using electrochemical techniques, Brunoro et al. [83] illustrated that the inhibition efficiency of BTA derivatives for copper alloys in the presence of alloying elements (Zn, Pb and Sn) possessing multiphase microstructures, is less than that of the pure copper since a weaker metal- triazole bond develops. 5-octyl-1,2,3-BTA (C8) was found with the highest inhibition efficiency. This is because C8 possesses a long aliphatic (non-aromatic) chain resulting in a much more hydrophobic protective film on the metal surface. Chemical composition of the bronzes used in this study is presented in Table 2-8. Figure 2-25 and 2-26 illustrate the Bode plots and variation of the polarization resistance of the C8 treated bronzes over time, respectively.

Table 2-8. Chemical composition (wt%) of the bronzes used [83].

Bronzes	Cu%	Sn%	Pb%	Zn%	Fe%	Ni%	Bi%
B6	Rest	6	–	–	–	–	–
G6	Rest	5.4	0.1	0.1	0.3	0.1	Traces
G12	Rest	10.6	1.9	1.1	0.1	0.4	Traces
G85	Rest	4.7	5.2	5.1	2.1	1.0	Traces

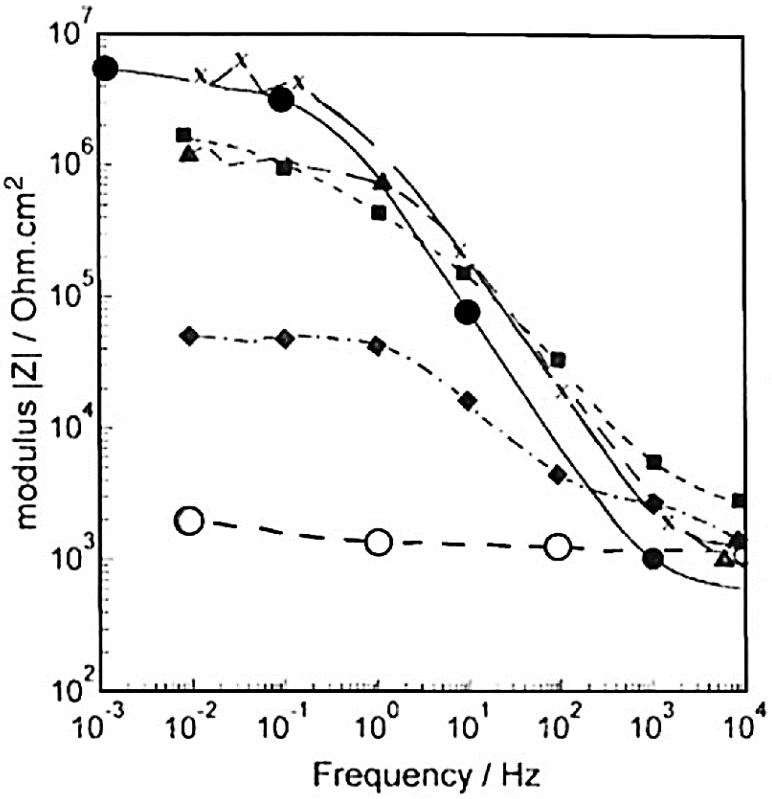

Figure 2-25. Bode plots measured after 1-hour immersion in synthetic acid rain for (O) non-treated Cu; C8 treated: (●) Cu; (×) B6; (▲) G6; (■) G12; (◆) G85 [83].

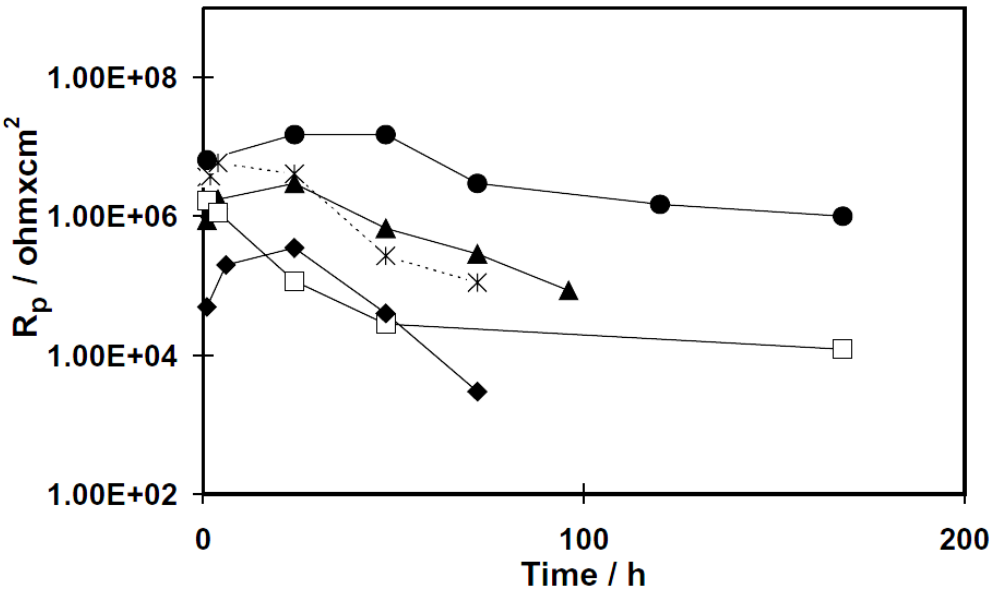

Figure 2-26. Polarization resistance over time of immersion in simulated acid rain for C8 treated samples of: (●) copper; (×) B6; (▲) G6; (□) G12; (◆) G85 [83].

2. 8. 2. Interaction of Ag with BTA

Few and contradictory studies have been conducted so far investigating the effect of BTA on the silver surface. Based on surface-enhanced Raman scattering of BTA in aqueous silver ions solution, Thomas et al. found that Ag(I)-BTA film is being formed and nitrogen atoms are involved in the interaction with surface [6]. DFT calculations by Naumov et al. showed that BTA binds to silver nanoparticles through N_1 and N_3 atoms of the triazole ring and the formed Ag(I)-BTA is energetically favorable [7]. However, adsorption of BTA on the surface of Cu-2 wt% Ag alloy was studied through X-ray photoelectron spectroscopy (XPS) and scanning electrochemical microscopy by Mansikkamäki et al. in Na_2SO_4 electrolyte and no evidence of Ag(I)-BTA film formation was found [5].

Generally, the inhibitor film acts as an insulator between the metal surface and tip of the scanning electrochemical microscope (SECM). In the absence of the film, when the SECM tip approaches the conductive surface, the current increases as displayed in Figure 2-27(a). On the other hand, having the insulating inhibitor on the surface of the metal results in current decreasing due to the blocking effect of the protective film as illustrated in Figure 2-27(b).

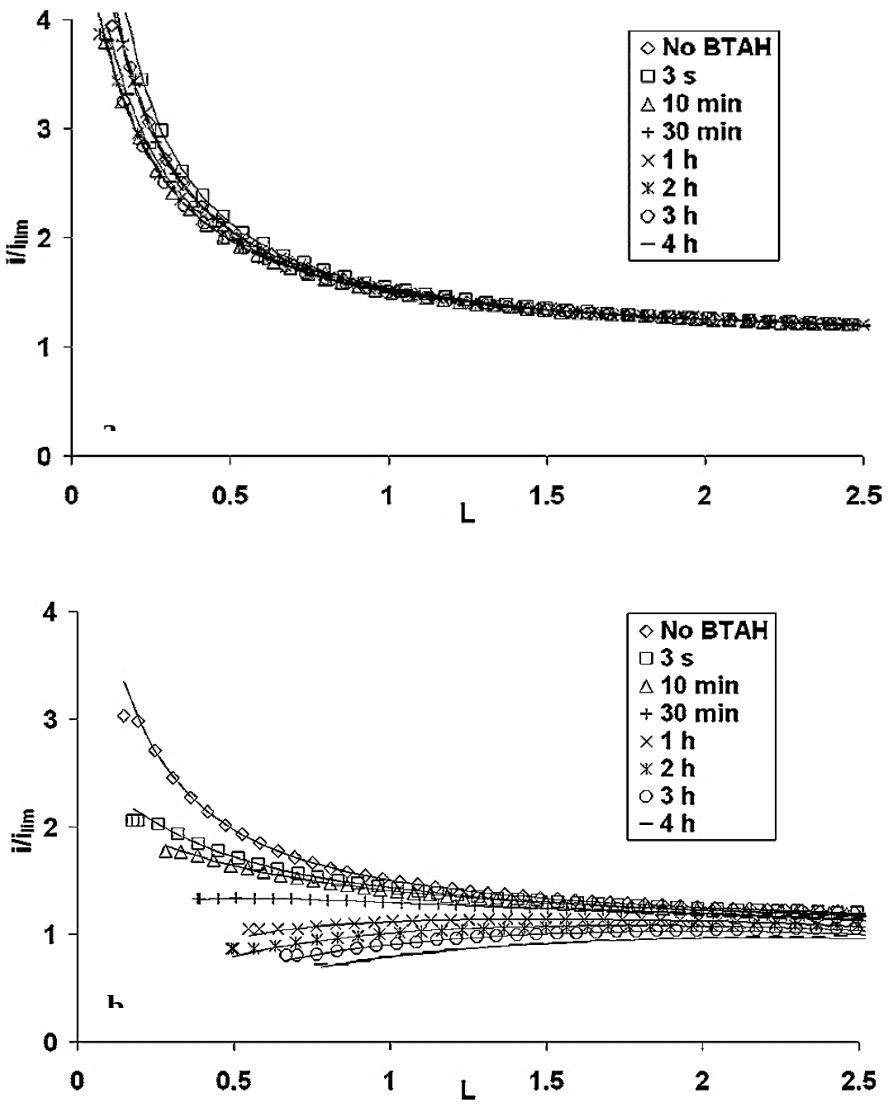

Figure 2-27. Approach SECM curves of (a) Cu-2 wt% Ag, (b) oxygen-free dehydrated Cu (OF-HC) measured at the substrate potential of OCP. i/i_{lim} is the dimensionless tip current, and L = d/a is the dimensionless distance between the sample and the tip [5].

In SECM, parameter *d* is the distance between the tip and the metal surface; *a* is the radius of the tip; and $i_{\lim}$ is the limiting current when the tip is far away from the surface. With respect to the XPS studies, no change in the silver (Ag 3d) spectra was observed after exposure to BTA solution, indicating no Ag-BTA interaction as shown in Figure 2-28 [5]. However, formation of the Cu-BTA organometallic complex was confirmed through the component of the Cu $2P_{3/2}$ peak with the binding energy at 934.8 eV corresponding to the inhibitive film in Figure 2-29 [5,84].

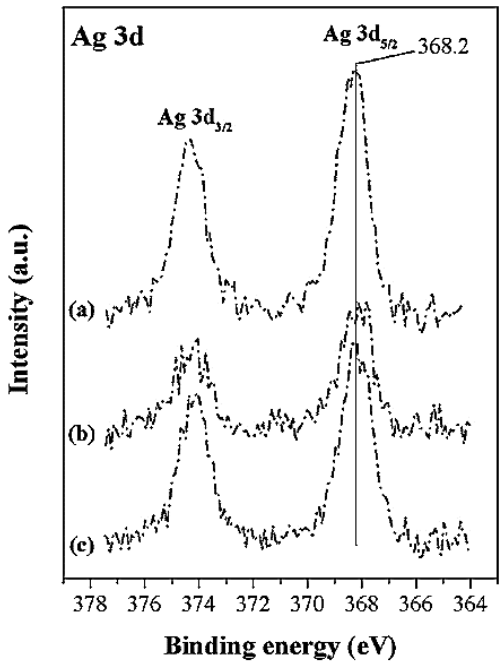

Figure 2-28. The Ag 3d XPS spectra of the Cu-2 wt% Ag sample. The spectrum of air-exposed sample (a) is uppermost, in the middle the one of BTA-treated sample (b), and lowermost is the spectrum of BTA-treated, sputtered sample (c) [5].

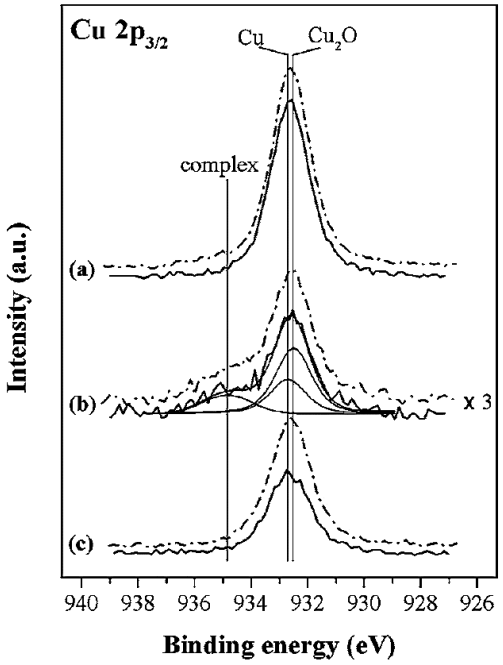

Figure 2-29. The XPS spectra of the Cu $2P_{3/2}$. Solid lines obtained on the OF-HC Cu and the dashed lines indicate the Cu-2wt%Ag sample. uppermost spectra (a) are for the air-exposed samples, in the middle (b) the BTA-treated samples, and lowermost (c) are the spectra of BTA-treated sputtered samples. Intensity of the spectrum pair b) is multiplied by 3 for better comparability. Peak-fittings has been carried out as follows: metallic Cu (932.7 eV), Cu_2O (932.5 eV), and Cu-BTA complex (934.8 eV) [5].

The polarization resistant and the chemical state of BTA on Cu, Ag, Au, Cr, Ni, Fe and Zn was studied by Notoya et al. via time-of-flight secondary ion mass spectroscopy in 0.1 M NaCl [9]. They observed that the corrosion inhibition is related to the degree of polymerization, following the order Cu>>Ag>>Zn>Ni, Fe representing the BTA molecular chain length on the metal surfaces. According to their results, less polymerized metal-BTA species were observed on Ag and Au compared to Cu. Figure 2-30 shows the ratio of polarization resistance of these elements in the absence and presence of BTA after 20 min immersion at room temperature.

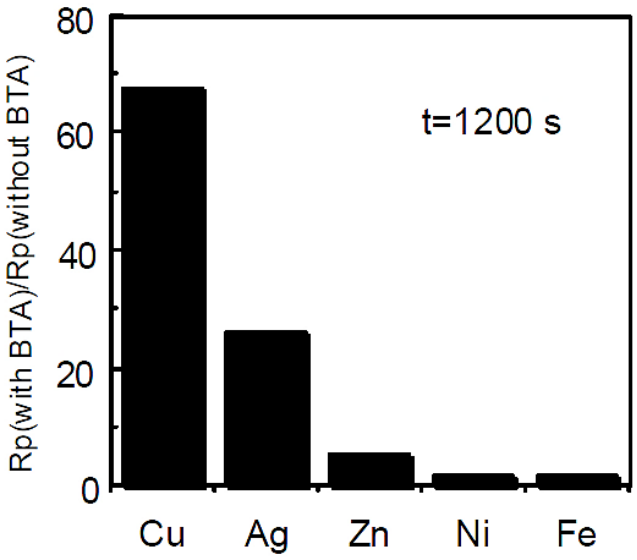

Figure 2-30. Ratio of polarization resistance in the presence over the absence of 0.01 M BTA in 0.1 M NaCl solution for some elements after 20 min of immersion at 298 K [9].

Since Cu showed the highest efficiency, the same polarization measurements were carried out to study the effect of pH level on the inhibition efficiency of BTA on Cu as presented in Figure 2-31. Results clearly show that BTA is essentially a good inhibitor for Cu in nearly neutral media rather than highly alkaline or acidic environments.

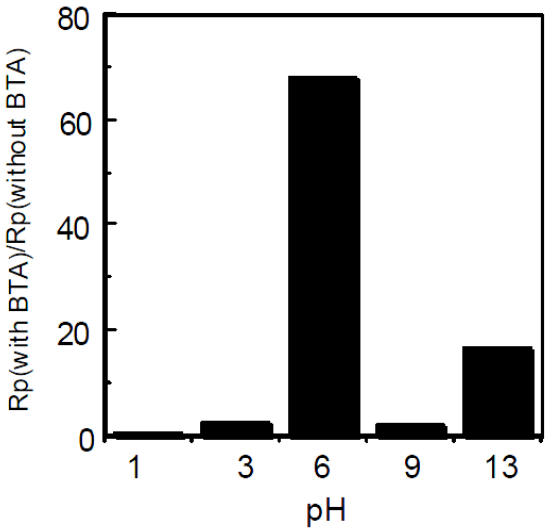

Figure 2-31. Effect of pH level on the inhibitory action of 0.01 M BTA on Cu in 0.1 M NaCl solution at 298 K [9].

2. 9. Effect of Surfactants

Surfactants composed of polar hydrophilic group attached to a non-polar hydrophobic section in their structure are being used for corrosion inhibition. The presence of multiple active centers for adsorption and a long hydrocarbon chain in the surfactants' structure results in a good surface coverage on the metal surface [66]. Surfactant's hydrophobicity stemming from the presence of the hydrocarbon chain can plug the defects in the adsorbed protective film [70]. The hydrophilic functional group is intended to interact with polar entities such as water, metals, and the present ions. Therefore, the hydrophilic section of the surfactant molecules is attached to the surface of the metal/metal oxide. In addition, the hydrophobic portion of the molecule is attracted to other hydrophobic portions of the adjacent surfactant molecules on the metal surface. As a result, a driving force exists for the adsorption of the surfactant on the metal/metal oxide surfaces directing the hydrophilic group at the solid interface and orienting the hydrophobic portion into the electrolyte. Therefore, a hydrophobic layer can develop over the metal surface [39]. Figure 2-32 demonstrates the formation of hydrophobic barrier at the solid interface over the concentration of the surfactant. With sufficient surfactant concentrations, one, two or multiple layers can form creating various adsorbed structures.

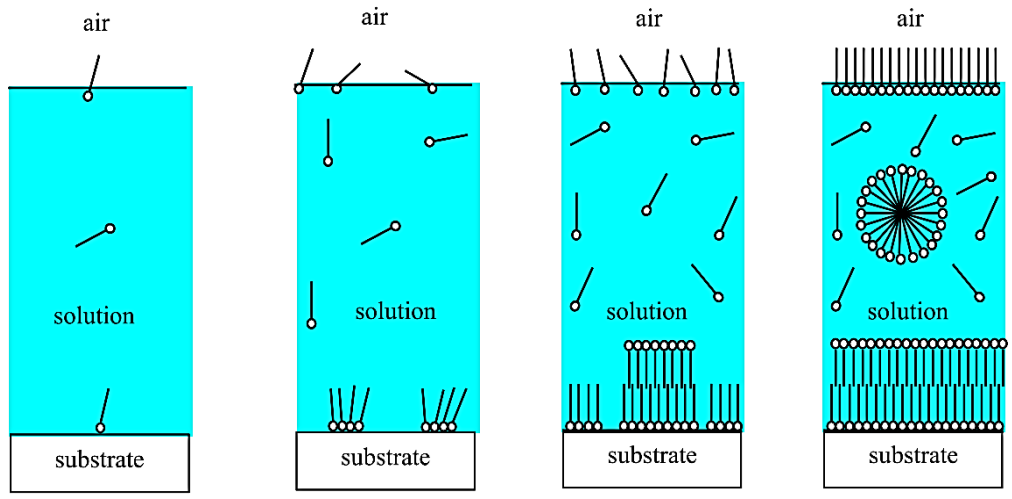

Figure 2-32. Comparison of surfactant aggregation in the electrolyte and on the metal surface versus concentration [39].

Accordingly, researchers have added various surfactants to increase the surface coverage of the adsorbed inhibitors used in their inhibition practices for various metals. Triton X-100 (TX-100) [70], cetyl trimethyl ammonium bromide (CTAB) [30,67], sodium dodecyl sulphate (SDS) [39,47,66], and molybdate (Mo) [66,85] are examples of the surfactants used to increase the inhibition efficiency.

The combination of surfactants has been also studied for higher protection. For instance, Gopi et al. [66] studied the inhibition of Cu in ground water medium at different temperatures with BTA and some of its derivatives such as 1-(2-Pyrrole carbonyl) benzotriazole (PBTA) and 1-(2-thienyl carbonyl)-benzotriazole (TBTA) in the presence of (sodium dodecyl sulphate (SDS), and molybdate (Mo). The highest inhibition efficiency was achieved for the ternary compound of PBTA + SDS + Mo. The results, presented in Table 2-9 and 2-10, show the positive role of surfactants in increasing the inhibition efficiency. As noted above, their inhibition role is attributed to their performance in the formation of a hydrophobic layer and somehow blocking the electrochemical reactions as well as plugging the defects in the adsorbed protective film.

Table 2-9. Potentiodynamic polarization results for Cu in ground water with different concentrations of BTA, TBTA, PBTA, SDS, and Mo at temperature range from 303 to 333 K [66].

Inhibitors	Conc. (mM)	$T = 303$ K			$T = 313$ K			$T = 323$ K			$T = 333$ K		
		E_{Corr} (mV)	j_{Corr} ($\mu A\ cm^{-2}$)	IE%	E_{Corr} (mV)	j_{Corr} ($\mu A\ cm^{-2}$)	IE %	E_{Corr} (mV)	j_{Corr} ($\mu A\ cm^{-2}$)	IE %	E_{Corr} (mV)	j_{Corr} ($\mu A\ cm^{-2}$)	IE%
Blank	—	-200	9.14	—	-179	10.2	—	-216	11.37	--	-212	12.64	--
BTA	0.1000	-208	5.36	41.4	-177	6.19	39.3	-210	6.97	38.7	-209	7.84	38.0
	0.1200	-214	4.47	51.1	-183	5.16	49.4	-216	5.82	48.8	-194	6.62	47.6
	0.1300	-210	3.96	56.7	-177	4.54	55.5	-221	5.16	54.6	-201	5.87	53.6
	0.1500	-207	4.45	51.3	-199	5.21	48.9	-211	5.94	47.8	-204	6.87	45.6
	0.1700	-204	5.01	45.2	-189	5.96	41.6	-216	6.72	40.9	-192	7.78	38.4
TBTA	0.0790	-260	4.99	45.4	-179	5.62	44.9	-219	6.41	43.6	-214	7.30	42.2
	0.0870	-195	3.14	65.6	-204	3.62	64.5	-208	4.10	63.9	-207	4.82	61.9
	0.0960	-240	2.80	69.4	-208	3.23	68.4	-218	3.73	67.2	-223	4.31	65.9
	0.1000	-198	3.45	62.2	-191	3.93	61.5	-216	4.44	60.9	-206	5.32	57.9
	0.1100	-255	3.96	56.7	-173	4.53	55.6	-222	5.27	53.6	-201	6.49	48.6
PBTA	0.0750	-215	4.45	51.3	-205	5.20	49.0	-218	5.87	48.4	-211	6.58	47.9
	0.0850	-198	3.53	61.4	-189	4.14	59.4	-217	4.73	58.4	-214	5.36	57.6
	0.0940	-200	2.48	72.9	-217	2.92	71.4	-217	3.42	69.9	-212	4.01	68.3
	0.1000	-195	4.46	51.2	-200	5.16	49.4	-220	5.83	48.7	-222	6.64	47.5
	0.1100	-198	5.00	45.3	-209	5.73	43.8	-207	6.49	42.9	-221	7.37	41.7
SDS	0.1390	-212	5.06	44.6	-183	5.87	42.4	-188	6.60	41.9	-205	7.49	40.7
	0.1560	-216	3.27	64.2	-200	3.76	63.1	-203	4.24	62.7	-215	4.83	61.8
	0.1730	-239	3.01	67.1	-208	3.45	66.2	-190	3.92	65.5	-206	4.47	64.6
	0.1910	-231	3.35	63.3	-204	3.89	61.9	-208	4.49	60,5	-205	5.21	58.8
	0.2080	-217	4.39	51.9	-182	5.11	49.9	-200	5.83	48.7	-192	6.76	46.5
Mo	0.0016	-222	5.13	43.9	-208	5.85	42.6	-206	6.68	41.2	-184	7.61	39.8
	0.0032	-217	4.29	53.1	-202	5.00	51.0	-210	5.72	49.7	-203	6.68	47.1
	0.0048	-230	3.80	58.4	-221	4.33	57.5	-197	4.92	56.7	-210	5.57	55.9
	0.0064	-217	4.65	49.1	-209	5.27	48.3	-203	5.96	47.6	-221	7.03	44.4
	0.0080	-224	4.88	46.6	-175	5.51	46.0	-204	6.31	44.5	-215	7.18	43.2

Table 2-10. Potentiodynamic polarization results for Cu in ground water with various binary and ternary compositions of inhibitors and surfactants at different temperatures [66].

Inhibitors	$T = 303$ K			$T = 313$ K			$T = 323$ K			$T = 333$ K		
	E_{Corr} (mV)	j_{Corr} ($\mu A\ cm^{-2}$)	IE %	E_{Corr} (mV)	j_{Corr} ($\mu A\ cm^{-2}$)	IE %	E_{Corr} (mV)	j_{Corr} ($\mu A\ cm^{-2}$)	IE %	E_{Corr} (mV)	j_{Corr} ($\mu A\ cm^{-2}$)	IE%
Blank	-200	09.14	—	-179	10.20	—	-216	11.37	—	-212	12.64	—
BTA + SDS	-217	01.21	86.8	-233	01.57	84.6	-236	02.03	82.1	-227	02.63	79.2
BTA + Mo	-310	02.56	72.0	-208	03.15	69.1	-217	03.73	67.2	-208	04.33	65.7
TBTA + SDS	-220	00.72	92.1	-296	00.94	90.8	-244	01.24	89.1	-242	01.62	87.2
TBTA + Mo	-217	02.37	74.1	-201	02.82	72.3	-222	03.28	71.1	-216	03.73	70.5
PBTA + SDS	-294	00.57	93.8	-268	00.77	92.4	-242	01.05	90.8	-250	01.44	88.6
PBTA + Mo	-204	02.10	77.0	-203	02.56	74.9	-222	03.07	73.0	-208	03.63	71.3
BTA + SDS + Mo	-278	00.94	89.7	-226	01.32	87.1	-270	01.82	84.0	-275	02.50	80.2
TBTA + SDS + Mo	-287	00.50	94.5	-312	00.71	93.0	-272	01.01	91.1	-312	01.41	88.8
PBTA + SDS + Mo	-295	00.29	96.8	-320	00.42	95.9	-275	00.61	94.6	-296	00.94	92.6

2. 10. Effect of Flow Rate on the Inhibition Mechanism with BTA

A few studies have been conducted on the corrosion inhibition of benzotriazole in dynamic flowing environment [45,86,87]. For instance, by utilizing a rotating cage inside the electrolyte, Khan et al. studied the effect of flow rate on the inhibition efficiency of BTA on Cu in 3.5% NaCl [45]. As it is shown in Figure 2-33, it was realized that the flow rate can help in the initial adsorption of the inhibitor while further increasing the flow rate can result in prevention and/or destruction of the initial formation of the protective film and causes localized corrosion. Besides, Hollander et al. observed that it is better to let the protective film form in a stagnant environment and then expose the pretreated metal surface to the solution flow. This way the initial adsorption and development of the film would not be impacted by the flow [65].

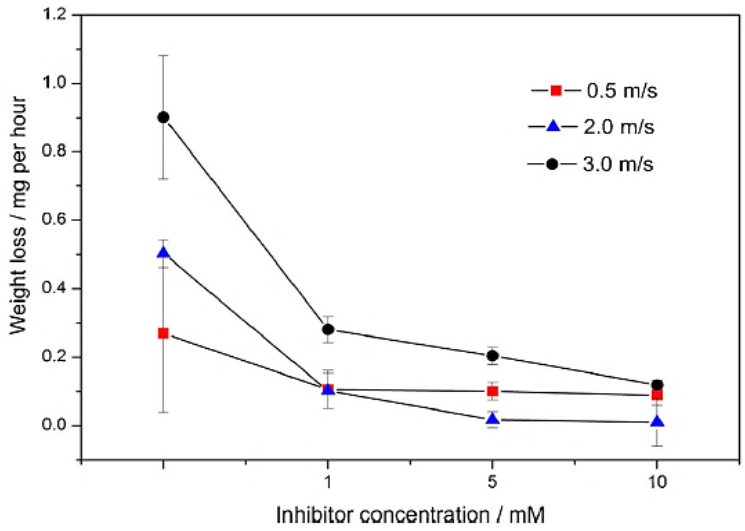

Figure 2-33. Cu weight loss in 3.5% NaCl in the absence and presence of 1-10 mM BTA at different velocities (0.5-3.0 m/s) [45].

2. 11. Summary

- Cu-Ag alloy is prone to corrode in neutral media.
- Application of inhibitors is one of the common remedies to decrease/ prevent corrosion.
- Inhibition of each phase of the alloy must be considered individually and in conjunction.
- Azole compounds, especially BTA and its derivatives, are the main type of inhibitors used for the inhibition of Cu in nearly neutral environments. There are contradictory reports on its

interaction with Ag.TD compounds with N and S heteroatoms in their structure can be good candidates for the inhibition of Ag.

- Inhibition efficiency of BTA, a well-known inhibitor for Cu, degrades over time and through increasing the temperature.
- BTA organometallic complex molecular chain length is different on Cu- and Ag-rich phases leading to different inhibition efficiencies on the metal surfaces. Inhibition reduction on alloys can be due to the disruptive effect these molecules have on each other.
- Coolant flushing periods should be determined to avoid further increase in the conductivity of the coolant and to maintain the inhibitor concentration and efficiency.
- Surfactants can provide a higher protection when accompanied by inhibitors.
- The presence of agitation in the system, to some extent can act as refurbishment of the protective layer. However, further increase in agitation rate can lead to the detachment of the inhibitor film from the metal surface.

Chapter 3 Experimental Methods

3. 1. Materials and Solutions

High purity copper plates and fine silver granules (K & K laboratories, Inc.) 99.999% were used to make alloys of pure Ag, Cu-60Ag, Cu-6Ag, and pure Cu; numbers denote atomic percent. Pure metals were included for comparison purposes. Furthermore, the alloys were added to study the composition effects on the corrosion process. The metals and alloys were prepared by utilizing an induction melting furnace under the flow of Ar gas followed by slow cooling. Cylindrical samples 7.6 mm in diameter were mounted in epoxy and polished down to 800-grid emery paper as the last step. Subsequently, the samples were ultrasonically cleaned in deionized water for 5 min, rinsed and dried before each electrochemical test. The microstructure of the eutectic (Cu-60Ag) and high copper (Cu-6Ag) alloys was observed by using the scanning electron microscopy (SEM, Hitachi S-3000N). DI water was used as the electrolyte with and without 100, 200, 500, and 1000 ppm BTA 99% and DMTD 98% (Sigma-Aldrich Co.). In addition, with the objective to increase the inhibition efficiency on the eutectic alloy, the effect of combining the two inhibitors was also measured in an electrolyte containing 1000 ppm BTA and 1000 ppm DMTD. To increase the accuracy in deriving the equivalent electrochemical circuit parameters from the impedance tests, 0.1 M KNO_3 ≥99% (Sigma-Aldrich Co.) was added to the electrolytes to increase the conductivity of the environment. Electrolytes containing the inhibitor were magnetically stirred for 15 min before each experiment for complete dissolution of the inhibitor. The ratio of the electrolyte volume to the metal surface was 10 ml/mm^2 for all experiments simulating the actual condition in the cooling systems in data center facilities.

3. 2. Electrochemical Measurements

A Parstat 2273 Potentiostat/Galvanostat (Princeton Applied Research) was used for all electrochemical testing. The exposed circular area of the mounted working electrode was 45.3 mm^2. A saturated calomel electrode (SCE) was used as a reference electrode and a platinized niobium mesh served as the counter electrode. The tip of the reference electrode was positioned close to the working electrode without using the Luggin capillary to minimize resistance in the cell. A hotplate stirrer was used to provide heat and agitation in the electrolytes. Figure 3-1 shows a scheme of the experimental set-up. Potentiodynamic tests were conducted after 10 min and 1 hour at the open circuit potential (OCP) in the absence and presence of different inhibitor concentrations. The 1-hour immersion tests were carried out to explore the nature of inhibitor adsorption. The potential was scanned from 250 mV below to 250 mV above the OCP at a sweep rate of 1 mV/s. At least three tests were conducted for each condition to ensure reproducibility. The PowerSuite software (version 2.60) was used to analyze the open circuit potential, potentiodynamic polarization, and impedance responses. Corrosion current densities were obtained by the Tafel extrapolation technique. Inhibition efficiency (η) and inhibitor surface coverage values (θ) were calculated using the corrosion current density (i_c) differences for each condition in the absence and presence of the inhibitor over i_c of the uninhibited condition.

The impedance tests were carried out at the OCP after an immersion time of 0, 2, 4, 6 hour(s) at room temperature (~298K) to explore the effect of time on the development of protective films and to investigate the effect of each inhibitor on the metal surfaces. The AC frequency range extended from 100 kHz to10 Hz with 10 points per decade and through an AC amplitude of ±10 mV in the absence and presence of the inhibitors in aerated electrolytes with 0.1 M KNO_3. In addition, the ZSimpWin software (version 3.30) which allows the chi-square (χ^2) value to judge the accuracy of the equivalent circuit fitting was used to fit the experimental results to the equivalent circuits and to obtain the EIS data (circuit parameter values).

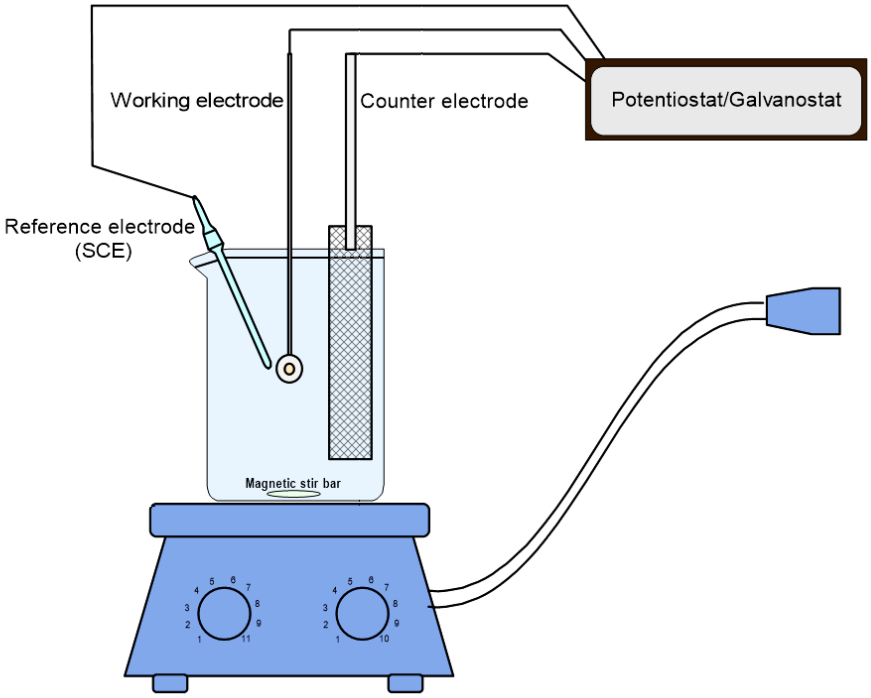

Figure 3-1. Scheme of the experimental set-up.

3. 3. XPS Characterization

XPS spectra were obtained from Cu and Ag samples after immersion in DI water with 1000 ppm BTA, and 1000 ppm DMTD for 10 min. Before each experiment, samples were dried in open atmosphere. XPS tests were conducted with a Perkin-Elmer Phi 560 ESCA/SAM system (Waltham, MA, USA) under vacuum pressure of 4.1×10^{-9} torr and utilizing a non-monochromated Al K_α excitation source. Each sample was scanned eight times in the 700-0 eV range with 0.1 s dwell time. The CasaXPS software (version 2.3.16) was used for high-resolution XPS peak deconvolution and data analysis. All XPS spectra were calibrated with respect to C1s peak at 284.5 eV.

Chapter 4 Results and Discussion

4. 1. Microstructural Investigations

The microstructures of the eutectic and high copper alloys are shown in Figure 4-1 in . The eutectic alloy exhibits a typical laminar structure composed of α (Cu-rich) and β (Ag-rich) phases. The high copper alloy shows large α-Cu grains and β phase segregation at the grain boundaries.

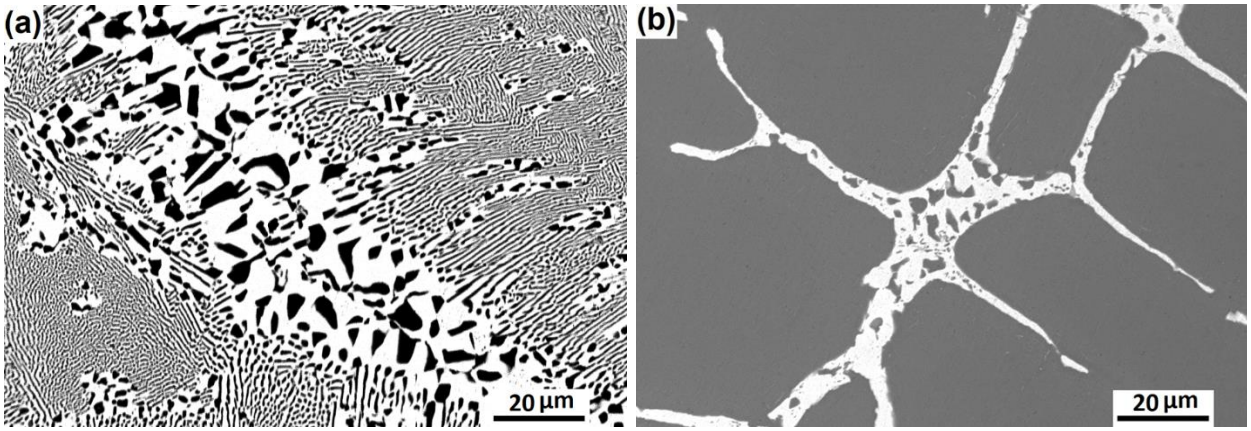

Figure 4-1. Scanning electron micrographs (BSE mode) of the (a) eutectic and (b) high copper alloy. The bright and dark regions corresponding to β-Ag and α-Cu areas, respectively.

4. 2. Electrochemical Studies

4. 2. 1. OCP and Potentiodynamic Polarization Curves

The results of the OCP measurements for Ag, Cu, Cu-60Ag, and Cu-6Ag in the absence and presence of 100 and 1000 ppm BTA in DI water are presented in Figure 4-2. Addition of BTA

moves Cu potential in the noble direction while the opposite effect is observed for Ag. It has been well established in the literature that BTA is a very effective inhibitor for copper [2,79,88]. The mechanism involves the adsorption of the inhibitor's molecules and formation of a polymeric Cu(I)-BTA and/or Cu(II)-BTA organometallic complex including Cu-N bonds [37,60,78]. However, reports for Ag are contradictory with some showing moderate or weak inhibition [6,7,9] while others show no effect [5]. This has been attributed to the weak adsorption of BTA on Ag surface [8]. Furthermore, the present results show that the presence of BTA activates the Ag surface. The reason for this behavior is not clear and can probably be attributed to either the oxidation of Ag due to the nucleophilic properties of BTA [89] or partial adsorption of BTA on the Ag surface causing activation of the adjacent uncovered areas.

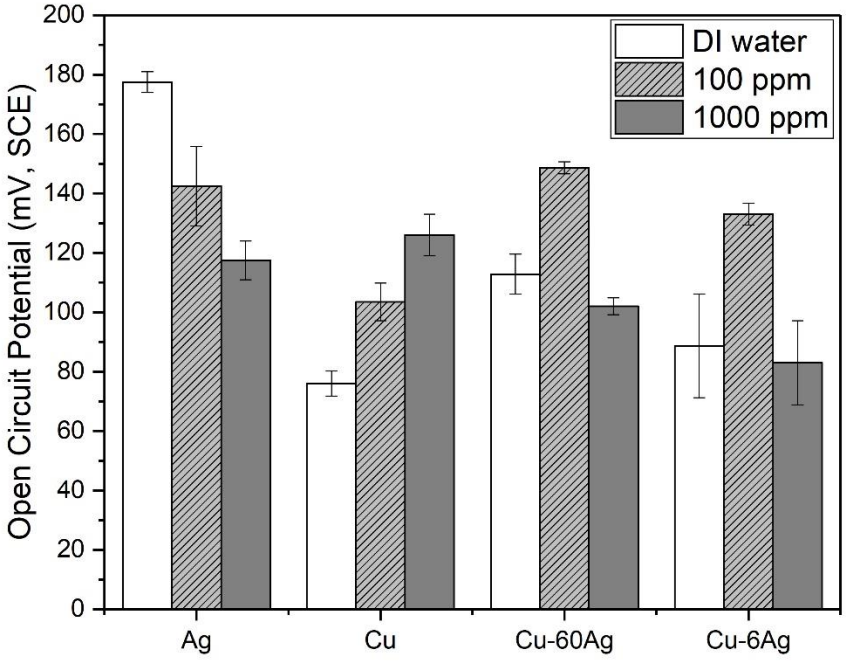

Figure 4-2. Open circuit potential values for Ag, Cu, Cu-60Ag, and Cu-6Ag without and with different BTA concentrations in DI water.

In the absence of the inhibitor, the eutectic and high Cu alloys are showing an OCP that is between those of pure Cu and Ag. However, addition of the inhibitor is showing a mixed behavior implying a competition between the α and β phase interaction with BTA. The results show that in the presence of 100 ppm BTA, the OCP is dominated by the behavior of Cu. In both alloys, the

OCP with 100 ppm BTA is higher than that in the absence of the inhibitor. This can be attributed to the strong inhibiting ability of BTA for Cu even when added in small amounts [1]. However, further addition of inhibitor to 1000 ppm causes the OCP to be dominated by silver, shifting it in the active direction. It is interesting to note that this behavior is observed even for the low Ag content alloy. An explanation for this behavior can be provided by considering the microstructure of the Cu-6Ag alloy, Figure 4-1. As noted above, 1000 ppm of BTA is not as effective for pure Ag as it is for pure Cu and in fact it drives its OCP to the active region. Since in the Cu-6Ag alloy all the silver is located at copper grain boundaries, it looks like the presence of Ag interrupts the formation of the BTA layer on the copper grains. Actually, the OCP of pure Cu and Cu-6Ag alloy in the absence of the inhibitor is similar to that of Cu-6Ag alloy in the presence of 1000 ppm BTA. It is possible that the presence of silver at the copper grain boundaries may destabilize the BTA layer preventing its formation on the surface of the copper grains.

Figure 4-3 presents the potentiodynamic polarization behavior of all four materials in the absence and presence of 100 and 1000 ppm BTA. Also, all electrochemical data from the potentiodynamic testing are summarized in Table 4-1. For an easy comparison, the corrosion potential (E_{Corr}) of all materials from these tests are shown in Figure 4-4. It is clear that the corrosion potentials follow the same trend and are in full agreement with the OCP presented in Figure 4-2. Also, Figure 4-3 shows that the anodic polarization of Cu and high Cu alloy is inhibited in the presence of BTA. On the contrary, the presence of BTA has no major effect on the anodic behavior of pure Ag and high Ag alloy. This difference in behavior is consistent with the effectiveness of BTA for Cu but not for Ag and high Ag alloy.

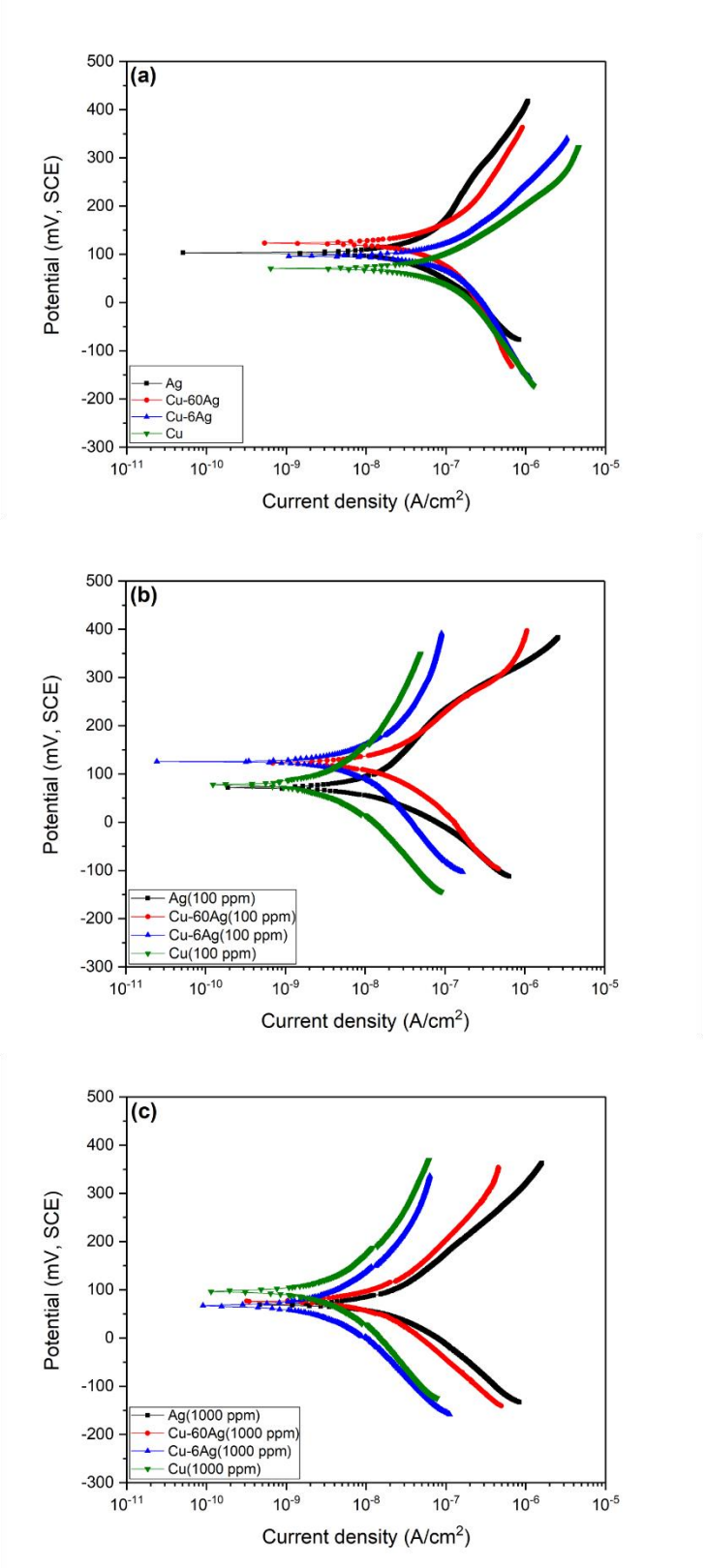

Figure 4-3. Potentiodynamic polarization responses of Ag, Cu, Cu-60Ag, and Cu-6Ag in the (a) absence and presence of (b) 100 ppm and (c) 1000 ppm BTA.

Table 4-1. Electrochemical data of the alloys in the absence and presence of 100 and 1000 ppm BTA.

Sample	E_{Corr} (mV)	i_C (nA/cm^2)	β_a (mV/decade)	β_c (mV/decade)
Ag	103.0	36.0	158.3	116.2
Cu-60Ag	121.8	53.8	137.0	159.6
Cu-6Ag	98.5	73.5	108.7	158.8
Cu	74.5	70.8	106.4	156.5
Ag (100 ppm)	77.4	11.0	149.1	91.3
Cu-60Ag (100 ppm)	115.1	13.7	126.2	96.1
Cu-6Ag (100 ppm)	130.7	6.1	102.5	147.3
Cu (100 ppm)	84.1	2.4	124.7	126.1
Ag (1000 ppm)	70.4	18.0	141.6	112.7
Cu-60Ag (1000 ppm)	76.3	6.3	108.2	110.3
Cu-6Ag (1000 ppm)	70.0	2.8	125.8	130.6
Cu (1000 ppm)	96.5	2.6	135.2	123.6

Table 4-1 shows that addition of the inhibitor lowers the corrosion rate of all four materials. For pure Cu and Cu-6Ag alloy, the reduction is more than one order of magnitude. This can be induced by the lower work function of Cu in the presence of BTA. Accordingly, diminishing any reaction that donates electrons; which is also consistent with the fact that BTA typically affects the anodic reaction [78]. However, the inhibitor shows a much lower impact on the corrosion rate of pure Ag and Cu-60Ag alloy.

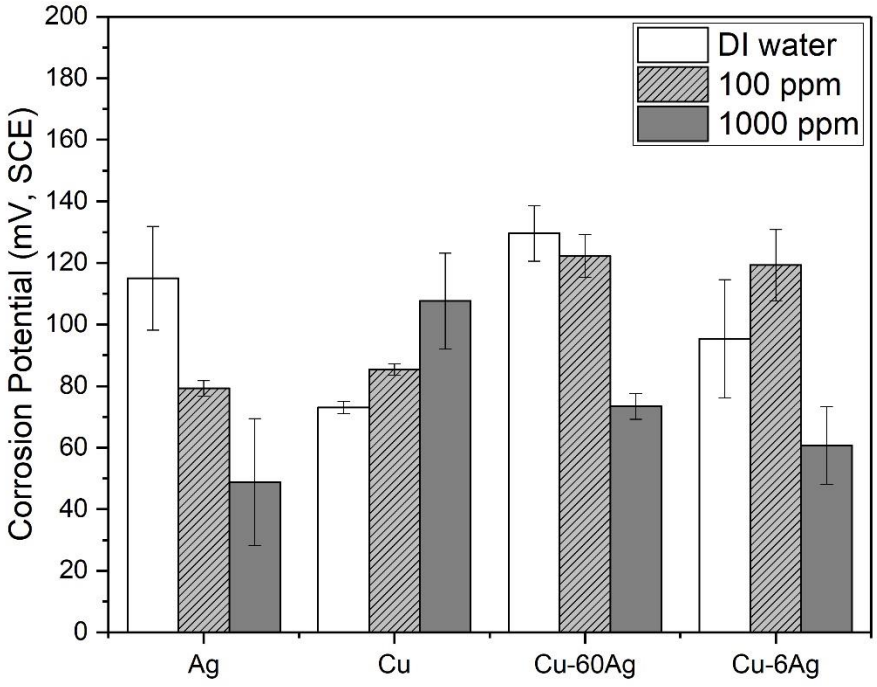

Figure 4-4. Corrosion potential in DI water in the absence and presence of different BTA concentrations.

Figure 4-5 demonstrates the inhibition efficiencies as derived using the corrosion rate data (Table 4-1). The corrosion inhibition efficiency (η) was calculated using the formula [44,66]:

$$\eta = \frac{i_c - i_{c(inh)}}{i_c} \times 100 \qquad (4\text{-}1)$$

where i_c and $i_{c(inh)}$ are the corrosion current densities from the potentiodynamic polarization responses in the absence and presence of inhibitor, respectively. For pure Cu and high Cu alloy, BTA shows a good surface coverage even with a small amount of BTA. This is because the Cu-azole film has hydrophobic character limiting the transport of hydrated ions to the metal surface [65]. However, for pure Ag and Cu-60Ag alloy, inhibition efficiency is significantly lower. In fact, addition of more BTA to pure Ag was found to further reduce the inhibition efficiency. This can be due to the partial and weak adsorption of BTA and/or detachment of the inhibitor as the chains become longer (heavier) on the Ag surface. Such a behavior leads to a weak coverage of the

inhibitor and limits the development of the organometallic complex providing a non-compact BTA-Ag film. Nevertheless, addition of more inhibitor (1000 ppm) to the Cu-60Ag alloy, has led to a higher inhibition efficiency and a better film coverage on the metal surface since it is dominated by the Cu behavior. It is interesting to note that further addition of the inhibitor reduced the OCP and E_{Corr} as thermodynamically-induced parameters by further activating the metal. However, its corrosion current density has been reduced too, as a kinetically-induced parameter in the presence of the α phase. Moreover, as corrosion rates are affected by the slopes of the polarization response, a further look into Table 4-1 can clarify as to how this kinetically-induced parameter is governed. It is clear that the addition of BTA, in all cases, has changed both the anodic and cathodic slopes of the polarization curves. This is because BTA is a mixed type inhibitor with more influence on the anodic reaction along with inhibition impacts on the cathodic reactions namely oxygen reduction [69]. That is also the reason for the fact that no definitive trend can be observed in the variation of the slopes with BTA concentration variations [44]. Generally, the consequence of changes of both the anodic and cathodic slopes is the variation of the corrosion current densities. Moreover, for the Cu-60Ag alloy due to the competition of α and β phases in interacting with BTA, the responses imply that the α phase is the dominant in controlling the kinetically-induced parameter of i_c, while the β phase is overcoming in controlling the thermodynamically-induced responses involving OCP and E_{Corr}.

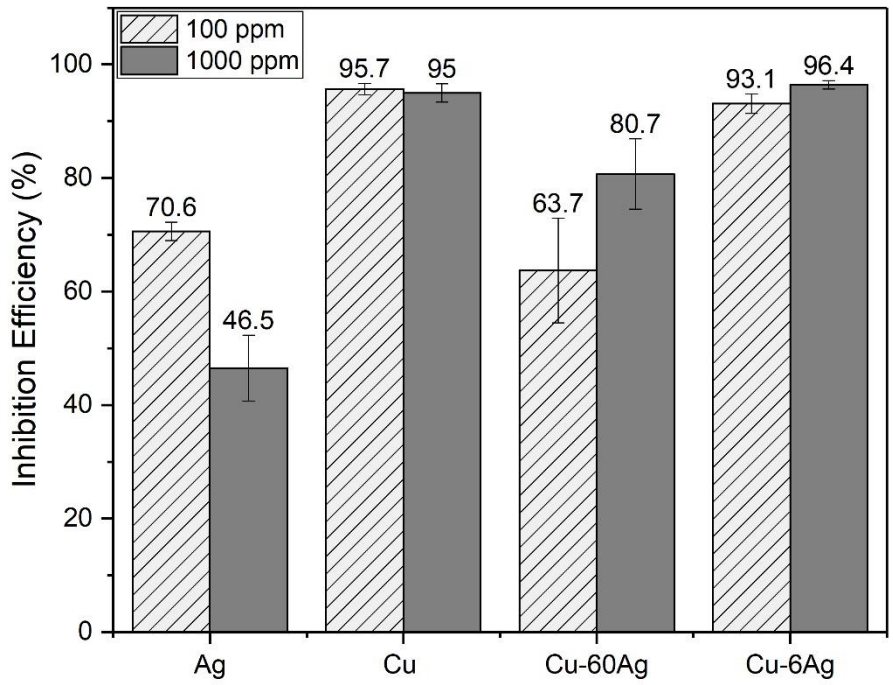

Figure 4-5. Inhibition efficiency in DI water with 100 and 1000 ppm BTA.

The OCP response of Cu and Ag with and without 500 rpm stirrer agitation of the electrolyte in the presence of 1000 ppm BTA at room temperature and 35˚C are shown in Figure 4-6. These measurements were carried out to resemble in some way the DI water circulation in the actual system that is operating at this temperature and 1000 ppm inhibitor concentration. Agitation in both cases has a minor positive impact by delivering more inhibitor to the surface of the metals [45] shifting their potential to a more noble direction with a somewhat higher impact on Cu. This again is attributed to the lower tendency of Ag to interact with BTA as was discussed earlier. Furthermore, increasing the electrolyte temperature was found to have no effect on Ag and only a minor initial effect on Cu surface. In the latter case, a higher kinetic energy in the electrolyte provides a better molecule diffusion shifting the potential to the noble direction with a higher rate compared to the situation at room temperature. However, after a period of time, this effect diminishes, and the potential stabilizes at the same level at both temperatures.

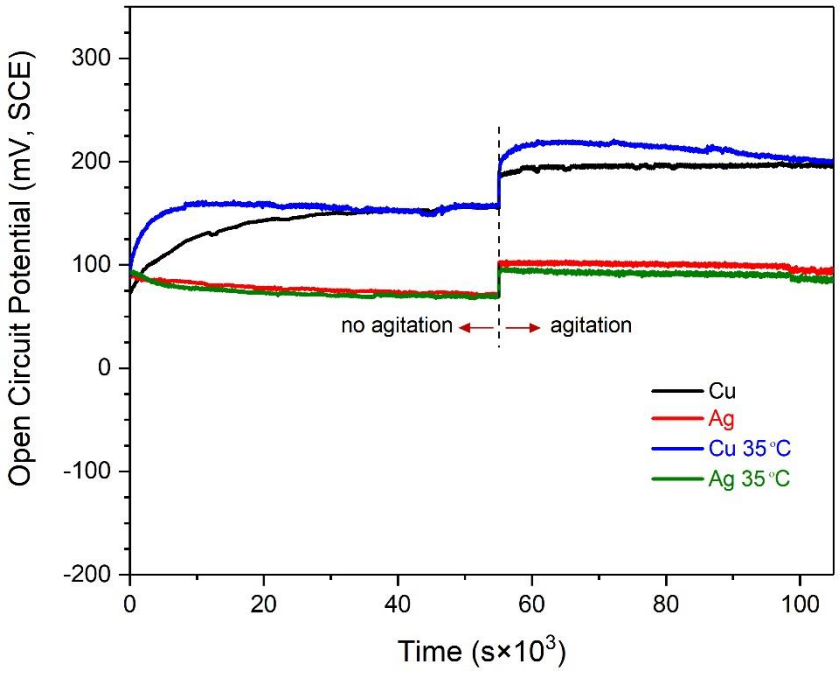

Figure 4-6. Open circuit potential for Cu and Ag with 1000 ppm BTA at room temperature and 35 ˚C with and without 500 rpm stirrer agitation of the electrolyte.

The present results show that in the presence of BTA in DI water, Cu exhibits a higher corrosion potential compared to Ag. In addition, the inhibitor shows a much higher efficiency compared to that of Ag. Both of the above factors indicate that in such a system, a galvanic couple is formed leading to higher corrosion of Ag that can be further exemplified by considering the high Cu over Ag surface area ratio in the water-cooling systems. It is noted that Ag is present in a small quantity of brazing alloy used to connect the large Cu fins in such water-cooling system.

In the search to increase the inhibition efficiency of the Ag-rich phase present in the Cu-Ag brazing eutectic alloy, by proposing an/a combination of effective inhibitor(s), 1,3,4-thiadiazole-2,5-dithiol (DMTD) was selected to be compared with BTA. Inhibition of DMTD molecule stems from the presence of two heteroatoms of N and S in its structure consisting of thiol (also known as sulfanyl or mercapto) group and azole functional group [16,57]. Figure 4-7 shows the molecular structure of these inhibitors using ACD/ChemSketch software (version C05E41). Heteroatoms are atoms other than carbon, including N, S, P, O, or Se present in the anchoring

groups through which the inhibitor molecule somehow anchors onto the metal surface [90]. These atoms are willing to participate in bonding with the metal surface [34]. Hence, they have the potential to increase the odds of adsorption. In general, thiadiazole and benzotriazole compounds are examples of the category of *"five-membered rings with two heteroatoms and fused carbocyclic derivative(s)"* heterocyclic compounds in organic chemistry [57,58]. They both possess features of a good inhibitor such as the presence of several heteroatoms to bond with the vacant orbitals of the metal, and complexity of the structure capable to make the molecule size big enough to properly block the electrochemical reactions, especially when fused with carbocyclic derivatives. It should be noted that, electron donating ability of S is higher than N [40]. Thus, DMTD can probably provide a better inhibition efficiency compared to BTA. However, the strength of adsorption depends on several other parameters such as the charge on the anchoring group in the specific environment, lateral interaction of the adsorbed molecules, etc. [41,91]. In addition, among different TD isomers, 1,3,4-thiadiazole probably provides a better inhibition efficiency as its heteroatoms are located at the both sides of the azole ring enhancing the odds of adsorption regardless of the direction of the molecule in the environment.

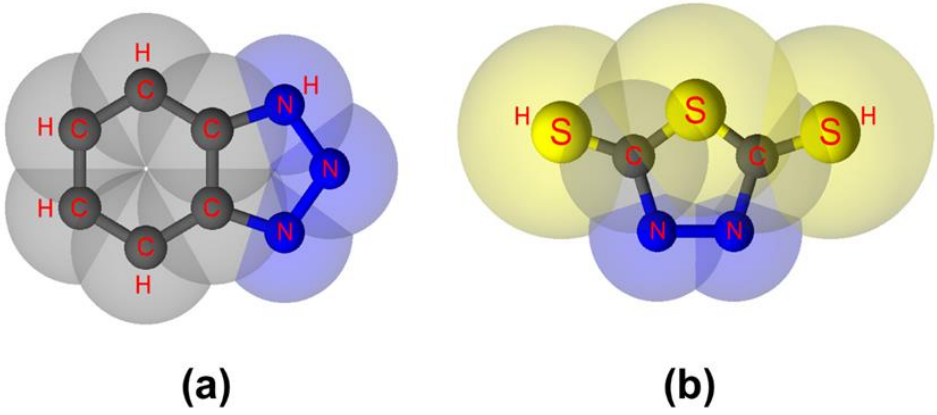

Figure 4-7. The chemical structure of (a) BTA, and (b) DMTD.

Figures 4-8 and 4-9 show the results of potentiodynamic polarization responses carried out after 1-h immersion in DI water with and without different inhibitor concentrations for Ag, Cu, and the Cu-60Ag alloy with BTA and DMTD, respectively. As the high Cu alloy showed an almost

identical behavior to the pure Cu, in terms of inhibition efficiency, it was excluded from these tests.

As illustrated in Figure 4-8(a), and with full agreement with our previous observations [92], BTA has shifted the corrosion potential to active regions for Ag. The reason for this behavior was attributed to either the oxidation of Ag due to the nucleophilic properties of BTA [89] or partial adsorption of BTA on the Ag surface causing activation of the adjacent uncovered areas. With respect to Cu, as demonstrated in Figure 4-8(b), BTA has shifted the corrosion potential towards the noble direction following the development of the Cu-BTA organometallic complex [37,60,78]. As shown in Figure 4-8(c), a mixed behavior in terms of corrosion potential is observed with the Cu-60Ag alloy implying a competition between the α and β phase interacting with BTA.

As shown in Figure 4-9, DMTD has shifted the corrosion potential towards the active region for all three metals. This can be attributed to the higher impact of DMTD molecule on the cathodic reaction. Cathodic inhibitors restrain the corrosion process by either decreasing the reduction rate or by selectively precipitating on the cathodic areas to increase the surface impedance and limit the diffusion of reducible species to these areas [16,28]. Nevertheless, given the change in the slope of both anodic and cathodic polarization curves, DMTD is acting as a mixed type inhibitor for all three metals. It also has thiol and azole anchoring groups in its structure through which the inhibitor can anchor onto the metal surface. Most organic (mixed) inhibitors have at least one functional group, considered as the reaction center or anchoring group [16]. The strength of adsorption depends on the charge on the anchoring group, rather than on the heteroatom. The structure of the rest of the molecule influences the charge density on the anchoring group [14,15]. Therefore, in light of the versatile structure of DMTD, it is expected that it would be in possession of an acceptable charge on its anchoring groups. Actually, this was the rationale for selecting this type of inhibitor in this study.

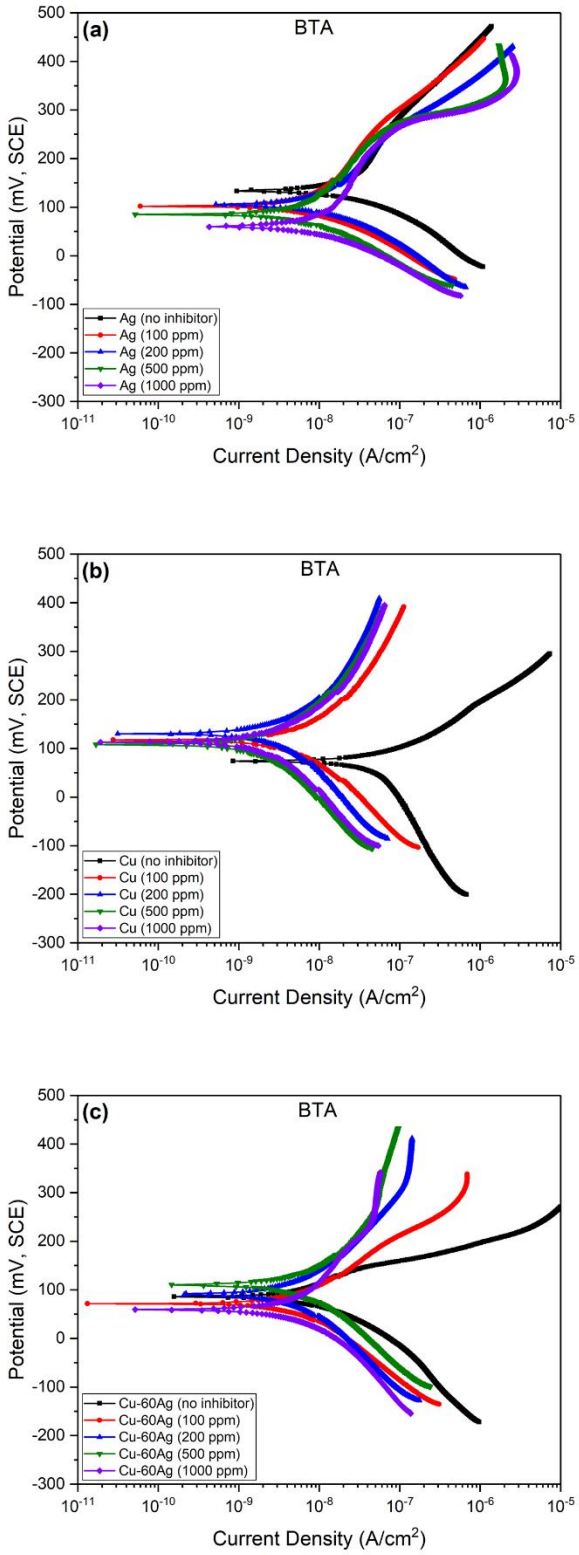

Figure 4-8. Potentiodynamic polarization responses in the absence and presence of different BTA concentrations for Ag, Cu, and Cu-60Ag alloy after 1-h immersion in DI water.

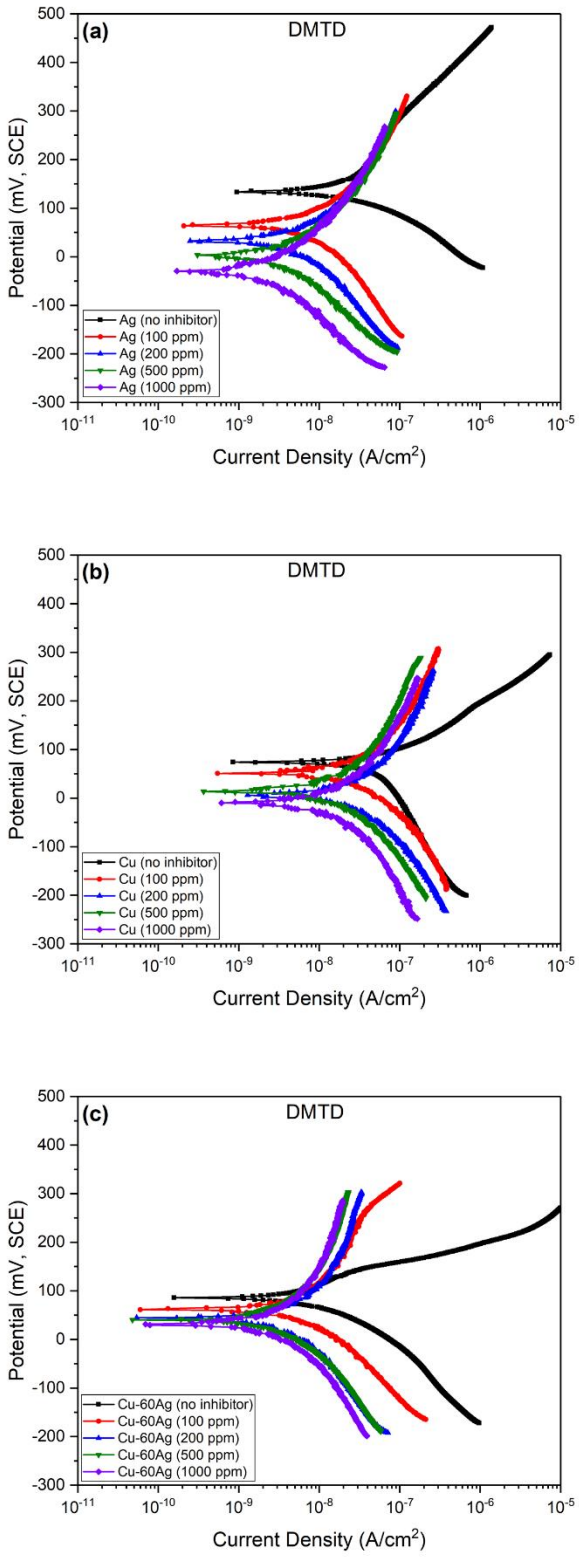

Figure 4-9. Potentiodynamic polarization surveys with and without different DMTD concentrations for Ag, Cu, and Cu-60Ag alloy after 1-h immersion in DI water.

With respect to the galvanic corrosion concern discussed earlier, DMTD is showing either an identical or higher corrosion potential in all concentrations for the brazing eutectic alloy compared to Cu. Although the corrosion potential for Ag is lower in different DMTD concentrations compared to Cu, the difference is much lower compared to the potential difference induced by BTA [92]. Therefore, DMTD seems to be a much safer inhibitor in this regard compared to BTA. Table 4-2 presents the corrosion rate for all the above anodic polarization tests as determined by Tafel extrapolation. It is clear that BTA and DMTD have lowered the rate with higher impact on Cu compared to Ag and Cu-60Ag alloy.

Table 4-2. Corrosion current densities in the absence and presence of different inhibitor concentrations.

	Blank	**BTA (ppm)**				**DMTD (ppm)**			
		100	200	500	1000	100	200	500	1000
		i_c (nA/cm^2)							
Ag	14	10.3	9.8	8.4	9.2	7	6.2	5	4.5
Cu	53	2.8	2.9	1.3	1.1	21.5	13.4	10.2	9.2
Cu-60Ag	10	4.9	4.1	3.7	3.4	4.8	4.3	3.7	3.2

Figure 4-10 presents the inhibition efficiencies as derived using the corrosion rate data extracted through the Tafel extrapolation technique from the polarization curves shown in Figures 4-8 and 4-9. The corrosion inhibition efficiency, η, were calculated using Equation (4-1) [1,41]. As shown in Figure 4-10(a), BTA has a very good coverage on Cu with above 90% efficiency even when added in a very small amount. This is in full agreement with our previous observations. The reason for this lies behind the strong hydrophobic character of Cu-azole film limiting the transport of hydrated ions to the metal surface [65]. However, for pure Ag and Cu-60Ag alloy, BTA inhibition efficiency is significantly lower in all concentrations. In fact, addition of more BTA to pure Ag was found to slightly reduce the inhibition efficiency. This can be due to the partial and weak adsorption of BTA and/or detachment of the inhibitor as the chains become longer (heavier) on the Ag surface [92]. Such a behavior leads to a weak coverage of the inhibitor and limits the development of the organometallic complex providing a non-compact BTA-Ag film. Nevertheless, addition of more inhibitor to the Cu-60Ag alloy has led to a higher inhibition efficiency and a better film coverage on the metal surface compared to Ag. Actually, in view of

the typical laminar structure of the Cu-60Ag eutectic alloy, it has an electrochemical behavior controlled by and between the two present α (Cu-rich) and β (Ag-rich) phases in its microstructure [92].

Figure 4-10(b) presents the inhibition efficiency of the DMTD molecule on all three metals. Interestingly enough, increasing the DMTD concentration has raised the inhibition efficiency for all three metals by covering more area on the metal surfaces. Compared to BTA, DMTD is providing a higher inhibition efficiency for Ag. This can be attributed to the higher electron donating ability of the S atom present in the DMTD molecule, along with the presence of the N heteroatom in its structure [40]. Providing a decent charge on the inhibitor anchoring groups seems to be effective in inhibition of Ag. This ultimately could have raised the odds of adsorption on the Ag surface [17]. With respect to Cu, BTA has higher inhibition efficiency in all concentrations compared to DMTD. This is due to the strong blocking effect of the Cu-BTA organometallic complex on the Cu surface involving Cu-N bonds [1,3,5]. Although DMTD possesses S and N heteroatoms with S comprising higher electron donating ability compared to the N heteroatoms of BTA, its molecule is somewhat smaller than BTA. This probably is providing a lower surface coverage on the Cu surface compared to BTA. Also, XPS results that are discussed in an upcoming section, showed that Cu does not bond with the N in DMTD. Therefore, it seems that the Cu-N bonding by BTA is much more effective compared to the Cu-S that can be obtained with DMTD. Another assumption can be the lower involved charge of the anchoring groups of DMTD compared to BTA leading to weaker adsorption on the Cu surface. Nonetheless, the inhibition efficiency depends on several other parameters such as electronic structure, chemical characteristics of the inhibitor being adsorbed, and especially the lateral interaction between the adsorbed molecules and the ability of the formed layer to become compact or cross-linked to develop a homogeneous film, etc. [41]. Thus, the plausible weaker lateral interaction of the adsorbed DMTD molecules on Cu compared to BTA, can be the third reason for the lower inhibition efficiency of DMTD on Cu compared to BTA. With respect to the Cu-60Ag alloy, much the same as in the presence of BTA, it delineates a behavior between the two pure metals in the presence of DMTD. Compared to BTA, DMTD is showing an almost identical efficiency for the Cu-60Ag alloy. This is because although DMTD has showed better affinity with Ag and has increased the coverage on the β phase, simultaneously it is demonstrating a lower interest towards the α phase compared to BTA, as

discussed above. Accordingly, the consequence of these two involved parameters has led to a virtually similar inhibition efficiency providing around 65% corrosion rate reduction in the presence of 1000 ppm of either of the two inhibitors for the eutectic alloy.

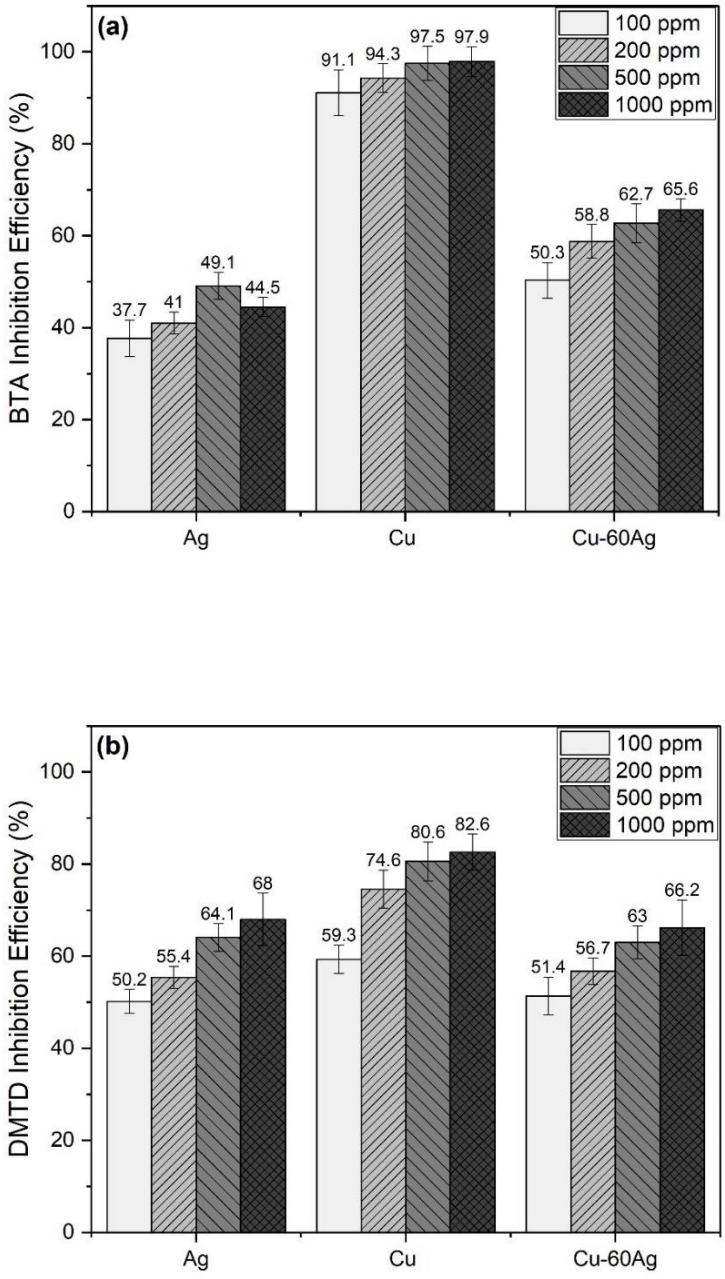

Figure 4-10. Inhibition efficiency with different (a) BTA and (b) DMTD concentrations for Ag, Cu, and Cu-60Ag alloy.

In an effort to further increase the inhibition efficiency of the brazing Cu-60Ag alloy, the effect of combining the two inhibitors on this alloy was explored. This was based on the obtained results regarding the influence of BTA and DMTD on the alloy's components. Figure 4-11 illustrates the potentiodynamic polarization surveys of Cu-60Ag alloy without and with BTA, DMTD and their combination. Also, the electrochemical data from these tests are summarized in Table 4-3. As discussed earlier, BTA and DMTD both are operating as mixed (organic) type inhibitors on the alloy. In view of the fact that both anodic and cathodic slopes are affected, combination of the two inhibitors is also providing a mixed behavior [59]. Employing the combination of the two inhibitors (1000 ppm from each) has reduced the corrosion rate down to 1.9 nA/cm^2 which is approaching over 80% corrosion inhibition efficiency. The rationale behind choosing 1000 ppm from each of the inhibitors was the fact that each separate inhibitor provided the highest efficiency with 1000 ppm concentration for the eutectic alloy. This promising increment in efficiency can probably be further improved by addition of appropriate surfactants to the environment. The presence of multiple active centers for adsorption and a long hydrocarbon chain present in the surfactants' structure can result in a good surface coverage on the metal surfaces [66]. Actually, surfactant's hydrophobicity stemming from the presence of the hydrocarbon chain can further plug the defects (uncovered areas) in the adsorbed protective film [70]. We plan to explore this route in an upcoming study.

The present results show that BTA has more affinity towards the α phase, whereas DMTD is more effective for the β phase. Nonetheless, both inhibitors adsorb on the other phase. But it seems they either cannot make a dense film or have lower adsorption energy on the other phase. Therefore, exploring the inhibitor adsorption as well as the bonding nature of the inhibitors to the metal surfaces are of utmost importance.

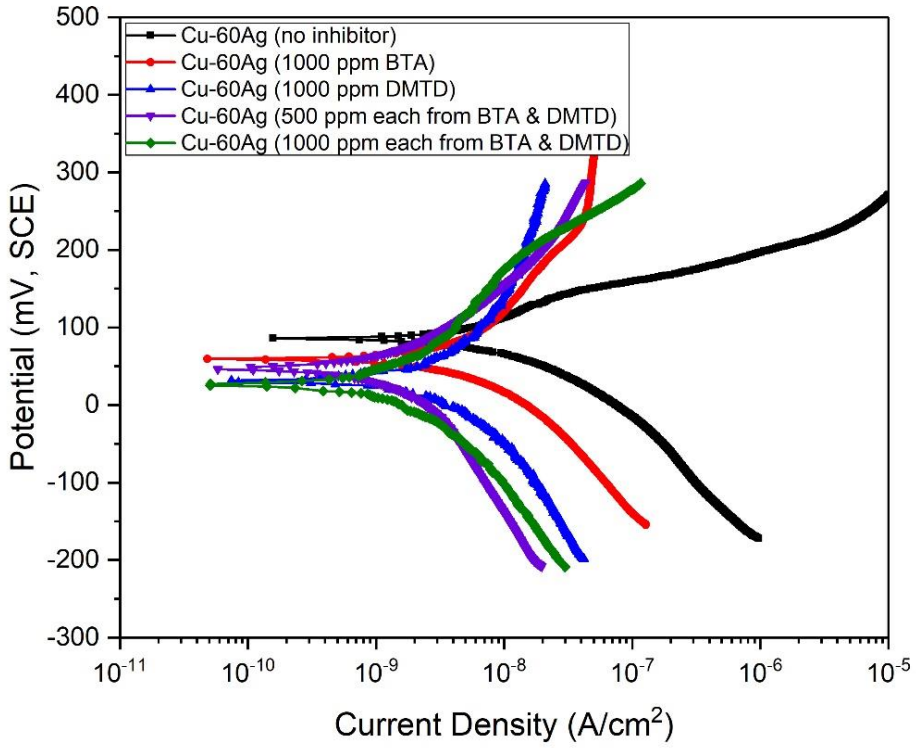

Figure 4-11. Potentiodynamic polarization curves without and with BTA, DMTD and their combination for Cu-60Ag alloy.

Table 4-3. Electrochemical data for the Cu-60Ag alloy in the absence and presence of BTA, DMTD, and their combination.

Inhibitor (ppm)	E_{Corr} (mV)	i_c (nA/cm^2)	η (%)	β_c (mV/decade)	β_a (mV/ decade)
Blank	82.9	10.0	-	101.1	68.0
BTA (10^3)	59.4	3.4	66	121.5	83.1
DMTD (10^3)	31.3	3.2	68	133.6	190.7
BTA + DMTD (500 each)	47.8	2.3	77	168.5	103.4
BTA + DMTD (10^3 each)	34.3	1.9	81	157.3	154.5

4. 2. 2. Adsorption Isotherm Investigations

Adsorption mechanism and strength can be deduced from the adsorption isotherm, which shows the relation between the concentration of inhibitor in the corrosive environment (electrolyte) and the inhibitor coverage on the metal surface [37,42,43]. To evaluate the nature and strength of adsorption, the experimental data obtained from the potentiodynamic polarization surveys illustrated in Figures 4-8 and 4-9 were employed. The degree of surface coverage, θ, in different BTA and DMTD inhibitor concentrations were calculated using Equation (4-2):

$$\theta = \frac{i_c - i_{c(inh)}}{i_c} \qquad (4\text{-}2)$$

Several adsorption isotherms including Langmuir, Temkin, and Frumkin isotherms were considered to achieve the best fit for the calculated surface coverage in order to extract the thermodynamic data of adsorption [16,44–46].

Langmuir adsorption isotherm, illustrated in Figure 4-12(a), was found to be the best fit for all three metals interacting with BTA. However, Temkin adsorption isotherm provided the best fit with regard to DMTD as presented in Figure 4-12(b). This indicates that the adsorption mechanisms are different. Langmuir model assumes that all metal surface adsorption sites are equal and molecular binding takes place independently of the neighboring sites regardless of whether or not the nearby sites are occupied [39,47]. The Temkin adsorption isotherm is also an empirical adsorption model that considers the chemisorption of molecules on materials surfaces [48]. The main assumption in this model is that heat of adsorption of all molecules in the adsorbed layer decreases linearly with an increase in the surface coverage [39]. Nevertheless, it would only seem natural to observe different adsorption mechanisms between BTA and DMTD. DMTD has two thiol and azole anchoring groups, two different (S and N) heteroatoms, and its plausible adsorption sites are at both sides of its molecule. Thus, DMTD can provide a somewhat heterogeneous adsorption nature compared to BTA with one active azole anchoring group, only one type of heteroatom (N), and possible adsorption sites at one side of its molecule. Although there are reports of BTA adsorption in different directions (perpendicular or tilted and/or parallel) relative to the metallic surface [2], it secures a virtually more homogeneous type of adsorption

compared to DMTD which has the potential for much more complexity and probabilities in its adsorption behavior.

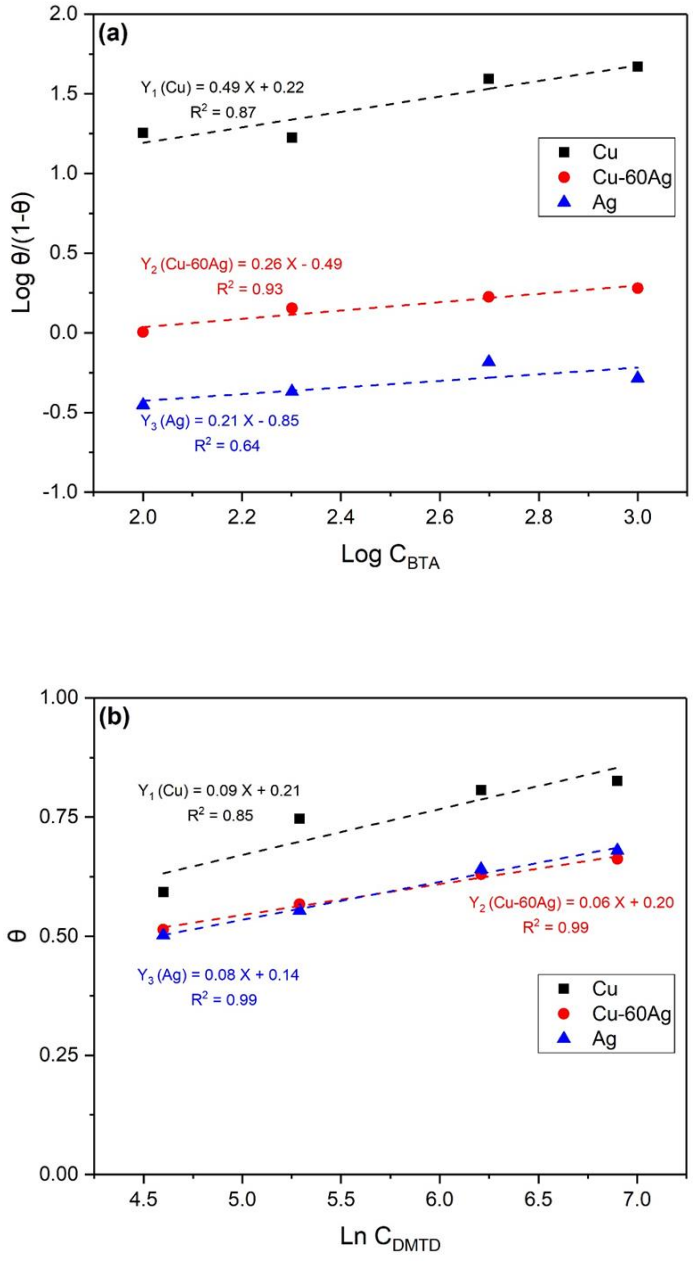

Figure 4-12. (a) Langmuir adsorption isotherm of BTA, (b) Temkin adsorption isotherm of DMTD on the surface of pure Cu, Cu-60Ag alloy, and pure Ag.

In the Langmuir model, Equation (4-3) and in Temkin model, Equation (4-4) rules between surface coverage, adsorption constant, and inhibitor concentration [49,93,94]. These two equations

were used to find the adsorption coefficient constants. Accordingly, standard free energies of adsorption were calculated using Equation (4-5):

$$\frac{\theta}{1-\theta} = K_{ads}c \tag{4-3}$$

$$e^{f\theta} = K_{ads}c \tag{4-4}$$

$$\Delta G_{ads} = -RTLn(55.5K_{ads}) \tag{4-5}$$

where K_{ads} (dm^3 mol^{-1}) is the equilibrium adsorption coefficient constant reflecting the affinity of the adsorbate molecules towards adsorption sites; c (mol dm^{-3}) the inhibitor concentration, and f the inhibitor molecular lateral interaction parameter (0 , for no interaction; +, for attraction; and —, for repulsion) between the adsorbed molecules. Moreover, ΔG_{ads} (J mol^{-1}) is the free energy of adsorption, R (J mol^{-1} K^{-1}) the universal gas constant, T (K) temperature, and 55.5 is the molar concentration of water in the electrolyte in (mol dm^{-3}) as the solvent [1,44,95].

In view of Equation (4-3), the y axis intercept of Log[θ/(1-θ)] vs. Log c plot is Log K_{ads}. Since the utilized concentrations were in ppm, in order to convert their units to mol/dm^3, the derived K_{ads}^{BTA} values from the fitted lines in Figure 4-12(a) were multiplied by 119127 (molar mass of BTA is 119.127 g mol^{-1}). In addition, as per Equation (4-4) and in light of DMTD's adsorbate-adsorbate attraction nature (making f : +) [41], the y axis intercept of θ vs. Lnc plot is LnK_{ads}. Meanwhile, the obtained K_{ads}^{DMTD} values from the fitted lines in Figure 4-12(b) were multiplied by 150250 (molar mass of DMTD is 150.250 g mol^{-1}) to turn the units to mol/dm^3.

The thermodynamic data of BTA and DMTD adsorption on all three metals are summarized in Tables 4-4 and 4-5, respectively. The standard free energy of adsorption was calculated to be -40.16 kJ mol^{-1} for Cu, -36.11 kJ mol^{-1} for Cu-60Ag, and -34.06 kJ mol^{-1} for Ag while interacting with BTA. This is indicative of *chemisorption*, *physisorption*/*chemisorption*, and *physisorption/weak chemisorption*, respectively [17,37,49]. However, the standard free energies of all three metals are somewhat identical while interacting DMTD as calculated to be -40.00, -39.97, and -39.83 kJ mol^{-1} for Cu, Cu-60Ag, and Ag, respectively. The results show that DMTD

has a strong chemisorption nature in all cases towards all three metals surfaces. As noted above, this can be attributed to the presence of two active anchoring groups involving S and N heteroatoms existing at both sides of the molecule. However, the inhibition difference observed by these metals while interacting DMTD can be related to other determining factors. The other contributing factors include the number and type of active bonding(s) between the inhibitor and the metal surface as well as the lateral interaction between adsorbed protective monolayers.

Physical adsorption is nonspecific with a low activation energy. This process is rapid and, in many cases, reversible [16]. It involves, electrostatic/ van der Waals forces [38]. On the other hand, the adsorbed molecules involved in chemical interaction (chemisorption) form bonds with the metal surface. Chemisorption entails a higher heat of energy and is persistent, specific and irreversible [17,39]. The bonding occurs with electron transfer or sharing between metal and inhibitor. The negativity of the standard free energies is an indication of the spontaneous nature of absorption, and their absolute value implies the degree of spontaneity [41,93,96]. It should be noted that using only ΔG_{ads} as a criterion to identify the type of adsorption might not be sufficient. This is because contribution of other enthalpies such as adsorbate/adsorbent electrostatic interaction enthalpy, and adsorbate conformation change enthalpy should also be considered. However, many studies have distinguished the nature of adsorption simply by the absolute value of standard free energy of adsorption in such a way that values greater than -40 kJ mol^{-1} are considered as chemisorption, for less than -20 kJ mol^{-1} are evaluated as physisorption, and the range between these two specified values is known for a mixed adsorption [49,90,97–99].

The adsorption types determined through the Langmuir isotherms are consistent with our foregoing observations confirming the lower affinity of the Ag-rich phase interacting with BTA ($\eta_{Cu} > \eta_{Cu\text{-}60Ag} > \eta_{Ag}$). Therefore, the fact that BTA is partially chemisorbed and to some extent physiosorbed on Ag can be another explanation for its weaker adsorption on the Ag-rich phase compared to the Cu-rich phase. The partial chemisorption of BTA on Ag through the N tail of the inhibitor is confirmed in this study by XPS [92]. Accordingly, the eutectic alloy suffers from this partial BTA chemisorption on its Ag-rich phase.

As illustrated in Figure 4-10(b), the same inhibition efficiency trend was also observed with respect to DMTD on the materials studied and is reflecting on the Temkin isotherms. Despite

the vicinity of the calculated standard free energies of DMTD adsorption presented in Table 4-5, they still follow much the same trend as that of the inhibition efficiencies. Especially, comparing DMTD adsorption coefficient constants as a criterion of the affinity of the adsorbate molecules towards adsorption sites, further illuminates this obedience [16,39,49].

Table 4-4. Thermodynamic parameters for the BTA adsorption in DI water.

Material	K_{ads} (dm^3 mol^{-1})	ΔG_{ads} (kJ mol^{-1})	Adsorption Type
Cu	197,701.60	-40.16	Chemisorption
Cu-60Ag	38,548.74	-36.11	Physisorption/ Chemisorption
Ag	16,827.13	-34.06	Physisorption/ Weak Chemisorption

Table 4-5. Thermodynamic parameters for the DMTD adsorption in DI water.

Material	K_{ads} (dm^3 mol^{-1})	ΔG_{ads} (kJ mol^{-1})	Adsorption Type
Cu	185,360.13	-40.00	Chemisorption
Cu-60Ag	183,515.76	-39.97	Chemisorption
Ag	172,828.63	-39.83	Chemisorption

Therefore, adsorption isotherm studies further clarified the appropriate candidacy of DMTD compared to BTA for the Ag-rich phase in DI water. It also shed light on the fundamental understanding behind the reasons for the distinct behavior of Cu and Ag while interacting with DMTD and BTA.

4. 2. 3. Electrochemical Impedance Spectroscopy Experiments

The electrochemical impedance spectroscopy (EIS) measurements were conducted to model the electrochemical performance through equivalent circuits and to shed light on the adsorption and inhibition mechanism. Figure 4-13 illustrates the Nyquist plots for Cu in the

absence and presence of 1000 ppm BTA and DMTD after certain time intervals. The observed flattening over time shown in Figure 4-13(a) is due to the formation of Cu_2O on the metal surface in the absence of the inhibitors [12]. Besides, a straight line attributed to the Warburg impedance in the low frequency regime is observed due to mass transport involving the diffusion of Cu^+ from the electrode surface into the bulk solution or diffusion of dissolved oxygen from the electrolyte to the Cu surface [100,101]. However, in the presence of BTA and DMTD, Nyquist plot flattening is caused by the formation of the organometallic protective film and is synchronized with significant increase in impedance [78]. Appearance of depressed capacitive loops, whose diameter increases over time propose a shift towards a more charge transfer-controlled process in which copper corrosion resistance has been notably improved [96]. Particularly, through the passage of time, the diffusion-controlled behavior is further weakened in the presence of the inhibitors.

Decreasing the slope of the straight line and increasing the impedance value especially at the low frequency range illustrated in Figure 4-13(d), indicates that both BTA and DMTD can efficiently inhibit the diffusion of Cu^+ or dissolved oxygen [97]. This is because, rise of impedance in the low frequency range is consistent with the sluggishness of any diffusion-controlled phenomenon [11]. This is consistent with our prior observations in which potentiodynamic polarization responses and adsorption isotherm studies confirmed the positive role of BTA and DMTD can play in reducing copper corrosion current density in DI water both through chemisorption [92,102]. Moreover, in the presence of BTA, Z' (the real part of impedance) shows a somewhat larger increase compared to Z'' (the imaginary part of impedance), while the opposite is observed with DMTD. This shows that the adsorption mechanism of BTA and DMTD is different in agreement with the finding that BTA follows Langmuir adsorption isotherm and DMTD obeys Temkin isotherm for these metals [102]. The role of these inhibitors has been attributed to the strong blocking effect and hydrophobic character of the formed Cu-azole complexes involving Cu-N bonding in the case of BTA and Cu-S bonding in the presence of DMTD [1,3,5,65,103]. Actually, the pyrrolic nitrogen of the triazole ring of BTA and the exocyclic mercapto group (-SH) of thiadiazole derivatives can be polymerized via the Cu^+ ion and form a polymer chain on the copper surface [92,103,104]. The higher impedance values by increasing the immersion time confirms the progressively increasing inhibiting role of the inhibitors studied. This

is due to the development and densification of the protective film with time by increasingly blocking the electrochemical reactions while gradually forming a compact film [96].

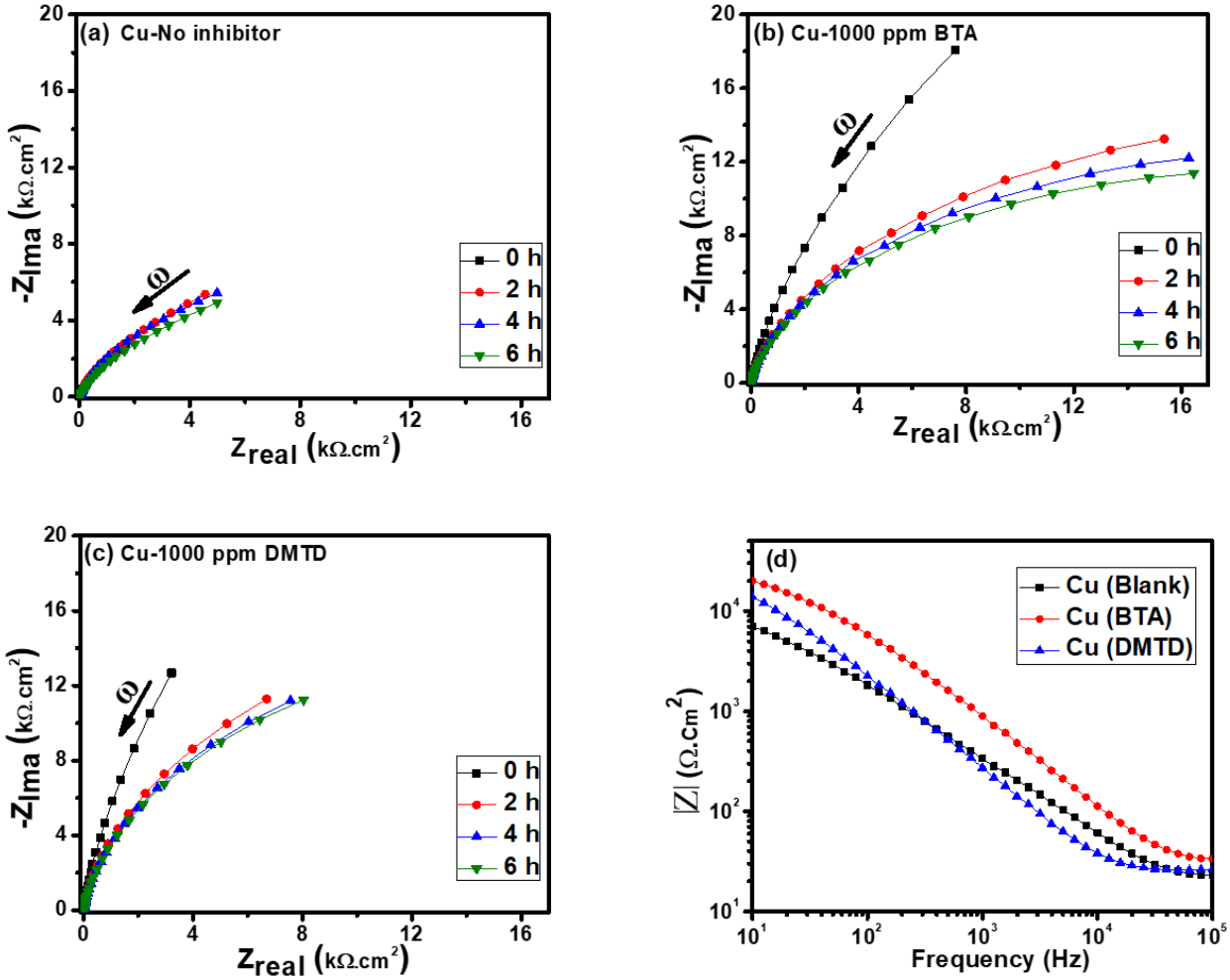

Figure 4-13. Temporal evolution of Nyquist plots for Cu in 0.1 M KNO_3 electrolyte containing (a) no inhibitor, (b) 1000 ppm BTA and (c) 1000 ppm DMTD. Corresponding Bode plots are shown in (d).

Figure 4-14 demonstrates the Nyquist plots for pure Ag in the absence and presence of the inhibitors. Much the same as for Cu in the absence of inhibitors, Ag is showing a Nyquist plot flattening over time owing to deviation from ideal conductive behavior caused by the formation of Ag_2O on the metal surface. The appearance of the straight line stems from the Warburg impedance in the low-frequency range due to diffusion of Ag^+ into the electrolyte from the metal surface or diffusion of dissolved oxygen from the bulk solution invading the Ag surface [100,105,106]. Nevertheless, in the presence of the inhibitors, the observed depressed curves are ascribed to the formation of the protective films acting as a barricade to the diffusion of silver ions or oxygen.

Similar to the behavior observed with Cu, impedance has been increased significantly in the presence of the inhibitors, and the depressed curves imply a shift to a charge transfer-control phenomenon while mass-transfer gradually diminishes, especially over time [107]. Comparing Nyquist plots of BTA- and DMTD-treated Ag shows that DMTD is much more successful in depressing the curves. In fact, the inhibition behavior of BTA and DMTD on Ag is due to formation of the protective films involving Ag-N bonding in the case of BTA along with Ag-S and Ag-N bonding in the case of DMTD based on XPS measurements. In addition, Langmuir isotherm has revealed the weaker adsorption of BTA on Ag via its simultaneous chemisorption and physisorption nature. On the other hand, Temkin adsorption isotherm has confirmed the stronger chemisorption nature of DMTD on Ag surface [102]. Immersion time also seems to have a positive role in increasing the film coverage/homogeneity on the metal surface. In fact, EIS data extracted from the equivalent circuit further sheds light on this in the following sections. Moreover, Bode |Z| plot illustrated in Figure 4-14(d) after 6-h immersion time, also shows that DMTD has led to a much higher impedance in the low frequency regime. This can be considered another evidence for the higher affinity and effectiveness of DMTD on Ag compared to BTA.

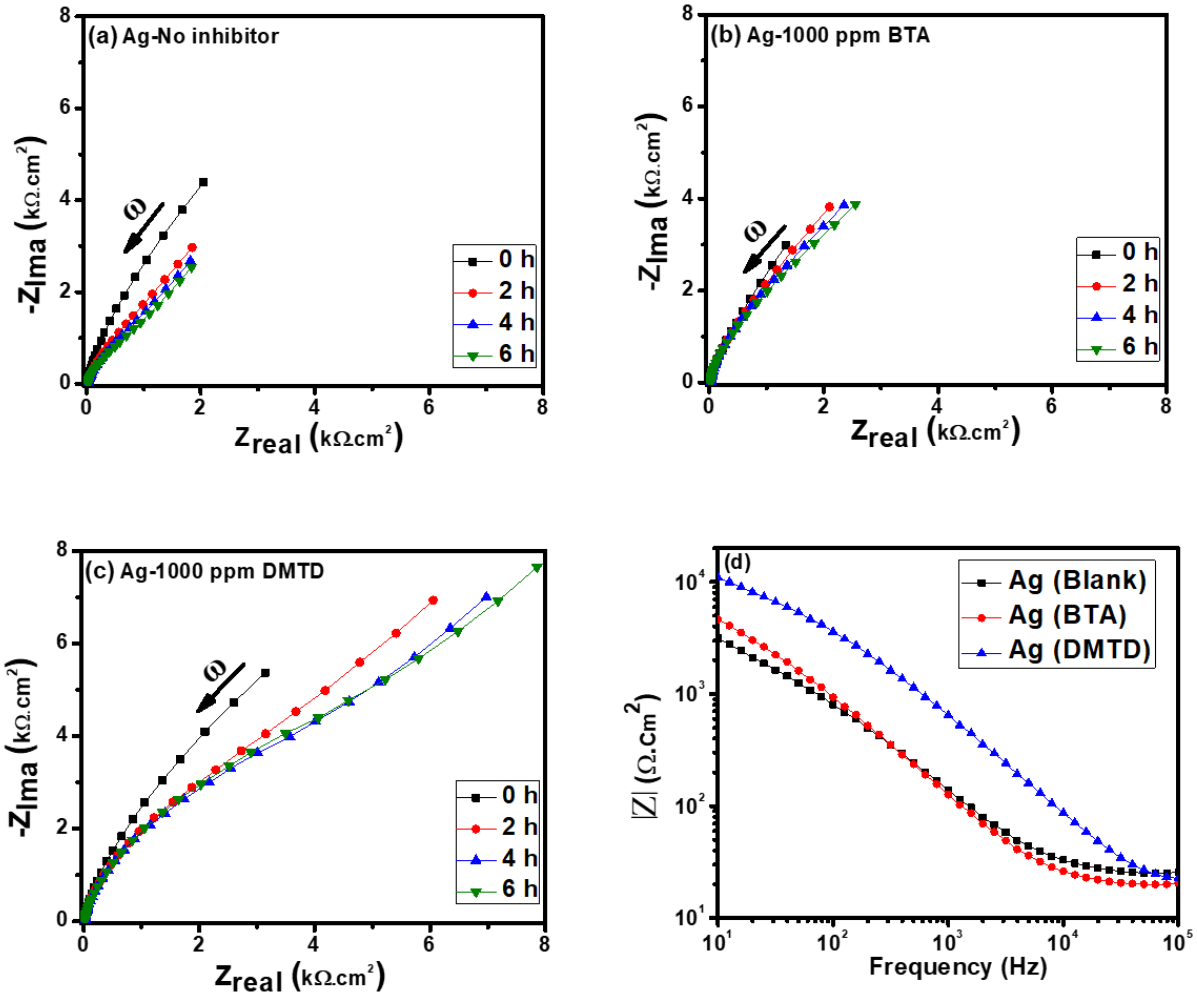

Figure 4-14. Temporal evolution of Nyquist plots for Ag in 0.1 M KNO_3 electrolyte containing (a) no inhibitor, (b) 1000 ppm BTA and (c) 1000 ppm DMTD. Corresponding Bode plots are shown in (d).

Nyquist plots for the Cu-60Ag alloy are shown in Figure 4-15. In the absence of the inhibitors, Warburg impedance is observed in the low frequency range. A mass-controlled process that has been depressed over time upon the formation of the surface oxides from the alloy mere components including α (Cu-rich) and β (Ag-rich) phases [50]. Addition of the inhibitors has led to the significant increase in the impedance particularly the imaginary part of impedance. However, for the pure metals, the real part of the impedance was somehow proportionately increasing with the imaginary part. This is an indication of a distinction in the inhibition mechanism that can further be clarified through equivalent circuit modeling. Figure 4-15(d) shows the Bode plot of the alloy after 6-h immersion in the absence and presence of the inhibitors.

Looking into to the low frequency range and consistent with our previous findings, an almost identical effective inhibition was obtained with both inhibitors. Despite the fact that DMTD provided a promising protection for the Ag-rich phase, it is showing a lower efficiency for the Cu-rich phase compared to BTA. Consequently, these two factors have led to a roughly similar inhibition condition for the alloy.

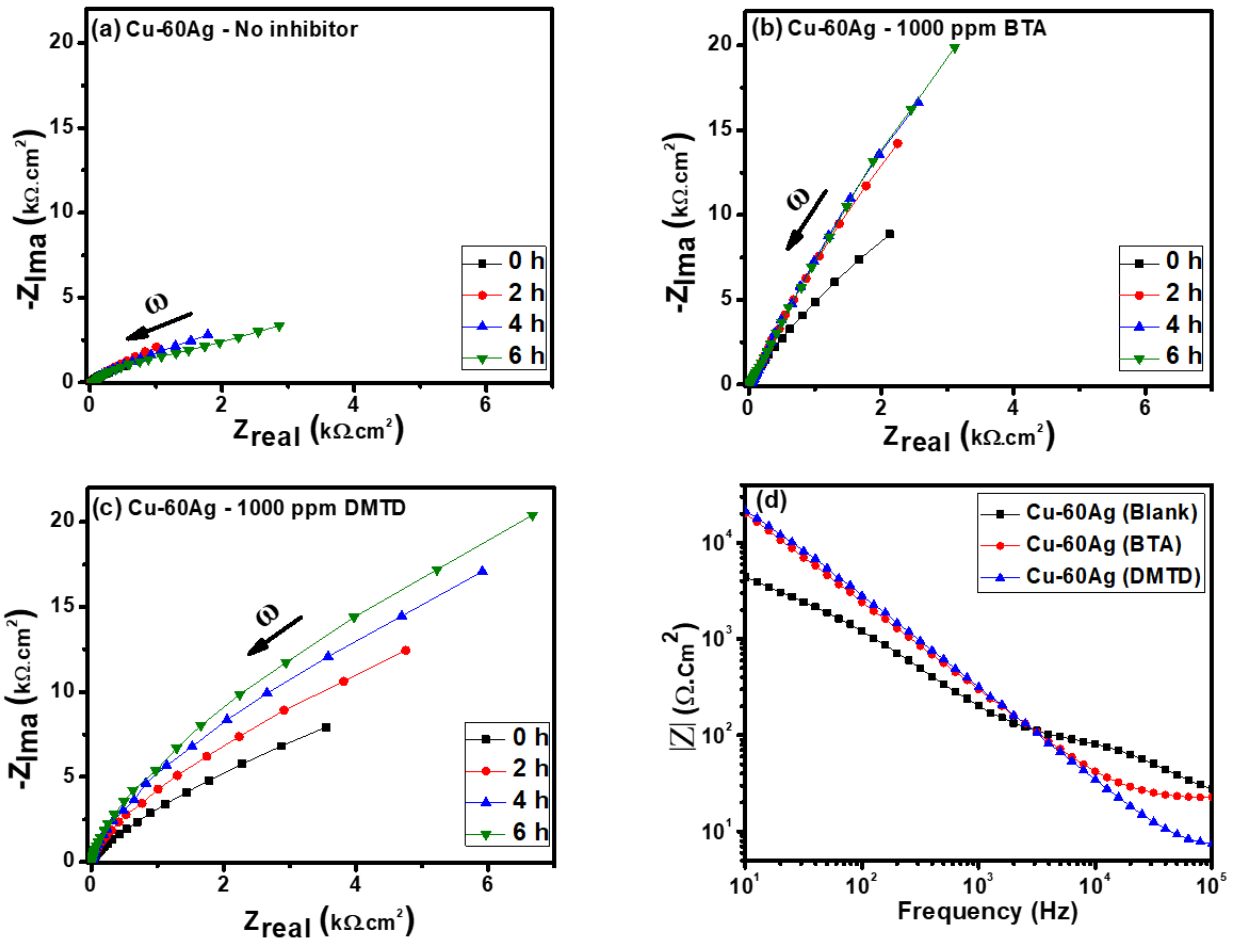

Figure 4-15. Temporal evolution of Nyquist plots for Cu-60Ag in 0.1 M KNO_3 electrolyte containing (a) no inhibitor, (b) 1000 ppm BTA and (c) 1000 ppm DMTD. Corresponding Bode plots are shown in (d).

The equivalent circuits in Figures 4-16(a) and (b) were used to fit the impedance responses for the pure metals, and the Cu-60Ag alloy, respectively. The utilized circuit models showed the least errors in fittings and were also judged by a chi-square value of $\chi^2 \leq 10^{-4}$ representing high accuracy of the fitted data [37,49]. Figure 4-17 exemplifies the high precision of the fitted data. R_s

is the solution resistance and was almost constant with time for each condition in the absence and presence of the inhibitors. This is consistent with reported negligible R_s variations [108]. In the absence of the inhibitors, solution resistance was around 24 $\Omega.cm^2$ owing to the mere effect of KNO_3 in the electrolyte, while addition of 10^3 ppm BTA slightly shifted it down to around 20 $\Omega.cm^2$ upon the separation of the hydrogen cations from pyrrolic nitrogen. In the presence of 10^3 ppm DMTD, R_s was found to be around 18 $\Omega.cm^2$ due to the breakdown of H-S bonding from the thiol anchoring groups of the inhibitor in the electrolyte. It is well established in the literature that solution resistance is dependent on the inhibitor concentration, type of ions, temperature, and geometry of electrodes in the bulk solution and all of which were kept constant over time in the measurements for each condition [16,19,24,28]. Therefore, no significant fluctuation was observed for the R_s values over time.

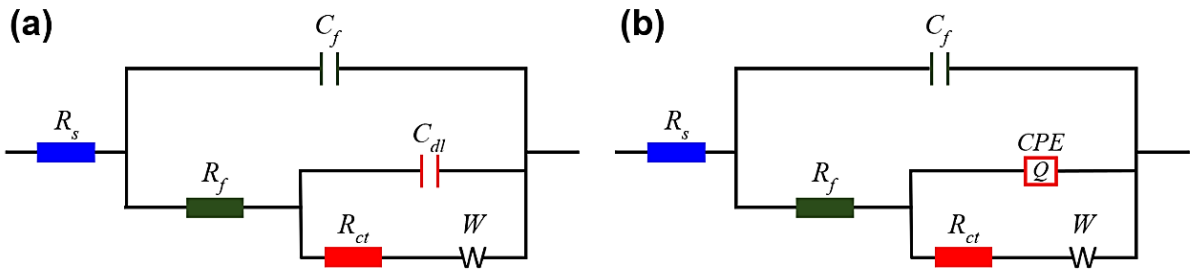

Figure 4-16 Equivalent circuit models for (a) the pure elements (b) for the Cu-60Ag alloy (b). Refer to the text for definition of the circuit elements.

Figures 4-18, 4-19, and 4-20 demonstrate changes of charge transfer resistance (R_{ct}), film resistance (R_f), double layer capacitance (C_{dl})/constant-phase-element (Q_{CPE}), and film capacitance (C_f) over time. In the absence of the inhibitors, "film" represents the formed oxide on the metal surfaces, while in the presence of the inhibitors, it stands for the formed organometallic protective film. Results show that R_{ct} and R_f have been significantly increased especially after 2 hours in the presence of the inhibitors except for Ag in the presence of BTA. The rather minor perturbations in the two resistance elements in this case is consistent with the weak interaction of the Ag surface with BTA.

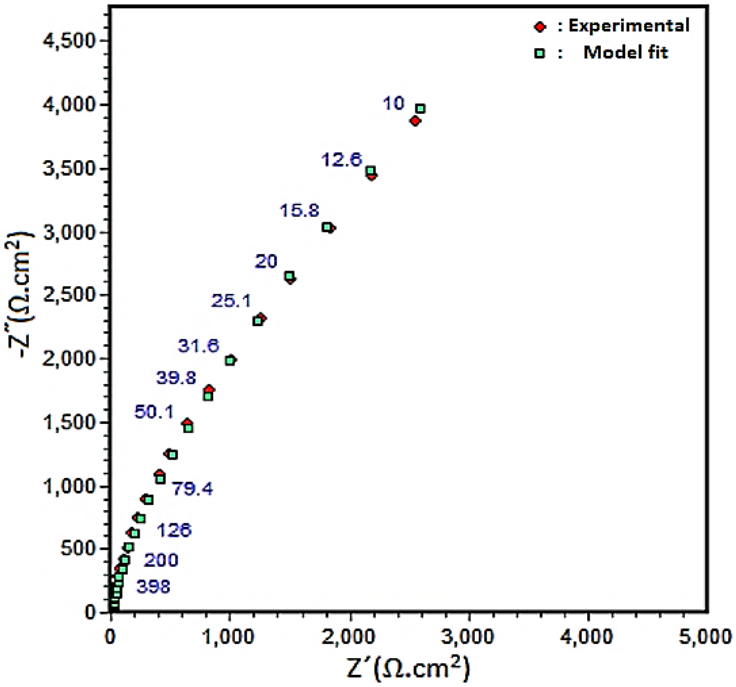

Figure 4-17. Representative ZSimpWin fit of EIS data for Ag in 1000 ppm BTA/0.1 M KNO_3 after 6-h immersion. The equivalent circuit model used for the fit is presented in Figure 4-16(a); the fit is just shown here for illustrative purposes only. The chi-square value for this fit was 4×10^{-4}. The numbers in blue are the AC signal frequency in Hz.

What about the changes in capacitive circuit element values with time? There is a notable reduction in the C_{dl}/Q_{CPE} and C_f confirming the effective inhibition of BTA and DMTD for the metals studied. This is in accordance with previously reported results [12,109,110]. Regarding the Cu-60Ag alloy, the C_{dl} is substituted with a constant-phase-element (CPE) upon the heterogeneity of the surface caused by the distinction in the nature of the formed oxides/protective films on the alloy surface. This inhomogeneity provides a non-ideal capacitive behavior ascribed to the difference in the oxides'/inhibiting films' dielectric constant [15,33]. Impedance of a CPE is obtained through Equation (4-6) [10,90,111,112]:

$$Z_{CPE} = [Q(j\omega)^n]^{-1} \qquad (4\text{-}6)$$

where Q represents CPE constant or amplitude, j is the imaginary root $(j^2 = -1)$, ω the angular frequency, and n is known as the deviation index or CPE power reflecting the degree of surface inhomogeneity [33,95,113,114]. The deviation exponent has a value of $-1 \le n \le 1$. An $n=1$ denotes

a pure capacitor, *n=0* represents a pure resistor, and *n=-1* implies a pure inductor [94,115,116]. However, when n≠-1, 0, 1 it signifies that the system is in possession of a behavior related to surface heterogeneity arising from different reasons such as changes in the conductivity of the formed layer on the surface, distinction on the type of the formed oxide or porosity, heterogeneous adsorption of inhibitors, etc., as noted above [94,111,112]. In addition, as per the Helmholtz model, C_{dl} and C_f can be expressed as follows [96,116,117]:

$$C_{dl} = \varepsilon^{o}\varepsilon\frac{S}{d} \tag{4-7}$$

$$C_{f} = \frac{F^{2}S}{4RT} \tag{4-8}$$

where ε^{o} and ε are the air dielectric permittivity constant and double layer local dielectric constant, respectively. *S* stands for the uninhibited metal/working electrode surface area exposed to the bulk solution, *d* is the double layer thickness, *F* Faraday's constant, *T* temperature, and *R* the universal gas constant [97,118,119]. Replacement of water molecules on the surface of the metals with BTA and DMTD molecules leads to a decline in the dielectric permittivity, and adsorption of the inhibitors increases the double layer thickness caused by the larger size of BTA and DMTD molecules compared to H_2O molecule. In addition, the metal surface area exposed to the solution has decreased [97,116,117]. Therefore, in view of Equation (4-7), these contributing factors have led to a downward trend for the double layer capacitance and CPE constant, accompanied by an upward trend for the film resistance and charge transfer resistance in the presence of the inhibitors through the passage of time. Besides, as per Equation (4-8), reduction of the exposed metal surface area to the bulk solution has also resulted in significant film capacitance reduction in the presence of BTA and DMTD over time. All of which confirming the positive inhibition of the utilized inhibitors on the studied metals.

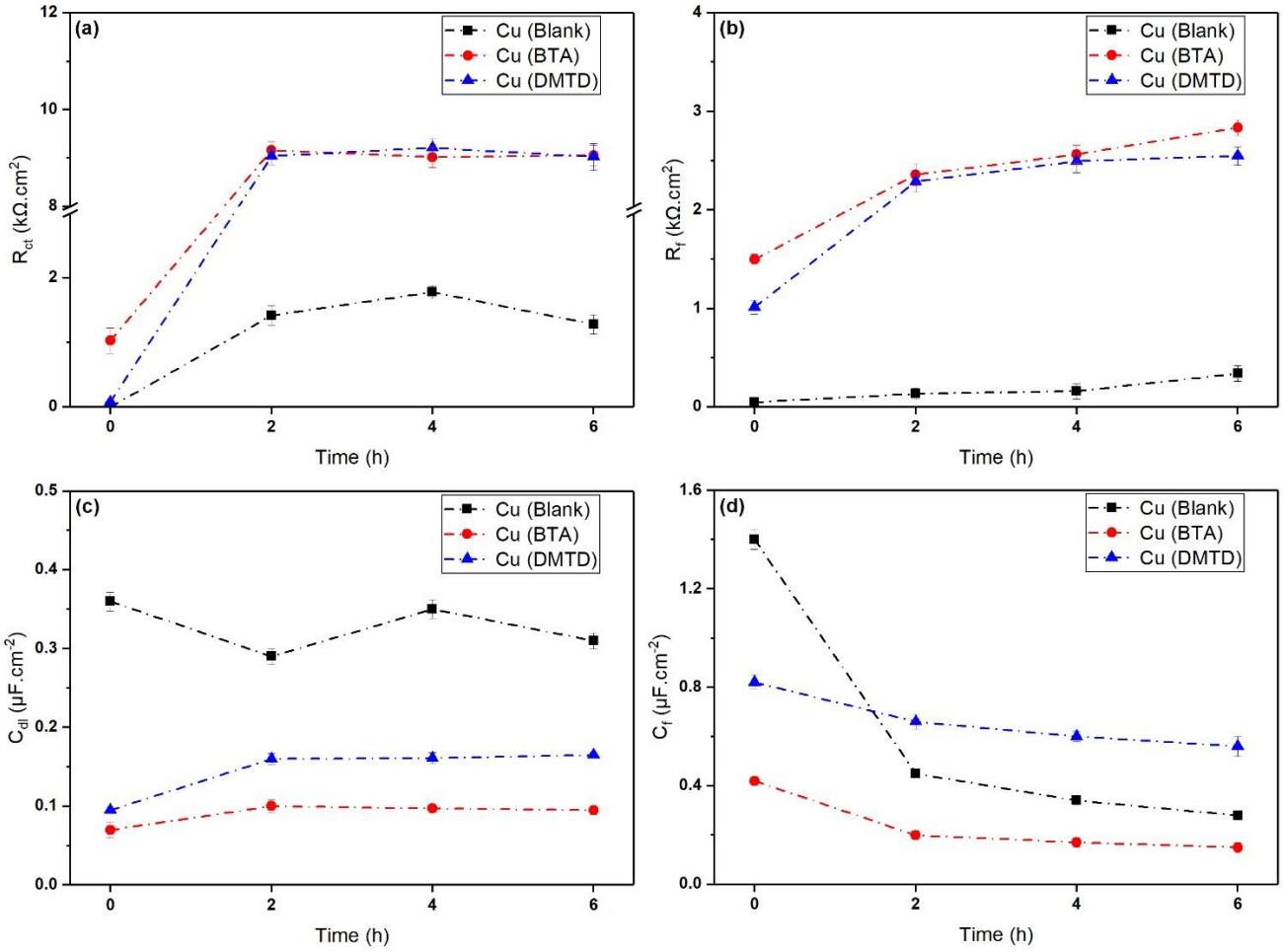

Figure 4-18. Temporal evolution of the equivalent circuit elements for Cu. Values for the circuit elements were obtained from ZSimpWin fits of EIS data as in Figure 4-17. The error bars denote one standard deviation from replicates.

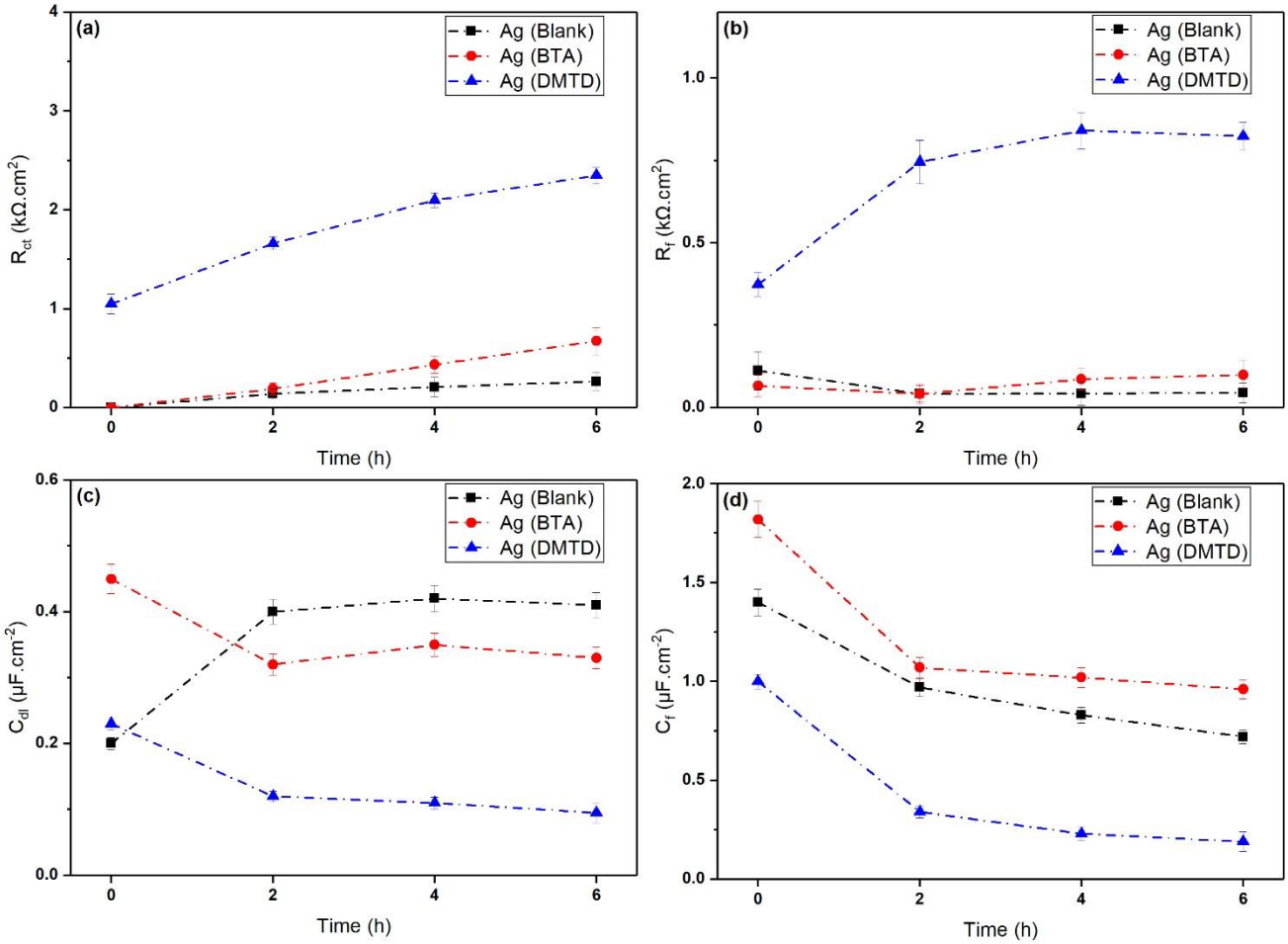

Figure 4-19. Temporal evolution of the equivalent circuit elements for Ag. Values for the circuit elements were obtained from ZSimpWin fits of EIS data as in Figure 4-17. The error bars denote one standard deviation from replicates.

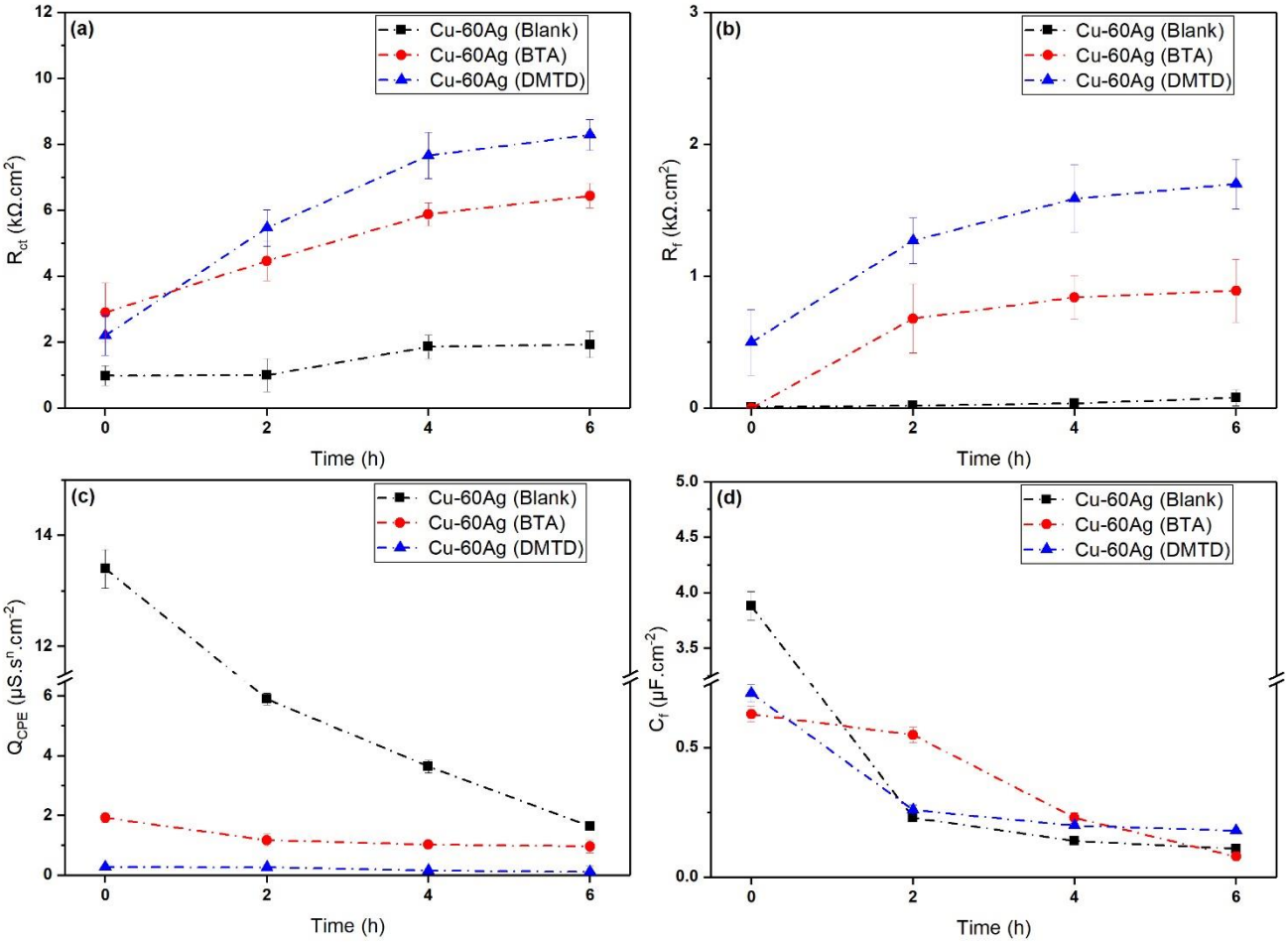

Figure 4-20. Temporal evolution of the equivalent circuit elements for Cu-60Ag. Values for the circuit elements were obtained from ZSimpWin fits of EIS data as in Figure 4-17. The error bars denote one standard deviation from replicates.

Table 4-6. Electrochemical impedance spectroscopy data after 6-h immersion in the absence and presence of 10^3 ppm BTA, and DMTD. The η´ is derived from the potentiodynamic polarization method.

	R_p (kΩ.cm^2)	C_{dl} (μF.cm^{-2})/Q_{CPE} (μS.s^n.cm^{-2})	n	W (μS.s$^{0.5}$.cm^2)	η_{6h} (%)	η_{2h} (%)	η_{4h} (%)	η' (%)
Cu (Blank)	1.61	0.31	1.00	16.9	-	-	-	-
Cu (BTA)	11.89	0.09	1.00	9.40	86.4	86.5	83.2	97.9
Cu (DMTD)	11.51	0.16	1.00	9.91	86.0	86.3	83.4	82.6
Ag (Blank)	0.30	0.41	1.00	35.1	-	-	-	-
Ag (BTA)	0.77	0.33	1.00	20.6	61.0	21.7	50.9	44.5
Ag (DMTD)	3.17	0.09	1.00	12.0	90.5	92.5	91.4	68.0
Cu-60Ag (Blank)	2.00	1.64	0.86	28.4	-	-	-	-
Cu-60Ag (BTA)	7.33	0.97	0.83	16.8	72.7	80.1	71.8	65.6
Cu-60Ag (DMTD)	9.99	0.12	0.79	9.29	80.0	84.8	79.5	66.2

Table 4-6 shows a summary of the extracted EIS data after 6-h immersion in the absence and presence of BTA and DMTD. Polarization resistance and inhibition efficiencies were calculated using Equation (4-9) and (4-10), respectively [44,70,77]:

$$R_p = R_{ct} + R_f \tag{4-9}$$

$$\eta = \frac{R_p - R_p^o}{R_p} \times 100 \tag{4-10}$$

where R_p^o and R_p is the polarization resistance in the absence and presence of the inhibitor, respectively. It is instructive to compare the values for η in Table 4-6 with those derived from corrosion rate data in the presence and absence of the inhibitor. Such values for η' are shown for comparison in the last column in Table 4-6. While comparison of the absolute values is complicated by the fact that η and η' are obtained from small-signal and large-signal perturbation techniques respectively, the relative trends in the two sets of values are internally consistent. In addition, no definitive trend is observed in the variation of inhibition efficiency derived from EIS responses over time as shown in this Table.

The data clearly show the notable increase in polarization resistance, synchronized with significant reduction in double layer capacitance/CPE constant and Warburg impedance verifying

the effective inhibition of BTA and DMTD. BTA is showing a somewhat better inhibition on the Cu surface compared to DMTD. Results imply that the Cu-N bonding on the BTA-treated surface can somehow better protect the Cu-rich phase compared to the Cu-S bonding that can be obtained with DMTD-modified surfaces. This is especially verified by the higher impedance and polarization resistance of Cu with BTA at the low frequency range illustrated in Figure 4-13(d) and Table 4-6, respectively. Furthermore, DMTD is showing a strong inhibiting effect on Ag with over 90% inhibition efficiency in the specific environment. In fact, the thiol *S* from the mercapto functional group with higher electron donating ability compared to *N*, along with the DMTD's pyrrolic *N* have provided a decent charge on the inhibitor anchoring groups. This could have raised the odds and strength of adsorption on the Ag surface [17]. A process that has resulted in the formation of a strong protective film capable to efficiently block the electrochemical reactions [40]. This has been verified in Figure 4-14(d), and Table 4-6 given the significant increase of the polarization resistances. However, inhibition efficiency can be induced by other factors including electronic structure, the lateral interaction between the adsorbed molecules and homogeneity of the protective film, etc. [41]. Therefore, probably the weaker lateral interaction of the adsorbed BTA molecules on the Ag-rich phase compared to DMTD, could be another reason for the lower inhibition efficiency of BTA on this phase.

4. 3. XPS Measurements

High resolution XPS spectra of BTA-treated pure Cu and Ag are shown in Figures 4-21 and 4-22. These measurements were carried out to explore the chemical state of the BTA interaction with Cu and Ag surface. The Cu $2p_{3/2}$ high resolution peak has three components at binding energies of 932.7, 932.5, and 934.8 eV corresponding to metallic Cu [5,49], Cu_2O [46,120], and inhibitive film (the Cu-BTA organometallic complex) [5,84], respectively. Oxidation of copper is unavoidable while is exposed to open atmosphere [11]. Formation of a thin layer of the inhibitive film is in agreement with the results from the electrochemical response. N 1s was recorded at binding energy of 399.7 eV consistent with binding energy of pyrrolic nitrogen [121,122] from the azole ring of the inhibitor. It is well established in the literature that carbon-containing compounds can be adsorbed on the metal surfaces, be oxidized during the sample preparation and exposure to air, and eventually appear in the XPS spectra [105,123]. That is why

O 1s exhibits three components of Cu_2O at 530.3 eV, oxidized carbon compounds (contaminants) at 531.7 eV, and partly oxidized Cu-BTA complex at 532.8 eV [5]. C 1s also involves two components of adventitious carbon compounds [11] at 284.5 eV [120] and carbon in the inhibitor structure at 286 eV [5]. Thus, the XPS results show the formation of Cu-BTA protective complex which is consistent with the electrochemical results.

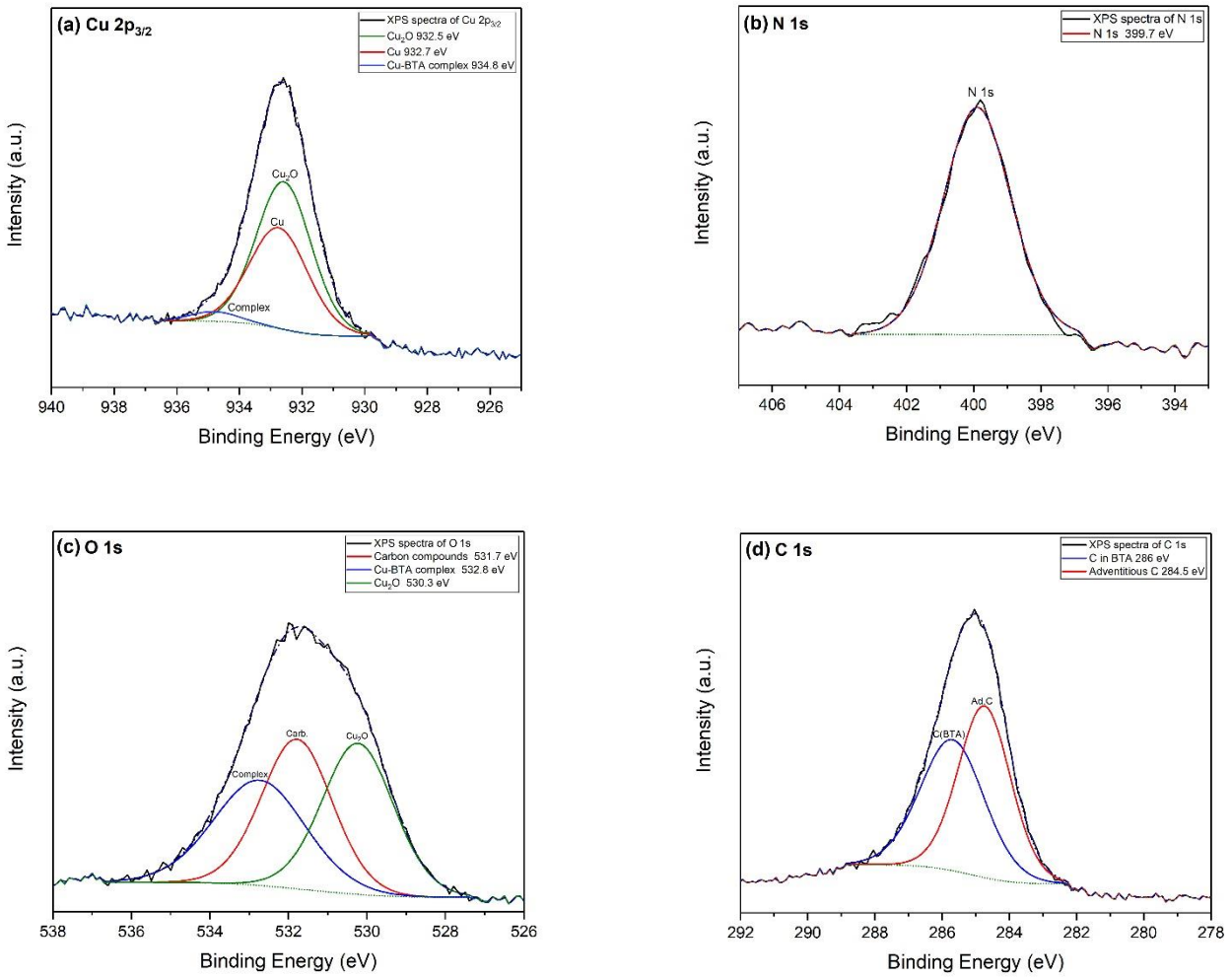

Figure 4-21. XPS high-resolution spectra of (a) Cu $2p_{3/2}$, (b) N 1s, (c) O 1s, and (d) C 1s for Cu after 10 min immersion in DI water with 1000 ppm BTA.

Figure 4-22 presents the high-resolution spectra for the Ag BTA-treated sample. The Ag 3d peaks show three components of metallic Ag, Ag-O, and Ag-N at binding energies of 368.2

[120,124,125], 367.5 [120,125,126] and 366.9 eV [126], for the Ag $3d_{5/2}$ peaks as well as 374.2 [127,128], 373.5 and 372.9 eV [126] for the Ag $3d_{3/2}$ peaks, respectively. Much the same as for Cu, exposure to the ambient has led to the bonding between Ag and O. Nonetheless, there is no previous XPS study reporting Ag-N binding from BTA treatment as an indication of formation of the protective film. Moreover, the N 1s peak is at binding energy of 399.5 eV showing a slight shift (0.2 eV) to lower binding energy compared to N 1s on Cu. This can be attributed to the different electronegativity of these two metals providing a different binding energy [129]. Given the fact that the probable different arrangement of BTA on the surface of these metals and whether the bonding is through N_1 and/or N_3 atom(s) [7] of the triazole ring, could have also indirectly influenced the N 1s peak's location and shape and has resulted in such a slight shift. The O 1s peak also involves three components of oxidized carbon compounds from the contaminants, Ag-O from the exposure of the metal to open atmosphere, and partly oxidized Ag-BTA complex from development of the inhibitive film in the presence of oxygen at 531.7 [5], 530.1 [120], and 533.2 eV, respectively. The C 1s has two components of adventitious carbon compounds at 284.5 eV and ca

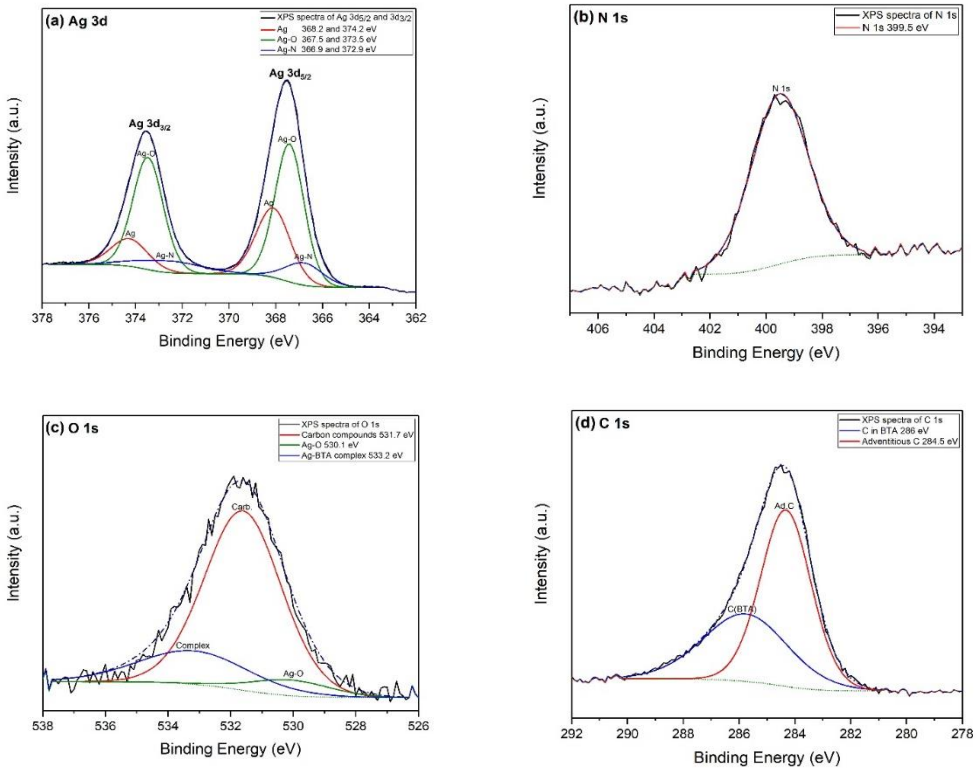

Figure 4-22. XPS high-resolution spectra of (a) Ag 3d, (b) N 1s, (c) O 1s, and (d) C 1s for Ag after 10 min immersion in DI water with 1000 ppm BTA.

Figures 4-23 and 4-24 show high-resolution XPS spectra of DMTD-treated pure Cu and Ag, respectively. These experiments were carried out to explore the chemical state and nature of the formed bonds on the metal surfaces interacting DMTD. The $Cu2p_{3/2}$ peak comprises three components including metallic Cu at 932.7 eV [5,49,92], Cu_2O at 932.5 eV [120,130], and the Cu-DMTD organometallic complex at 934.4 eV. It is well established in the literature that the exocyclic mercapto group (-SH) of thiadiazole derivatives can be polymerized via the Cu^+ ion and form a one-dimensional polymer chain or even just an infinite monolayer on the copper surface [103,104]. Formation of a thin organometallic film is consistent with the electrochemical responses illustrated in Figure 4-9(b). Presence of copper oxide is inevitable and could be due to sample preparation, drying procedure, or transfer to the spectrometer. All of which have exposed the sample to open atmosphere [11]. According to Figure 4-23(b), the N1s bonding energy is at 398.8 eV corresponding to 3- and 4- positions of pyrrolic nitrogen $(-N=)$ from the DMTD's azole ring [90,131,132]. In contrast with Cu-BTA interaction mechanism [92], DMTD did not show any bonding from its N tail with the Cu surface. This can be a plausible reason for the lower inhibition efficiency of DMTD compared to BTA on Cu. The O1s spectrum presented in Figure 4-23(c), shows the presence of Cu_2O at 530.3 eV [5], oxidized carbon compounds at 531.7 eV [92], and partially oxidized Cu-DMTD organometallic complex at a binding energy of 533.4 eV [132]. As demonstrated in Figure 4-23(d), C1s involves three components of adventitious carbon compounds at 284.5 eV [120], (C=N) at 286.7 eV [133], and (C-S) at 285.6 eV [134] where the two latter of which are from the DMTD molecule. As noted above, the presence of all O1s components, and adventitious carbon compounds appeared under the C1s spectra are related to the exposure of the sample to open atmosphere during different stages of lab work [123]. As shown in Figure 4-23(e), the S2p spectrum was deconvoluted into four peaks. These are the $S2p_{3/2} \equiv 161.4$ eV, and $S2p_{1/2} \equiv 162.3$ eV [135], corresponding to (S-Cu) from the thiol anchoring group, as well as $S2p_{3/2} \equiv 163.4$ eV, and $S2p_{1/2} \equiv 164.9$ eV ascribed to (S-C) from the lone thiophene sulfur in DMTD molecule [120,136]. As discussed above, the two exocyclic thiol sulfurs of DMTD have the affinity to bond with the Cu surface to form a thin protective film [103,104]. Thus, XPS results show the formation of the Cu-DMTD organometallic film through the bonding between Cu and S atoms present in the inhibitor's thiol group (-SH) corresponding to 2- and 5- positions of its azole ring in DI water. This is in full agreement with the electrochemical surveys. In addition, no evidence was found about any plausible bonding between DMTD's pyrrolic nitrogen atoms and the Cu surface.

Figure 4-24 shows the high-resolution XPS spectra for the DMTD-treated pure Ag sample. The Ag3d spectra were deconvoluted into four distinct components corresponding to metallic Ag at binding energies of 368.2 [120,124,125] and 374.2 eV [127,128], (Ag-O) at 367.5 [120,125] and 373.5 eV [126], (Ag-N) at 366.9 and 372.9 eV [92,126], and (Ag-S) at 368.0 and 374.0 eV [120,137] for $Ag3d_{5/2}$ and $Ag3d_{3/2}$, respectively. Similar to that for Cu, bonding between Ag and O is due to exposure to open atmosphere. Results show that DMTD has formed bonding with Ag through its S and N atoms. Therefore, the higher inhibition efficiency of DMTD on Ag compared to BTA, demonstrated in Figure 4-10, can be attributed to the simultaneous involvement of S and N atoms in the adsorption process. Regarding the Ag-BTA interaction, the protective film only bonds through its N tail to the Ag surface [92]. As shown in Figure 4-24(b), the N1s peak involves two components of (N-Ag) at 397.8 eV [126], and pyrrolic nitrogen at 398.8 eV from DMTD, similar to what observed for Cu [90,131,132]. The O1s spectrum illustrated in Figure 4-24(c) was deconvoluted into oxidized carbon compounds from contaminants, along with (Ag-O) and partially oxidized Ag-DMTD organometallic complex coming from exposure to the ambient at 531.7 eV [5], 530.1 eV [120], and 532.3 eV, respectively. As presented in Figure 4-24(d), C1s has three constituent of adventitious carbon compounds at 284.5 eV [120], along with (C=N) at 286.7 eV [133], and (C-S) at 285.9 eV from the DMTD molecule. The (C-S) bond from DMTD's azole ring on Ag is with a slight shift (0.3 eV) to higher binding energies compared to that on Cu. This is ascribed to the different adsorption behavior and involved charge state of DMTD on Ag compared to Cu with a different electronegativity [129]. The S2p spectrum, shown in Figure 4-24(e), involves two components of (S-Ag) at 161.8 eV and 163.0 eV [138] attributed to the thiol sulfur bonded with Ag [104], as well as (S-C) at 163.4 eV and 164.9 eV from the thiophene sulfur bonded with carbon from the inhibitor [120,136]. Therefore, the XPS results show the development of a protective Ag-DMTD organometallic complex film on the Ag surface through Ag atoms bonding with pyrrolic N and exocyclic thiol S from the inhibitor. This is consistent with the electrochemical findings shown in Figure 4-9(a). It is also a plausible reason for the higher inhibition efficiency of DMTD compared to BTA for Ag, as discussed above.

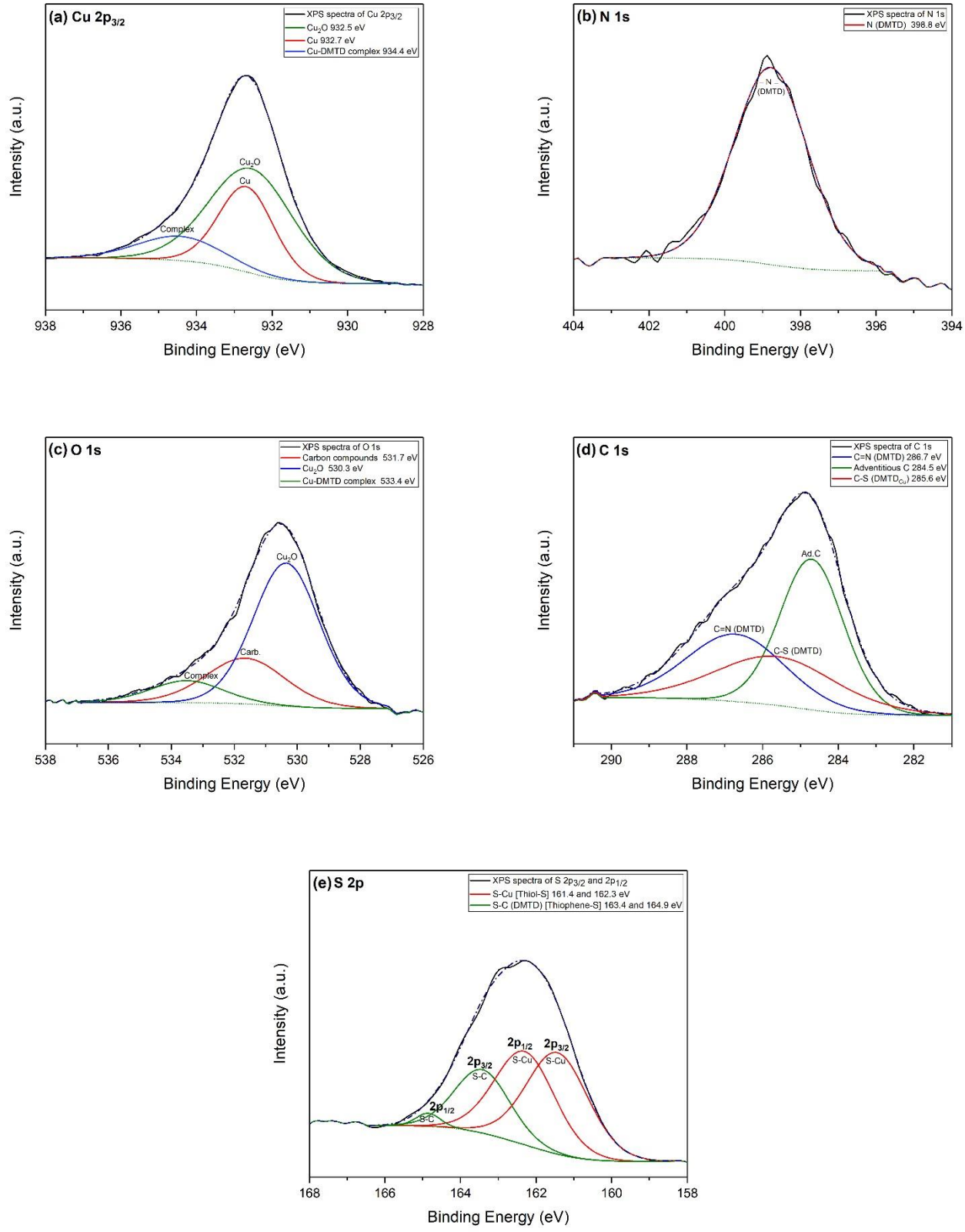

Figure 4-23. XPS high-resolution spectra of (a) Cu $2p_{3/2}$, (b) N 1s, (c) O 1s, (d) C 1s, and (e) S 2p for Cu after 10 min immersion in DI water with 1000 ppm DMTD.

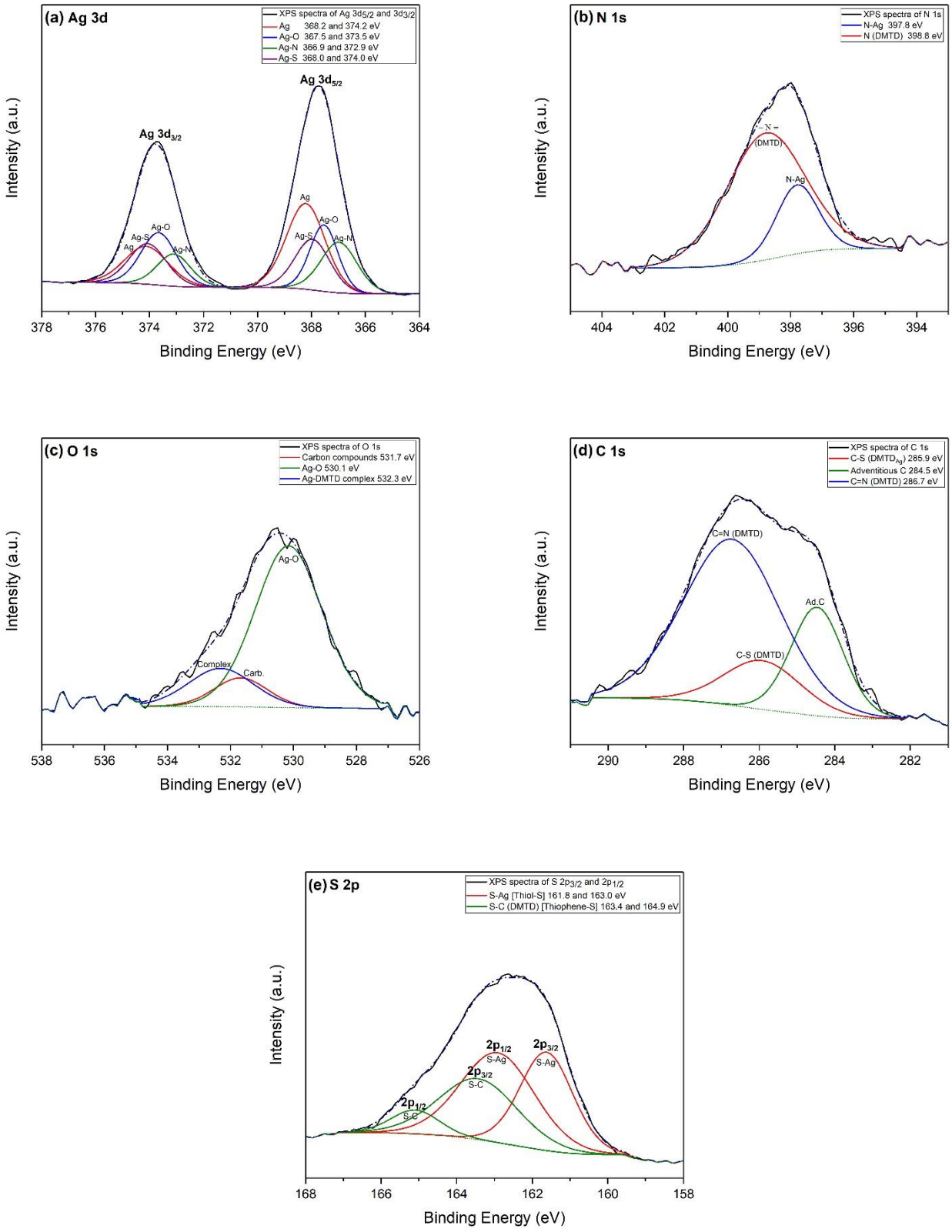

Figure 4-24. XPS high-resolution spectra of (a) Ag 3d, (b) N 1s, (c) O 1s, (d) C 1s, and (e) S 2p for Cu after 10 min immersion in DI water with 1000 ppm DMTD.

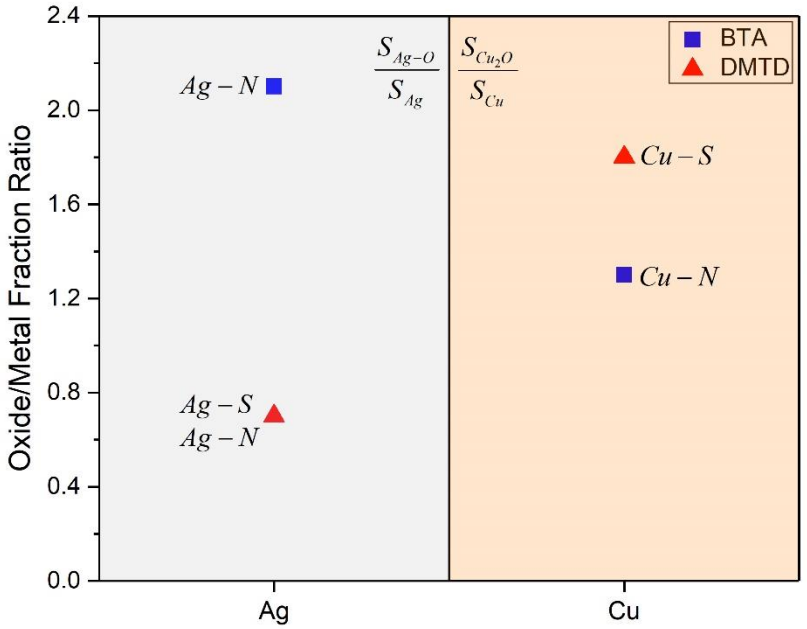

Figure 4-25. An estimate of the oxide/metal fraction ratio for Ag and Cu in the presence of BTA and DMTD and the formed chemical bonding with the inhibitors acquired from XPS measurements.

Figure 4-25 compares the approximate surface oxide/metal fraction ratios acquired from the XPS high-resolution peaks from the of BTA-treated and DMTD-modified specimens. It also demonstrates the type of chemical bonds each metal has formed with the inhibitors. Considering each individual metal, these results imply that the inhibitor producing a lower oxide/metal ratio has also provided a higher surface coverage and inhibition efficiency. This would seem natural since most of the oxide would have formed after electrochemical testing during exposure to atmosphere. For example, DMTD for Ag, and BTA for Cu, has less oxide/metal fraction ratio consistent with higher inhibition efficiency and stronger inhibitor adsorption behavior, i.e., merely chemisorption. However, comparing the oxide/metal fraction in the presence of each individual inhibitor on different metals is not an appropriate method to infer the prohibitive behavior. Particularly, when an inhibitor forms different type and number of bonding with different metals (e.g., in case of DMTD), the oxide/metal fraction is not a valid criterion in determining the inhibition efficiency.

Chapter 5 Conclusions

5. 1. Conclusions

The corrosion behavior of pure Cu, pure Ag, Cu-60Ag and Cu-6Ag alloys was studied in DI water in the absence and presence of benzotriazole. Results show that BTA shifts the corrosion potential of Cu to the noble direction but has the opposite effect for Ag. For the alloys, a mixed quantitatively-induced behavior was observed implying a competition between the α and β phases in interacting with BTA. BTA was found to decrease the corrosion rate of Cu and high Cu alloy by more than one order of magnitude while it resulted in a much lower decrease for the Ag and the brazing Cu-60Ag alloy. As a result, a high inhibition efficiency (around 95%) was obtained for Cu and the Cu-6Ag alloy. Only a lower inhibition effect was observed for Ag and the brazing alloy.

Corrosion inhibition and adsorption behavior of BTA and DMTD was studied on pure Ag, pure Cu, and Cu-60Ag alloy in DI water. Results show that BTA has a very good coverage on the Cu-rich phase, and DMTD provides a much better inhibition efficiency for the Ag-rich phase. In addition, combining the two inhibitors demonstrates a promising increment in the efficiency of the Cu-Ag alloy. This was attributed to fact that the inhibition of α phase with BTA is synchronized with the appropriate coverage of the β phase with DMTD, together blocking the electrochemical reactions on the alloy.

Adsorption isotherm investigations revealed that BTA follows Langmuir adsorption isotherm while DMTD obeys Temkin adsorption isotherm for the metals studied. This shows the

distinct adsorption mechanism of these two inhibitors on the metal surfaces. Also, it was found that BTA chemisorbs on Cu, but with respect to Cu-60Ag alloy and Ag, it shows a combination of chemisorption and physisorption behavior consistent with the observed reductions in inhibition efficiencies. Moreover, DMTD showed chemisorption towards all the three metals, having standard free energies of adsorption values following the same trend as acquired with the inhibition efficiencies ($\eta_{Cu} > \eta_{Cu\text{-}60Ag} > \eta_{Ag}$), much the same as for BTA. Transition from the adsorption mechanism observed with BTA as partially chemisorbed/ partially physisorbed to the stronger merely chemisorption of DMTD on the Ag surface was recognized as a possible reason for the higher inhibition efficiency of DMTD on Ag.

XPS results of BTA-treated samples were compared with DMTD-modified specimens. Results showed the formation of Cu- and Ag-BTA organometallic complexes through the N tail of the inhibitor. In addition, the measurements show the formation of Cu-DMTD protective film through the (Cu-S) bonding with the exocyclic thiol S of DMTD. However, the (Cu-N) bonding of Cu-BTA film seems more favorable to cover the Cu surface. Results also demonstrate the development of Ag-DMTD organometallic complex through the (Ag-S) bonding with the mercapto/thiol S anchoring site as well as (Ag-N) bonding. The involvement of DMTD's two anchoring sites with Ag surface led to higher inhibition efficiency compared to BTA. Having less oxide/metal fraction ratio on each individual metal in the presence of inhibitors was in accordance with higher inhibition efficiency leaving less uncovered surface area to be exposed to the aerated environment.

The temporal changes in the EIS Nyquist profiles or Bode plots seen in the present study, were useful for gauging the relative efficacy of the two organic additives for passivation of Cu, Ag, or Cu-60Ag alloy surfaces. Diagnostics furnished by the Nyquist and Bode EIS profiles were shown to reaffirm the importance of passivating film formation in the inhibition. Further advances in the fundamental, atomic level understanding of how the two inhibitors work on these metal surfaces would require the development of operando measurement tools that in turn facilitate real time correlation of the changes in the interfacial chemistry with structural/morphological alterations. Admittedly, EIS is handicapped in this regard and must be supplemented in its use by other interfacial probes.

References

[1] A. Kokalj, S. Peljhan, M. Finšgar, I. Milošev, What determines the inhibition effectiveness of ATA, BTAH, and BTAOH corrosion inhibitors on copper?, J. Am. Chem. Soc. 132 (2010) 16657–16668. doi:10.1021/ja107704y.

[2] M. Finšgar, I. Milošev, Inhibition of copper corrosion by 1,2,3-benzotriazole: A review, Corros. Sci. 52 (2010) 2737–2749. doi:10.1016/j.corsci.2010.05.002.

[3] F. Grillo, D.W. Tee, S.M. Francis, H. Früchtl, N. V. Richardson, Initial stages of benzotriazole adsorption on the Cu (111) surface, Nanoscale. 5 (2013) 5269–5273. doi:10.1039/c3nr00724c.

[4] M. M. Antonijevic and M. B. Petrovic, Copper Corrosion Inhibitors. A review, Int. J. Electrochem. Sci. 3 (2008) 1–28. http://www.electrochemsci.org/papers/vol3/3010001.pdf.

[5] K. Mansikkamäki, U. Haapanen, C. Johans, K. Kontturi, M. Valden, Adsorption of Benzotriazole on the Surface of Copper Alloys Studied by SECM and XPS, J. Electrochem. Soc. 153 (2006) B311–B318. doi:10.1149/1.2208912.

[6] S. Thomas, S. Venkateswaran, S. Kapoor, R. D'Cunha, T. Mukherjee, Surface enhanced Raman scattering of benzotriazole: A molecular orientational study, Spectrochim. Acta - Part A Mol. Biomol. Spectrosc. 60 (2004) 25–29. doi:10.1016/S1386-1425(03)00213-0.

[7] S. Naumov, S. Kapoor, S. Thomas, S. Venkateswaran, T. Mukherjee, SERS of benzotriazole on Ag colloid: Surface structure characterization using the DFT approach, J. Mol. Struct. 685 (2004) 127–131. doi:10.1016/j.theochem.2004.06.026.

[8] E.J. Ahn, J.J. Kim, Additives for Superconformal Electroplating of Ag Thin Film for ULSIs, Electrochem. Solid-State Lett. 7 (2004) C118–C120. doi:10.1149/1.1793811.

[9] T. Notoya, M. Satake, T. Ohtsuka, H. Yashiro, M. Sato, T. Yamauchi, D.P. Schweinsberg,

Structures of metal-benzotriazole films on copper and other metals, J. Corros. Sci. Eng. 6 (2003) 1–10. http://www.jcse.org/volume6/preprints/v6preprint31.pdf.

[10] M.E. Orazem, N. Pébère, B. Tribollet, Enhanced Graphical Representation of Electrochemical Impedance Data, J. Electrochem. Soc. 153 (2006) B129–B136. doi:10.1149/1.2168377.

[11] M. Finšgar, D. Kek Merl, An electrochemical, long-term immersion, and XPS study of 2-mercaptobenzothiazole as a copper corrosion inhibitor in chloride solution, Corros. Sci. 83 (2014) 164–175. doi:10.1016/J.CORSCI.2014.02.016.

[12] T. Kosec, D.K. Merl, I. Milošev, Impedance and XPS study of benzotriazole films formed on copper, copper–zinc alloys and zinc in chloride solution, Corros. Sci. 50 (2008) 1987–1997. doi:10.1016/J.CORSCI.2008.04.016.

[13] A.S.H. Makhlouf, V. Herrera, E. Muñoz, Corrosion and protection of the metallic structures in the petroleum industry due to corrosion and the techniques for protection, in: Handb. Mater. Fail. Anal., Elsevier, 2018: pp. 107–122. doi:10.1016/B978-0-08-101928-3.00006-9.

[14] R.W. Revie, H.H. Uhlig, Corrosion and Corrosion Control: An Introduction to Corrosion Science and Engineering, Fourth, John Wiley & Sons, Inc., Hoboken, New Jersey, 2008. doi:10.1002/9780470277270.

[15] P.R. Roberge, Corrosion Engineering Principles and Practice, McGraw-Hill Companies, Inc., New York City, New York, 2008.

[16] R.W. Revie, Uhlig's Corrosion Handbook, Third, John Wiley & Sons, Inc., Hoboken, New Jersey, 2011. doi:10.1002/9780470872864.

[17] E. Mccafferty, Introduction to Corrosion Science, Springer, New York City, New York, 2010. doi:10.1007/978-1-4419-04553.

[18] E.E. Stansbury, R.A. Buchanan, R.M. Condra, Fundamentals of Electrochemical Corrosion, ASM International, Materials Park, Ohio, 2000.

[19] M. Fontana, Corrosion Engineering, Third, McGraw-Hill, New York City, New York, 1987.

[20] A. Kvryan, K. Livingston, C.M. Efaw, K. Knori, B.J. Jaques, P.H. Davis, D.P. Butt, M.F. Hurley, Microgalvanic corrosion behavior of cu-Ag active braze alloys investigated with SKPFM, Metals (Basel). 6 (2016) 1–17. doi:10.3390/met6040091.

[21] M.K. Lee, J.J. Park, J.G. Lee, C.K. Rhee, Phase-dependent corrosion of titanium-to-stainless steel joints brazed by Ag-Cu eutectic alloy filler and Ag interlayer, J. Nucl. Mater. 439 (2013) 168–173. doi:10.1016/j.jnucmat.2013.04.002.

[22] M.K. Lee, J.J. Park, G.J. Lee, J.G. Lee, D.W. Kim, C.H. Lim, C.K. Rhee, Y.B. Lee, J.K. Lee, S.J. Hong, Corrosion of Ti–STS dissimilar joints brazed by a Ag interlayer and Ag–Cu–(Pd) alloy fillers, J. Nucl. Mater. 409 (2011) 183–187. doi:10.1016/j.jnucmat.2010.12.003.

[23] M. Dighe, Corrosion of Brazed and Soldered Joints, in: ASM Handbook, Vol. 13B Corros. Mater., ASM International, Materials Park, Ohio, 2005: pp. 418–421. doi:10.31399/asm.hb.v13b.a0003831.

[24] ASM International Handbook Committee, ASM Handbook, Volume 13: Corrosion, Ninth, ASM International, Materials Park, Ohio, 1992.

[25] A.M. Aminazad, A.M. Hadian, F. Ghasimakbari, Investigation on Corrosion Behaviour of Copper Brazed Joints, Procedia Mater. Sci. 11 (2015) 672–678. doi:10.1016/j.mspro.2015.11.024.

[26] R. Javaherdashti, K. Alasvand, Why Corrosion and Particularly Microbial Corrosion Are Important?, in: Biol. Treat. Microb. Corros., Elsevier, 2019: pp. 1–9. doi:10.1016/B978-0-12-816108-1.00001-X.

[27] Q. Bai, Y. Bai, Corrosion Prevention and Advanced CP Design, in: Subsea Pipeline Des. Anal. Install., Elsevier, 2014: pp. 451–464. doi:10.1016/B978-0-12-386888-6.00019-5.

[28] P.R. Roberge, Handbook of Corrosion Engineering, McGraw-Hill Companies, Inc., New York City, New York, 2000.

[29] W.S. Tait, Controlling Corrosion of Chemical Processing Equipment, in: Handb. Environ. Degrad. Mater., William Andrew Publishing, Madison, Wisconsin, 2018: pp. 583–600. doi:10.1016/B978-0-323-52472-8.00028-9.

[30] A. Fateh, M. Aliofkhazraei, A.R. Rezvanian, Review of corrosive environments for copper and its corrosion inhibitors, Arab. J. Chem. (2017). doi:10.1016/j.arabjc.2017.05.021.

[31] Z. Tang, A review of corrosion inhibitors for rust preventative fluids, Curr. Opin. Solid State Mater. Sci. 23 (2019). doi:10.1016/j.cossms.2019.06.003.

[32] D.M. Bastidas, E. Cano, E.M. Mora, Volatile corrosion inhibitors: a review, Anti-Corrosion Methods Mater. 52 (2005) 71–77. doi:10.1108/00035590510584771.

[33] U. Rammelt, S. Koehler, G. Reinhard, Use of vapour phase corrosion inhibitors in packages for protecting mild steel against corrosion, Corros. Sci. 51 (2009) 921–925. doi:10.1016/j.corsci.2009.01.015.

[34] C.G. Dariva, A.F. Galio, Corrosion Inhibitors – Principles, Mechanisms and Applications, in: Dev. Corros. Prot., InTech, 2014: pp. 365–379. doi:10.5772/57255.

[35] M. Szociński, K. Darowicki, Assessment of copper surface coverage with corrosion inhibitor using AFM-based local electrical measurements, Corros. Eng. Sci. Technol. 52 (2017) 520–525. doi:10.1080/1478422X.2017.1341221.

[36] J. Baux, N. Caussé, J. Esvan, S. Delaunay, J. Tireau, M. Roy, D. You, N. Pébère, Impedance analysis of film-forming amines for the corrosion protection of a carbon steel, Electrochim. Acta. 283 (2018) 699–707. doi:10.1016/J.ELECTACTA.2018.06.189.

[37] J.M. Bastidas, P. Pinilla, E. Cano, J.L. Polo, S. Miguel, Copper corrosion inhibition by triphenylmethane derivatives in sulphuric acid media, Corros. Sci. 45 (2003) 427–449. doi:10.1016/S0010-938X(02)00123-3.

[38] C. Gattinoni, A. Michaelides, Understanding corrosion inhibition with van der Waals DFT methods: the case of benzotriazole., Faraday Discuss. 180 (2015) 439–458. doi:10.1039/c4fd00273c.

[39] Y. Zhu, M.L. Free, R. Woollam, W. Durnie, A review of surfactants as corrosion inhibitors and associated modeling, Prog. Mater. Sci. 90 (2017) 159–223. doi:10.1016/j.pmatsci.2017.07.006.

[40] L. Guo, I.B. Obot, X. Zheng, X. Shen, Y. Qiang, S. Kaya, C. Kaya, Theoretical insight into an empirical rule about organic corrosion inhibitors containing nitrogen, oxygen, and sulfur

atoms, Appl. Surf. Sci. 406 (2017) 301–306. doi:10.1016/j.apsusc.2017.02.134.

[41] L. Liu, X. Pan, J. Xing, J. Qian, Anti-corrosion behavior of thiadiazole derivatives for silver strip in hydrogen sulfide solutions, Anti-Corrosion Methods Mater. 62 (2015) 353–362. doi:10.1108/ACMM-03-2014-1364.

[42] J.M. Bastidas, P. Pinilla, J.L. Polo, E. Cano, Adsorption of Benzotriazole on Copper Electrode Surfaces in Citric Acid Media, Corrosion. 58 (2002) 922–931. doi:https://doi.org/10.5006/1.3280782.

[43] W.A. Badawy, K.M. Ismail, A.M. Fathi, Corrosion control of Cu-Ni alloys in neutral chloride solutions by amino acids, Electrochim. Acta. 51 (2006) 4182–4189. doi:10.1016/j.electacta.2005.11.037.

[44] H. Gerengi, P. Slepski, G. Bereket, Dynamic electrochemical impedance spectroscopy and polarization studies to evaluate the inhibition effect of benzotriazole on copper-manganese-aluminium alloy in artificial seawater, Mater. Corros. 64 (2013) 1024–1031. doi:10.1002/maco.201206565.

[45] P.F. Khan, V. Shanthi, R.K. Babu, S. Muralidharan, R.C. Barik, Effect of benzotriazole on corrosion inhibition of copper under flow conditions, J. Environ. Chem. Eng. 3 (2015) 10–19. doi:10.1016/j.jece.2014.11.005.

[46] T. Kosec, I. Milošev, B. Pihlar, Benzotriazole as an inhibitor of brass corrosion in chloride solution, Appl. Surf. Sci. 253 (2007) 8863–8873. doi:10.1016/J.APSUSC.2007.04.083.

[47] M. Hosseini, S.F.L. Mertens, M.R. Arshadi, Synergism and antagonism in mild steel corrosion inhibition by sodium dodecylbenzenesulphonate and hexamethylenetetramine, Corros. Sci. 45 (2003) 1473–1489. doi:10.1016/S0010-938X(02)00246-9.

[48] S.A. El Wanees, A.A. El Aal Mohamed, M.A. El Azeem, R. El Said, Inhibition of Silver Corrosion in Nitric Acid by Some Aliphatic Amines, J. Dispers. Sci. Technol. 31 (2010) 1516–1525. doi:10.1080/01932690903294022.

[49] C. Jing, Z. Wang, Y. Gong, H. Huang, Y. Ma, H. Xie, H. Li, S. Zhang, F. Gao, Photo and thermally stable branched corrosion inhibitors containing two benzotriazole groups for copper in 3.5 wt% sodium chloride solution, Corros. Sci. 138 (2018) 353–371.

doi:10.1016/J.CORSCI.2018.04.027.

[50] F.H. Assaf, A.M. Zaky, S.S. Abd El-Rehim, Cyclic voltammetric studies of the electrochemical behaviour of copper–silver alloys in NaOH solution, Appl. Surf. Sci. 187 (2002) 18–27. doi:10.1016/S0169-4332(01)00462-7.

[51] M. Rajčić-Vujasinovic, S. Nestorović, V. Grekulović, I. Marković, Z. Stević, Electrochemical behavior of sintered CuAg4 at. pct alloy, Metall. Mater. Trans. B Process Metall. Mater. Process. Sci. 41B (2010) 955–961. doi:10.1007/s11663-010-9405-1.

[52] E.-S.M. Sherif, Corrosion Behavior of Copper in 0.50 M Hydrochloric Acid Pickling Solutions and its Inhibition by 3-Amino-1,2,4-triazole and 3-Amino-5-mercapto-1,2,4-triazole, Int. J. Electrochem. Sci. 7 (2012) 1884–1897.

[53] F. Cardarelli, Materials Handbook, Third, Springer International Publishing, Cham, Switzerland, 2018. doi:10.1007/978-3-319-38925-7.

[54] P. Vassiliou, V. Gouda, Ancient silver artefacts: corrosion processes and preservation strategies, in: Corros. Conserv. Cult. Herit. Met. Artefacts, Elsevier, 2013: pp. 213–235. doi:10.1533/9781782421573.3.213.

[55] T.E. Graedel, Corrosion Mechanisms for Silver Exposed to the Atmosphere, J. Electrochem. Soc. 139 (1992) 1963–1969. doi:10.1149/1.2221162.

[56] E. Topal, G. Gece, Untangling the Inhibition Effects of Aliphatic Amines on Silver Corrosion: a Computational Study, Chem. J. Mold. 12 (2017) 64–70. doi:10.19261/cjm.2017.411.

[57] G.I. Kornis, 1,3,4-Thiadiazoles, in: Compr. Heterocycl. Chem. II, Elsevier, 1996: pp. 379–408. doi:10.1016/B978-008096518-5.00088-5.

[58] A.K. Jain, S. Sharma, A. Vaidya, V. Ravichandran, R.K. Agrawal, 1,3,4-Thiadiazole and its Derivatives: A Review on Recent Progress in Biological Activities, Chem. Biol. Drug Des. 81 (2013) 557–576. doi:10.1111/cbdd.12125.

[59] R. Ravichandran, S. Nanjundan, N. Rajendran, Effect of benzotriazole derivatives on the corrosion of brass in NaCl solutions, Appl. Surf. Sci. 236 (2004) 241–250. doi:10.1016/j.apsusc.2004.04.025.

[60] D.M. Bastidas, P.P. Gómez, E. Cano, The isotherm slope. A criterion for studying the adsorption mechanism of benzotriazole on copper in sulphuric acid, Rev. Metal. 41 (2005) 98–106. doi:10.3989/revmetalm.2005.v41.i2.192.

[61] E. Cano, J.L. Polo, A.L.A. Iglesia, J.M. Bastidas, A study on the adsorption of benzotriazole on copper in hydrochloric acid using the inflection point of the isotherm, Adsorption. 10 (2004) 219–225. doi:10.1023/B:ADSO.0000046358.35572.4c.

[62] K. Wall, I. Davies, Corrosion control in a water-cooled stator, J. Appl. Chem. 15 (1965) 389–392. doi:10.1002/jctb.5010150808.

[63] M. Finšgar, J. Kovač, I. Milošev, Surface Analysis of 1-Hydroxybenzotriazole and Benzotriazole Adsorbed on Cu by X-Ray Photoelectron Spectroscopy, J. Electrochem. Soc. 157 (2010) C52–C60. doi:10.1149/1.3261762.

[64] M.R. Choudhury, R.D. Vidic, D.A. Dzombak, Inhibition of Copper Corrosion by Tolyltriazole in Cooling Systems Using Treated Municipal Wastewater as Makeup Water, Arab. J. Sci. Eng. 39 (2014) 7741–7749. doi:10.1007/s13369-014-1385-z.

[65] O. Hollander, R.C. May, The Chemistry of Azole Copper Corrosion Inhibitors in Cooling Water, Corrosion. 41 (1985) 39–45. doi:https://doi.org/10.5006/1.3581967.

[66] D. Gopi, E.S.M. Sherif, M. Surendiran, D.M. Angeline Sakila, L. Kavitha, Corrosion inhibition by benzotriazole derivatives and sodium dodecyl sulphate as corrosion inhibitors for copper in ground water at different temperatures, Surf. Interface Anal. 47 (2015) 618–625. doi:10.1002/sia.5755.

[67] S. Ramesh, S. Rajeswari, Evaluation of inhibitors and biocide on the corrosion control of copper in neutral aqueous environment, Corros. Sci. 47 (2005) 151–169. doi:10.1016/j.corsci.2004.05.013.

[68] F.M. Al Kharafi, I.M. Ghayad, R.M. Abdullah, Corrosion Inhibition of Copper in Non-polluted and Polluted Sea Water Using 5-phenyl-1-H-tetrazole, Int. J. Electrochem. Sci. 7 (2012) 3289–3298.

[69] P. Yu, D.-M.M. Liao, Y.-B.B. Luo, Z.-G.G. Chen, Studies of benzotriazole and tolytriazole as inhibitors for copper corrosion in deionized water, Corrosion. 59 (2003) 314–318.

doi:10.5006/1.3277563.

[70] D. Gopi, K.M.M. Govindaraju, V. Collins Arun Prakash, D.M.M. Angeline Sakila, L. Kavitha, A study on new benzotriazole derivatives as inhibitors on copper corrosion in ground water, Corros. Sci. 51 (2009) 2259–2265. doi:10.1016/j.corsci.2009.06.008.

[71] G.T. Hefter, N.A. North, S.H. Tan, Organic Corrosion Inhibitors in Neutral Solutions; Part 1 - Inhibition of Steel, Copper, and Aluminum by Straight Chain Carboxylates, CORROSION. 53 (1997) 657–667. doi:10.5006/1.3290298.

[72] M. Emad, M. AL-Rasheedi, Nigella Sativa and Natural Honey as Corrosion Inhibitors for Copper in Cooling Water Systems, J. Mater. Environ. Sci. 6 (2015) 201–206.

[73] M.-M. Li, Q.-J. Xu, J. Han, H. Yun, Y. Min, Inhibition Action and Adsorption Behavior of Green Inhibitor Sodium Carboxymethyl Cellulose on Copper, Int. J. Electrochem. Sci. 10 (2015) 9028–9041.

[74] P.D. Rani, S. Selvaraj, Emblica officinalis (AMLA) leaves extract as corrosion inhibitor for copper and its alloy (CU-27ZN) in natural sea water., Arch. Appl. Sci. Res. 2 (2010) 140–150.

[75] P. Deepa Rani, S. Selvaraj, Inhibitive action of Vitis vinifera (grape) on copper and brass in natural sea water environment, 3 (2010) 473–482.

[76] Z. Pengxiang, L. Erjun, L. Xiuying, A SERS study of 1. 2. 3-benzotriazole adsorbed on silver surface, Chinese Phys. Lett. 5 (1988) 329–332. doi:10.1088/0256-307X/5/7/011.

[77] X. Pan, L. Liu, Q. Zhang, J. Qian, Corrosion inhibition and performance evaluation on 2,5-diaryl-1,3,4-thiadiazole and its derivatives, Surf. Interface Anal. 48 (2016) 373–382. doi:10.1002/sia.5994.

[78] A. Kokalj, Ab initio modeling of the bonding of benzotriazole corrosion inhibitor to reduced and oxidized copper surfaces, Faraday Discuss. 180 (2015) 415–438. doi:10.1039/c4fd00257a.

[79] M. Finšgar, I. Milošev, Corrosion study of copper in the presence of benzotriazole and its hydroxy derivative, Mater. Corros. 62 (2011) 956–966. doi:10.1002/maco.201005645.

[80] N.K. Allam, H.S. Hegazy, E.A. Ashour, Adsorption–Desorption Kinetics of Benzotriazole

on Cathodically Polarized Copper, J. Electrochem. Soc. 157 (2010) C174–C177. doi:10.1149/1.3332578.

[81] N. Khalil, Quantum chemical approach of corrosion inhibition, Electrochim. Acta. 48 (2003) 2635–2640. doi:10.1016/S0013-4686(03)00307-4.

[82] B.A. Johnson, The Dissolution of Metal Corrosion Products in Deionized Water at 38° C (100° F), Nucl. Appl. Technol. 8 (1970) 58–61. doi:10.13182/NT70-A28634.

[83] G. Brunoro, A. Frignani, A. Colledan, C. Chiavari, Organic films for protection of copper and bronze against acid rain corrosion, Corros. Sci. 45 (2003) 2219–2231. doi:10.1016/S0010-938X(03)00065-9.

[84] D. Gelman, D. Starosvetsky, Y. Ein-Eli, Copper corrosion mitigation by binary inhibitor compositions of potassium sorbate and benzotriazole, Corros. Sci. 82 (2014) 271–279. doi:10.1016/J.CORSCI.2014.01.028.

[85] K. Sabet Bokati, C. Dehghanian, S. Yari, Corrosion inhibition of copper, mild steel and galvanically coupled copper-mild steel in artificial sea water in presence of 1H-benzotriazole, sodium molybdate and sodium phosphate, Corros. Sci. 126 (2017) 272–285. doi:10.1016/j.corsci.2017.07.009.

[86] R. Alkire, A. Cangellari, Effect of Benzotriazole on Dissolution of Copper in the Presence of Fluid Flow, J. Electrochem. Soc. 136 (1989) 913–919. doi:10.1149/1.2096887.

[87] G. Xue, J. Ding, Chemisorption of a compact polymeric coating on copper surfaces from a benzotriazole solution, Appl. Surf. Sci. 40 (1990) 327–332. doi:10.1016/0169-4332(90)90032-U.

[88] F. Grillo, D.W. Tee, S.M. Francis, H.A. Früchtl, N. V. Richardson, Passivation of copper: Benzotriazole films on Cu(111), J. Phys. Chem. C. 118 (2014) 8667–8675. doi:10.1021/jp411482e.

[89] S. Kapoor, Preparation, Characterization, and Surface Modification of Silver Particles, Langmuir. 14 (1998) 1021–1025. doi:10.1021/la9705827.

[90] Q.H. Zhang, B.S. Hou, N. Xu, W. Xiong, H.F. Liu, G.A. Zhang, Effective inhibition on the corrosion of X65 carbon steel in the oilfield produced water by two Schiff bases, J. Mol.

Liq. 285 (2019) 223–236. doi:10.1016/j.molliq.2019.04.072.

[91] S. Peljhan, A. Kokalj, DFT study of gas-phase adsorption of benzotriazole on Cu(111), Cu(100), Cu(110), and low coordinated defects thereon, Phys. Chem. Chem. Phys. 13 (2011) 20408–20417. doi:10.1039/c1cp21873e.

[92] H. Rahmani, E.I. Meletis, Corrosion study of brazing Cu-Ag alloy in the presence of benzotriazole inhibitor, Appl. Surf. Sci. 497 (2019) 143759. doi:10.1016/j.apsusc.2019.143759.

[93] Y.-M. Tang, W.-Z. Yang, X.-S. Yin, Y. Liu, R. Wan, J.-T. Wang, Phenyl-substituted amino thiadiazoles as corrosion inhibitors for copper in 0.5 M H2SO4, Mater. Chem. Phys. 116 (2009) 479–483. doi:10.1016/j.matchemphys.2009.04.018.

[94] H. Tian, W. Li, K. Cao, B. Hou, Potent inhibition of copper corrosion in neutral chloride media by novel non-toxic thiadiazole derivatives, Corros. Sci. 73 (2013) 281–291. doi:10.1016/j.corsci.2013.04.017.

[95] R. Babić, M. Metikoš-Huković, M. Lončar, Impedance and photoelectrochemical study of surface layers on Cu and Cu–10Ni in acetate solution containing benzotriazole, Electrochim. Acta. 44 (1999) 2413–2421. doi:10.1016/S0013-4686(98)00367-3.

[96] F. Ma, W. Li, H. Tian, B. Hou, The Use of a New Thiadiazole Derivative as a Highly Efficient and Durable Copper Inhibitor in 3.5% NaCl Solution, Int. J. Electrochem. Sci. 10 (2015) 5862–5879. doi:http://www.electrochemsci.org/papers/vol10/100705862.pdf.

[97] B. Tan, S. Zhang, Y. Qiang, W. Li, H. Liu, C. Xu, S. Chen, Insight into the corrosion inhibition of copper in sulfuric acid via two environmentally friendly food spices: Combining experimental and theoretical methods, J. Mol. Liq. 286 (2019) 1–13. doi:10.1016/j.molliq.2019.110891.

[98] R.T. Loto, A. Ogaga, Inhibition effect of the combined admixture of l-leucine and 5-bromovanilin on the corrosion of P4 low carbon mold steel, Procedia Manuf. 35 (2019) 315–320. doi:10.1016/j.promfg.2019.05.046.

[99] R.T. Loto, O. Olowoyo, Synergistic effect of sage and jojoba oil extracts on the corrosion inhibition of mild steel in dilute acid solution, Procedia Manuf. 35 (2019) 310–314.

doi:10.1016/j.promfg.2019.05.045.

[100] T. Hong, Y.H. Sun, W.P. Jepson, Study on corrosion inhibitor in large pipelines under multiphase flow using EIS, Corros. Sci. 44 (2002) 101–112. doi:10.1016/S0010-938X(01)00052-X.

[101] S.Y. Sayed, M.S. El-Deab, B.E. El-Anadouli, B.G. Ateya, Synergistic effects of benzotriazole and copper ions on the electrochemical impedance spectroscopy and corrosion behavior of iron in sulfuric acid, J. Phys. Chem. B. 107 (2003) 5575–5585. doi:10.1021/jp034334x.

[102] H. Rahmani, E.I. Meletis, Corrosion inhibition of brazing Cu-Ag alloy with 1,2,3-benzotriazole and 2,5-dimercapto-1,3,4-thiadiazole, Submitt. to Corros. (2020).

[103] L. Huang, J. Shen, J. Ren, Q. Meng, T. Yu, The adsorption of 2,5-dimercapto-1,3,4-thiadiazole (DMTD) on copper surface and its binding behavior, Chinese Sci. Bull. 46 (2001) 387–389. doi:10.1007/bf03183270.

[104] L. Huang, F. Tang, B. Hu, J. Shen, T. Yu, Q. Meng, Chemical reactions of 2,5-dimercapto-1,3,4-thiadiazole (DMTD) with metallic copper, silver, and mercury, J. Phys. Chem. B. 105 (2001) 7984–7989. doi:10.1021/jp004385j.

[105] M. Finšgar, D.K. Merl, 2-Mercaptobenzoxazole as a copper corrosion inhibitor in chloride solution: Electrochemistry, 3D-profilometry, and XPS surface analysis, Corros. Sci. 80 (2014) 82–95. doi:10.1016/J.CORSCI.2013.11.022.

[106] T.T. Qin, J. Li, H.Q. Luo, M. Li, N.B. Li, Corrosion inhibition of copper by 2,5-dimercapto-1,3,4-thiadiazole monolayer in acidic solution, Corros. Sci. 53 (2011) 1072–1078. doi:10.1016/j.corsci.2010.12.002.

[107] C. Cleveland, S. Moghaddam, M.E. Orazem, Nanometer-Scale Corrosion of Copper in De-Aerated Deionized Water, J. Electrochem. Soc. 161 (2013) C107–C114. doi:10.1149/2.030403jes.

[108] E.M. Sherif, S.-M. Park, Inhibition of Copper Corrosion in 3.0% NaCl Solution by N-Phenyl-1,4-phenylenediamine, J. Electrochem. Soc. 152 (2005) B428–B433. doi:10.1149/1.2018254.

[109] A.M. Fenelon, C.B. Breslin, An electrochemical study of the formation of benzotriazole surface films on copper, zinc and a copper-zinc alloy, J. Appl. Electrochem. 31 (2001) 509–516. doi:10.1023/A:1017503031045.

[110] Z. Tao, G. Liu, Y. Li, R. Zhang, H. Su, S. Li, Electrochemical Investigation of Tetrazolium Violet as a Novel Copper Corrosion Inhibitor in an Acid Environment, ACS Omega. 5 (2020) 4415–4423. doi:10.1021/acsomega.9b03475.

[111] V.M.-W. Huang, V. Vivier, I. Frateur, M.E. Orazem, B. Tribollet, The Global and Local Impedance Response of a Blocking Disk Electrode with Local Constant-Phase-Element Behavior, J. Electrochem. Soc. 154 (2007) C89–C98. doi:10.1149/1.2398889.

[112] T.X. Shi, J. Henry, J. Schlueter, Electrochemical Characterizations and CMP Performance of Ru Slurry, ECS Trans. 50 (2013) 17–27. doi:10.1149/05039.0017ecst.

[113] Z. Tao, S. Zhang, W. Li, B. Hou, Corrosion inhibition of mild steel in acidic solution by some oxo-triazole derivatives, Corros. Sci. 51 (2009) 2588–2595. doi:10.1016/j.corsci.2009.06.042.

[114] A. Liu, X. Ren, Q. Yang, J. Sokolowski, J. Guo, Y. Li, L. Gao, M. An, G. Wu, Theoretical and Experimental Studies of the Prevention Mechanism of Organic Inhibitors on Silver Anti-Tarnish, J. Electrochem. Soc. 165 (2018) H725–H732. doi:10.1149/2.0081811jes.

[115] F. Reshadi, G. Faraji, M. Baniassadi, M. Tajeddini, Surface modification of severe plastically deformed ultrafine grained pure titanium by plasma electrolytic oxidation, Surf. Coatings Technol. 316 (2017) 113–121. doi:10.1016/j.surfcoat.2017.03.016.

[116] L. Guo, Y. El Bakri, R. Yu, J. Tan, E.M. Essassi, Newly synthesized triazolopyrimidine derivative as an inhibitor for mild steel corrosion in HCl medium: an experimental and in silico study, J. Mater. Res. Technol. 9 (2020) 6568–6578. doi:10.1016/j.jmrt.2020.04.044.

[117] W. Plieth, Electrochemistry for Materials Science, Elsevier, Dresden, 2008. doi:https://doi.org/10.1016/B978-0-444-52792-9.X5001-5.

[118] F.J. Martin, G.T. Cheek, W.E. O'Grady, P.M. Natishan, Impedance studies of the passive film on aluminium, Corros. Sci. 47 (2005) 3187–3201. doi:10.1016/j.corsci.2005.05.058.

[119] K. Hu, J. Zhuang, J. Ding, Z. Ma, F. Wang, X. Zeng, Influence of biomacromolecule DNA

corrosion inhibitor on carbon steel, Corros. Sci. 125 (2017) 68–76. doi:10.1016/j.corsci.2017.06.004.

[120] J.F. Moulder, W.F. Stickle, P.E. Sobol, K.D. Bomben, Handbook of X-ray Photoelectron Spectroscopy, Perkin-Elmer Corporation, 1992.

[121] P. Lazar, R. Mach, M. Otyepka, Spectroscopic Fingerprints of Graphitic, Pyrrolic, Pyridinic and Chemisorbed Nitrogen in N-Doped Graphene, J. Phys. Chem. C. (2019) 1–30. doi:10.1021/acs.jpcc.9b02163.

[122] J.-Y. Jhuang, S.-H. Lee, S.-W. Chen, Y.-H. Chen, Y.-J. Chen, J.-L. Lin, C.-H. Wang, Y.-W. Yang, Adsorption and Reaction Pathways of 1H-Pyrazole on Cu(100) and O/Cu(100), J. Phys. Chem. C. 122 (2018) 6195–6208. doi:10.1021/acs.jpcc.8b00042.

[123] A. Mirarco, S.M. Francis, C.J. Baddeley, A. Glisenti, F. Grillo, Effect of the pH in the growth of benzotriazole model layers at realistic environmental conditions, Corros. Sci. 143 (2018) 107–115. doi:10.1016/J.CORSCI.2018.08.008.

[124] J. Gupta, J. Mohapatra, D. Bahadur, Visible light driven mesoporous Ag-embedded ZnO nanocomposites: reactive oxygen species enhanced photocatalysis, bacterial inhibition and photodynamic therapy, Dalt. Trans. 46 (2017) 685–696. doi:10.1039/C6DT03713E.

[125] T.C. Kaspar, T. Droubay, S.A. Chambers, P.S. Bagus, Spectroscopic evidence for Ag(III) in highly oxidized silver films by X-ray photoelectron spectroscopy, J. Phys. Chem. C. 114 (2010) 21562–21571. doi:10.1021/jp107914e.

[126] L. Duan, P. Wang, X. Yu, X. Han, Y. Chen, P. Zhao, D. Li, R. Yao, The synthesis and characterization of Ag–N dual-doped p-type ZnO: experiment and theory, Phys. Chem. Chem. Phys. 16 (2014) 4092–4097. doi:10.1039/c3cp53067a.

[127] Y. Liu, C. Tian, B. Yan, Q. Lu, Y. Xie, J. Chen, R. Gupta, Z. Xu, S.M. Kuznicki, Q. Liu, H. Zeng, Nanocomposites of graphene oxide, Ag nanoparticles, and magnetic ferrite nanoparticles for elemental mercury (Hg 0) removal, RSC Adv. 5 (2015) 15634–15640. doi:10.1039/C4RA16016A.

[128] J. Wang, J. Li, G. Guo, Q. Wang, J. Tang, Y. Zhao, H. Qin, T. Wahafu, H. Shen, X. Liu, X. Zhang, Silver-nanoparticles-modified biomaterial surface resistant to staphylococcus: new

insight into the antimicrobial action of silver, Sci. Rep. 6 (2016) 32699. doi:10.1038/srep32699.

[129] S. Tardio, P.J. Cumpson, Practical estimation of XPS binding energies using widely available quantum chemistry software, Surf. Interface Anal. 50 (2018) 5–12. doi:10.1002/sia.6319.

[130] T. Shinagawa, G.O. Larrazábal, A.J. Martín, F. Krumeich, J. Pérezpérez-Ramírez, Sulfur-Modified Copper Catalysts for the Electrochemical Reduction of Carbon Dioxide to Formate, 8 (2018) 837–844. doi:10.1021/acscatal.7b03161.

[131] Q.H. Zhang, B.S. Hou, G.A. Zhang, Inhibitive and adsorption behavior of thiadiazole derivatives on carbon steel corrosion in CO2-saturated oilfield produced water: Effect of substituent group on efficiency, J. Colloid Interface Sci. 572 (2020) 91–106. doi:10.1016/j.jcis.2020.03.065.

[132] P. Kalimuthu, P. Kalimuthu, S.A. John, Leaflike structured multilayer assembly of dimercaptothiadiazole on gold surface, J. Phys. Chem. C. 113 (2009) 10176–10184. doi:10.1021/jp810337s.

[133] A. Abdul Razzaq, Y. Yao, R. Shah, P. Qi, L. Miao, M. Chen, X. Zhao, Y. Peng, Z. Deng, High-performance lithium sulfur batteries enabled by a synergy between sulfur and carbon nanotubes, Energy Storage Mater. 16 (2019) 194–202. doi:10.1016/j.ensm.2018.05.006.

[134] Z. Wang, Y. Dong, H. Li, Z. Zhao, H. Bin Wu, C. Hao, S. Liu, J. Qiu, X.W.D. Lou, Enhancing lithium-sulphur battery performance by strongly binding the discharge products on amino-functionalized reduced graphene oxide, Nat. Commun. 5 (2014) 1–8. doi:10.1038/ncomms6002.

[135] M. Panthakkal Abdul Muthalif, C. Damodharan Sunesh, Y. Choe, C.D. Sunesh, Y. Choe, H3PO4 treated surface modified CuS counter electrodes with high electrocatalytic activity for enhancing photovoltaic performance of quantum dot-sensitized solar cells, Appl. Surf. Sci. 440 (2018) 1022–1026. doi:10.1016/j.apsusc.2018.01.233.

[136] J.C. Bernède, Y. Trégouet, E. Gourmelon, F. Martinez, G. Neculqueo, On the degradation of some thiophene oligomers after doping by ion chloride, Polym. Degrad. Stab. 55 (1997) 55–64. doi:10.1016/S0141-3910(96)00110-3.

[137] S. Kadian, G. Manik, N. Das, P. Nehra, R.P. Chauhan, P. Roy, Synthesis, characterization and investigation of synergistic antibacterial activity and cell viability of silver-sulfur doped graphene quantum dot (Ag@S-GQDs) nanocomposites, J. Mater. Chem. B. 8 (2020) 3028–3037. doi:10.1039/c9tb02823d.

[138] C. Battocchio, I. Fratoddi, L. Fontana, E. Bodo, F. Porcaro, C. Meneghini, I. Pis, S. Nappini, S. Mobilio, M. V. Russo, G. Polzonetti, Silver nanoparticles linked by a Pt-containing organometallic dithiol bridge: study of local structure and interface by XAFS and SR-XPS, Phys. Chem. Chem. Phys. 16 (2014) 11719–11728. doi:10.1039/C4CP01264J.